A FACILE EFFECTIVE METHOD FOR THE SYNTHESIS OF Au-CdSe NANOSTRUCTURES AND THEIR CHARACTERISATIONS

by

NELISA NCUMISA GAXELA

A dissertation submitted in fulfillment of the requirements for the degree of

MASTER OF SCIENCE

CHEMISTRY

at

WALTER SISULU UNIVERSITY

SUPERVISOR: PROF. S. O. OLUWAFEMI

MAY 2016

ABSTRACT

We report the synthesis of aqueous and organically soluble cadmium selenide (CdSe) nanoparticles (NPs) doped with gold via a facile and effective method. Briefly the synthesis involves the reduction of selenium powder using sodium sulphite to produce sodium selenosulphate which acts as the selenium source, followed by the addition of CdX (X = Cl_2, CH_3COO, NO_3). The nanoparticles were passivated with trisodium citrate, mercaptopropanoic acid (MPA), potassium sodium tartarate (PST) and L-cysteine which rendered them soluble in water and also acted as stabilizing agents, while passivation with hexadecylamine (HDA) made them soluble in organic solvent which also enhanced their stability. The high quality of the as-synthesized nanoparticles was confirmed using absorption and photoluminescence (PL) spectroscopy, Fourier transform infrared spectroscopy (FTIR), transmission electron microscopy (TEM) and high resolution TEM (HRTEM).

The systematic study of the effect of mole ratio, temperature, capping agent, growth time, cadmium precursor and ratio of Au on the size, optical and structural properties on the water soluble CdSe nanoparticles were investigated. All the as-synthesised particles, are blue-shifted in relation to the bulk band gap of CdSe. As the Cd: Se mole ratio increases, the intensity of the citrate capped CdSe materials also increases and the particle sizes are in the range of 2.06 – 4.00 nm. When the temperature was increased, the luminescence intensity quenched whereas the particle size increased. As the growth time increased, the intensity increased and then decreased again towards the end of

the reaction. When different capping agents were used the particle sizes range from 2.06 – 3.36 nm for citrate, 2.08 – 3.33 nm for MPA, 2.01 – 2.28 nm for L-cysteine and polydispersed for PST. The luminescence intensity decreased in the order citrate > cysteine > PST > MPA when $CdCl_2$ was used as cadmium precursor. When different cadmium precursors were used for L-cysteine, the particle sizes range from 2.06 – 2.31 nm for $Cd(CH_3COO)_2$ and 2.00 – 2.37 nm for $Cd(NO_3)_2$ while the intensity increased as the reaction time increased, however, still lower than the $CdCl_2$ materials. The effect of Au ratio showed that the intensity of Au-doped cysteine capped-CdSe increased as the Au ratio decreased.

The systematic study of the effect of temperature and growth time in the organic soluble CdSe nanoparticles on the size, optical and structural properties was also investigated. All the as-synthesised particles were blue-shifted in relation to the bulk CdSe. As the temperature increased the particle sizes of the undoped materials range between 2.92 – 2.95 nm at 160 °C and 5.35 – 5.39 nm at 200 °C while for the doped materials the particle size range from 2.53 – 2.61 nm at 160 °C, 3.97 nm at 200 °C and 4.20 – 4.72 nm at 240 °C. The intensity of the doped materials increased as the reaction time increased and then decreased again towards the end of the reaction. After ligand exchange the intensity of the as-synthesized doped and undoped-CdSe NPs was very low compare to the parent organically capped doped and un-doped CdSe.

It was discovered that without any further purification, the quality of the materials formed by this method is comparable to that of the best CdSe NPs reported in the literature. This method is safe, inexpensive and reproducible.

DECLARATION

I, Nelisa Ncumisa Gaxela student number 202607763, declare that this paper entitled "**A facile effective method for the synthesis of Au-CdSe nanostructures and their characterizations**" which I submit for the degree of MASTER OF SCIENCE (CHEMISTRY) at Walter Sisulu University is my original work. This study has not previously in its entirety or in part been submitted at any university in order to obtain an academic qualification.

CANDIDATE: Nelisa Ncumisa Gaxela

SIGNITURE: _____

DATE: _____

SUPERVISOR: Prof SO Oluwafemi

SIGNITURE: _____

DATE: _____

DEDICATIONS

This work is dedicated to my family. My mother Mrs. Weziwe Gaxela, my sisters Gcobisa and Andisiwe, my brother Aseko, my nephews Live and Amila and nieces Liphulaphule and Amkhitha. They could have discouraged me from pursuing my studies and told me to get a job but because of their unconditional love they were fully supportive of my desire to obtain this degree.

ACKNOWLEDGEMENTS

To my Heavenly Father for granting me the opportunity to further my studies while some who wish for the same could not. He gave me strength to pull through all the darkness and even when there were temptations to give up but thou lifted me up so I could fulfill thy promise about my life. My Redeemer, my solid foundation, once again gave me victory.

To my family who never gave up on me even when I came home crying and wanting to quit but always reminded me that I am a winner and nothing ever comes easy in life. Because of your confidence in me, I thank you from the bottom of my heart. God bless you all with love.

To my supervisor Prof. O. S. Oluwafemi for believing in me and giving me a chance when I didn't believe in my own self. You have been patient with me till this far and I am entirely grateful. God bless you and your family.

To the Department of Chemistry and Chemical Technology I show my sincerest gratitude for allowing me to enroll in this programme and helping with chemicals when I was in need. My knowledge has broadened and I owe it all to you.

To the Nano group at large (Mbande Z., Lucwaba Y., Zekani S., Mochochoko T., Stofile Y., Gura A., Deramola O., Tshikovhi A., Khanyisile and Linoyolo) and also my fellow researchers in the department (Rwexwana A. and Thungatha L.) for all the support you

have given me and help with all the discussions that strengthened me as a researcher. God bless you all.

To NRF for financial assistance. I wouldn't have done it all without all the aid you have given me.

To the CSIR for opening its doors and allowing me to perform my analyses. It is highly appreciated.

TABLE OF CONTENTS

ABSTRACT i

DECLARATION iv

DEDICATIONS v

ACKNOWLEDGEMENTS vi

LIST OF TABLES xiv

LIST OF FIGURES xvi

CHAPTER 1 1

1. INTRODUCTION AND LITERATURE REVIEW 1

1.1 BACKGROUND 1

1.2 HETEROSTRUCTURED MATERIALS 2

1.3 PHOTOCATALYSIS 3

1.4 SYNTHESIS OF HETEROSTRUCTURED MATERIALS 5

1.5 SYNTHESIS OF Au-CdSe NANOSTRUCTURES 9

1.6 APPLICATIONS OF HETEROSTRUCTURED MATERIALS 14

1.7 SYNTHETIC ROUTE PROBLEMS 16

1.8 AIM 19

1.9 OBJECTIVES 19

CHAPTER 2 20

2. EXPERIMENTAL 20

2.1 Chemicals 20

2.2 Apparatus 20

2.3 Synthesis 21

2.3.1 Synthesis of water soluble CdSe nanoparticles 21

2.3.1.1 Effect of Cd:Se mole ratio 22

2.3.1.2 Effect of temperature 22

2.3.1.3 Effect of capping agent 22

2.3.1.4 Effect of cadmium precursor 22

2.3.2 Synthesis of water soluble Au-doped CdSe 23

2.3.2.1 Effect of gold ratio 23

2.3.3 Synthesis of organic soluble CdSe nanostructures 23

2.3.4 Synthesis of organic soluble Au-doped CdSe nanostructures 24

2.3.4.1 Effect of temperature 25

2.4 Quantum yield determination 25

2.5 Ligand exchange 26

2.6 Characterization 26

2.6.1 Ultraviolet/visible (UV/vis) Spectroscopy 26

2.6.2 Photoluminescence (PL) Spectroscopy 27

2.6.3 Fourier Transform Infrared Spectroscopy (FTIR) 27

2.6.4 Transmission Electron Microscopy (TEM) and High Resolution TEM (HRTEM) 27

CHAPTER 3 29

3. RESULTS AND DISCUSSIONS 29

3.1 Synthesis of water soluble CdSe nanoparticles 29

3.1.1 Citrate-capped CdSe nanoparticles 29

3.1.1.1 Optical properties 29

3.1.1.2 Structural properties 32

3.1.1.2.1 Fourier Transform Infrared Spectroscopy (FTIR) 32

3.1.1.2.2 TEM, HRTEM and FFT 34

3.1.2 Effect of cadmium to selenium ratio 35

3.1.2.1 Optical properties 35

3.1.2.2 Structural properties 38

3.1.2.2.1 Fourier Transform Infrared Spectroscopy 38

3.1.2.2.2 TEM, HRTEM and FFT 39

3.1.3 Effect of temperature 40

3.1.3.1 Optical properties 41

3.1.3.2 Structural properties 43

3.1.3.2.1 TEM, HRTEM and FFT 43

3.1.4 Effect of capping agent 44

3.1.4.1 Optical properties 45

3.1.5 Effect of growth time 47

3.1.5.1 Optical properties 47

3.1.6 Effect of cadmium precursor 53

3.1.6.1 Optical properties 53

3.1.6.2 Structural properties 69

3.1.6.2.1 Fourier Transform Infrared Microscopy (FTIR) 69

3.1.6.2.2 TEM, HRTEM and FFT 72

3.2 Synthesis of water soluble Au-CdSe nanostructures 73

3.2.1 Cysteine-capped Au-CdSe nanostructures 74

3.2.1.1 Optical properties 74

3.2.2 Effect of Au ratio 75

3.2.2.1 Optical properties 75

3.2.2.2 Structural properties 79

3.2.2.2.1 Fourier Transform Infrared Microscopy (FTIR) 79

3.3 Synthesis of organic soluble CdSe nanostructures 81

3.3.1 HDA-capped CdSe nanostructures 81

3.3.1.1 Optical properties 81

3.3.2 Structural properties 86

3.3.2.1 Fourier Transform Infrared Microscopy (FTIR) 86

3.3.2.2 TEM, HRTEM and FFT 87

3.4 Synthesis of Au doped CdSe nanostructures 88

3.4.1 HDA-capped Au-CdSe nanostructures 88

3.4.1.1 Optical properties 88

3.4.2 Structural properties 95

3.4.2.1 Fourier Transform Infrared Microscopy (FTIR) 95

3.4.2.2 TEM, HRTEM and FFT 96

3.5 Ligand Exchange 97

3.5.1 Optical Properties 97

CHAPTER 4 99

4.1 Conclusion 99

4.2 Recommendations 104

REFERENCES 106

Appendix A 116

Appendix B 117

LIST OF TABLES

Table 1: Optical properties of citrate-capped CdSe NPs at ratio 1:1 using $CdCl_2$. 32

Table 2: IR bands for the citrate and citrate-capped CdSe NPs. 34

Table 3: Optical properties of citrate-capped CdSe NPs at different ratios at 1 hour reaction time. 37

Table 4: Optical properties of CdSe NPs using different capping agents. 46

Table 5: Optical properties of citrate-capped CdSe NPs using $CdCl_2$ precursor. 51

Table 6: Optical properties for MPA-capped CdSe NPs. 52

Table 7: Optical properties of cysteine-capped CdSe NPs. 53

Table 8: Optical properties of citrate-capped CdSe NPs using $Cd(CH_3COO)_2$ precursor. 56

Table 9: Optical properties of citrate-capped CdSe NPs using $Cd(NO_3)_2$ precursor. 57

Table 10: Optical properties of MPA-capped CdSe NPs using $Cd(CH_3COO)_2$ precursor. .60

Table 11: Optical properties of MPA-capped CdSe NPs using $Cd(NO_3)_2$ precursor. 61

Table 12: Optical properties of cysteine-capped CdSe NPs using $Cd(CH_3COO)_2$ precursor. 64

Table 13: Optical properties of cysteine-capped CdSe NPs using $Cd(NO_3)_2$ precursor. ..65

Table 14: Optical properties for PST-capped CdSe NPs using $Cd(CH_3COO)_2$ precursor. 68

Table 15: Optical properties of PST-capped CdSe NPs using $Cd(NO_3)_2$ precursor. 69

Table 16: Optical properties of cysteine-capped Au-doped CdSe NPs at ratio 1:40. 77

Table 17: Optical properties of cysteine-capped Au doped CdSe NPs at ratio 1:60.....79

Table 18: Optical properties of HDA-capped CdSe NPs at 160 °C. 83

Table 19: Optical properties of HDA-capped CdSe NPs at 200 °C. 85

Table 20: Optical properties of HDA-capped Au doped CdSe NPs at 160 °C. 90

Table 21: Optical properties of HDA-capped Au doped CdSe NPs at 200 °C. 92

Table 22: Optical properties of HDA-capped Au doped CdSe NPs at 240 °C. 95

Table 23: Optical properties after ligand exchange for both doped and undoped CdSe NPs at 160, 200 and 240 °C. 98

LIST OF FIGURES

Figure 1: A photograph of the colour of the CdSe solution after the addition of selenium precursor.....30

Figure 2: Absorption spectra of citrate-capped CdSe NPs at ratio 1:1 (Cd:Se) at different reaction times.....31

Figure 3: Photoluminescence spectra (λ_{400}) of citrate-capped CdSe NPs at ratio 1:1 (Cd:Se) at different reaction times. 31

Figure 4: FTIR spectra for citrate and citrate-capped CdSe NPs.....33

Figure 5: TEM (a) FFT (b) HRTEM (c) images of citrate-capped CdSe at ratio 1:1 at 1 hour.....35

Figure 6: (a) Absorption and (b) photoluminescence ($\lambda_{400\ nm}$) spectra of citrate-capped CdSe NPs at different ratios at 3 h reaction time. 37

Figure 7: FTIR spectra of citrate and citrate-capped CdSe NPs at different Cd:Se mole ratio. 38

Figure 8: TEM images of citrate-capped CdSe NPs [insets: HRTEM and FFT] at Cd:Se ratio of (a) 1:1 (b) 2:1 (c) 3:1 (d) 4:1. 40

Figure 9: Photographs showing the (a) reflux setup (b) colour change during the reaction of citrate-capped CdSe at ratio 2:1 in the order 0 mins, 15 mins, 30 mins and 1h. 41

Figure 10: Typical (a) Absorption and (b) photoluminescence (PL $\lambda_{400\ nm}$) spectra of citrate-capped CdSe NPs at room temperature and under reflux [Inset: PL under reflux]. 42

Figure 11: TEM images of citrate-capped CdSe NPs [insets: HRTEM and FFT] for Cd:Se ratio 2:1 at (a) room temperature (b) reflux. 43

Figure 12: The colour of the CdSe NPs after the addition of selenium precursor to the (a) Cd-citrate complex (b) Cd-MPA complex (c) Cd-cysteine complex and (d) Cd-PST complex solution. 44

Figure 13: (a) Absorption and (b) photoluminescence ($\lambda_{400\ nm}$) spectra of CdSe NPs using different capping agents 46

Figure 14: Absorption spectra of CdSe NPs using different capping agents: (a) citrate (b) MPA (c) cysteine and (d) PST at different reaction times. 48

Figure 15: Photoluminescence ($\lambda_{400\ nm}$) spectra of CdSe NPs using different capping agents: (a) citrate (b) MPA (c) cysteine and (d) PST at different reaction times. 50

Figure 16: Absorption spectra of citrate-capped CdSe NPs using (a) $Cd(CH_3COO)_2$ and (b) $Cd(NO_3)_2$ precursors and Photoluminescence ($\lambda_{400\ nm}$) spectra of citrate-capped

CdSe NPs using (c) $Cd(CH_3COO)_2$ and (d) $Cd(NO_3)_2$ precursors at different reaction times.....55

Figure 17: Absorption spectra of MPA-capped CdSe NPs using (a) $Cd(CH_3COO)_2$ and (b) $Cd(NO_3)_2$ and Photoluminescence ($\lambda_{400\ nm}$) spectra of MPA-capped CdSe NPs (c) $Cd(CH_3COO)_2$ and (d) $Cd(NO_3)_2$ at different reaction times. 59

Figure 18: Absorption spectra of cysteine-capped CdSe NPs using (a) $Cd(CH_3COO)_2$ and (b) $Cd(NO_3)_2$ and Photoluminescence ($\lambda_{350\ nm}$) spectra of cysteine-capped CdSe NPs (c) $Cd(CH_3COO)_2$ and (d) $Cd(NO_3)_2$ at different reaction times. 63

Figure 19: Absorption spectra of PST-capped CdSe NPs using (a) $Cd(CH_3COO)_2$ and (b) $Cd(NO_3)_2$ and Photoluminescence ($\lambda_{400\ nm}$) spectra of PST-capped CdSe NPs (c) $Cd(CH_3COO)_2$ and (d) $Cd(NO_3)_2$ at different reaction times. 67

Figure 20: FTIR spectra of CdSe NPs synthesised using different cadmium precursors capped with (a) citrate (b) MPA (c) cysteine and (d) PST. 72

Figure 21: (a) TEM (b) HRTEM (c) FFT images and (d) size distribution of MPA-capped CdSe NPs synthesised using $Cd(CH_3COO)_2$.....73

Figure 22: (a) Absorption and (b) photoluminescence ($\lambda_{400\ nm}$) spectra of cysteine-capped Au-doped CdSe NPs using 1:20 Cd:Au ratio at different reaction times. 75

Figure 23: (a) Absorption and (b) photoluminescence ($\lambda_{400\ nm}$) spectra of cysteine-capped Au-doped CdSe NPs using 1:40 Cd: Au ratio at different reaction times. 76

Figure 24: (a) Absorption and (b) photoluminescence ($\lambda_{400\ nm}$) spectra of cysteine-capped Au-doped CdSe NPs using 1:40 ratio at different reaction times. 78

Figure 25: FTIR spectra of cysteine and cysteine-capped Au doped CdSe NPs using different Cd:Au ratio. 80

Figure 26: A photograph showing the change in the colour of the CdSe NPs as at reaction time of 0, 8 and 15 mins. 81

Figure 27: (a) Absorption and (b) photoluminescence ($\lambda_{400\ nm}$) spectra of HDA-capped CdSe NPs at 160 °C at different reaction times. 82

Figure 28: Photographs showing the colour of HDA-capped CdSe NPs at 160 °C under (a) visible light and under (b) UV light at 0, 5, 10, 20, 30 and 60 min. 83

Figure 29: (a) Absorption and (b) photoluminescence ($\lambda_{400\ nm}$) spectra of HDA-capped CdSe NPs at 200 °C at different reaction times. 84

Figure 30: Photographs showing the colour of HDA-capped CdSe NPs at 200 °C under (a) visible light and under (b) UV light at 0, 5, 10, 20, 30 and 60 min. 85

Figure 31: FTIR spectra for HDA and HDA-capped CdSe NPs at 160 and 200 °C. 86

Figure 32: TEM (a) HRTEM (b) FFT (c) images and size distribution (d) of HDA-capped CdSe NPs at 200 °C. 87

Figure 33: A photograph showing the colour of the CdSe NPs after the addition of selenium precursor to the Au-Cd complex.....88

Figure 34 (a) Absorption and (b) photoluminescence ($\lambda_{400\ nm}$) spectra of Au doped HDA-capped CdSe at 160 °C at different reaction times.....89

Figure 35: Photographs showing the colour of Au-doped HDA-capped CdSe NPs at 160 °C under (a) visible light and under (b) UV light at 0, 5, 10, 20, 30 and 60 min. 90

Figure 36: (a) Absorption and (b) photoluminescence ($\lambda_{400\ nm}$) spectra of Au doped HDA-capped CdSe NPs at 200 °C at different reaction times. 91

Figure 37: Photographs showing the colour of Au-doped HDA-capped CdSe NPs at 200 °C under (a) visible light and under (b) UV light at 0, 5, 10, 20 and 30 min. 92

Figure 38: (a) Absorption and (b) photoluminescence ($\lambda_{400\ nm}$) spectra for Au doped HDA-capped CdSe NPs at 240 °C at different reaction times. 94

Figure 39: Photographs showing the colour of Au-doped HDA-capped CdSe NPs at 240 °C under (a) visible light and under (b) UV light at 0, 5, 10, 20, 30 and 60 min. 94

Figure 40: FTIR spectra for HDA and HDA-capped Au doped CdSe NPs at 160, 200 and 240 ° C. 96

Figure 41: TEM (a) HRTEM (b) FFT (c) images and size distribution (d) of HDA-capped Au-CdSe NPs at 160 °C 97

Figure 42: Absorption spectra after ligand exchange for (A) Au doped CdSe NPs at 160 °C, (B) HDA-capped CdSe NPs at 160 °C, (C) Au doped CdSe NPs at 200 °C, (D) HDA-capped CdSe NPs at 200 °C and (E) Au -doped CdSe NPs at 240 °C.....98

CHAPTER 1

1. INTRODUCTION AND LITERATURE REVIEW

1.1 BACKGROUND

There is an adage that reads "small is beautiful". However, today we know that small is not only beautiful but also powerful. With the range of applications that nanomaterials find in various fields of engineering and science, these materials look more promising than conventional bulk materials. Nanomaterials are particles that have at least one dimension less than 100 nm. They have a high surface to volume ratio and their mass and heat transfer properties are better than those of bulk materials. These materials as a result of their diverse architectures due to the various synthetic approaches are being referred to in literature as quantum dots (QD), nanoparticles, nanowires, nanorods, nanobelts, nanodisks and so on (Malik *et al.,* 2000; Malik and O'Brien 2005). These particles exhibit unique electronic and chemical properties which are attributed to two main factors: the large surface area –to – volume ratio and their reduced dimensions in relation to the excitonic radius of the bulk material known as quantum confinement (Green and O'Brien 1999). This quantum size effect causes structural and electronic changes that in-turn induce other novel properties that largely dominate the behavior of these materials and make them different from that of the bulk materials. The increase in the surface-area-to-volume ratio, which is a gradual progression as the particle gets smaller, leads to an increasing dominance of the behavior of the atoms on the surface

of the particle over those in the interior of the particle. This affects both the properties of the particle in isolation and its interaction with other materials (Hines and Guyot-Sionnest 1996). Hence they find enormous applications in fields such as optics, electronics, biomedicine, magnetics, catalysis, mechanics, energy science, physics and others (Pissuwan *et al.,* 2006).

1.2 HETEROSTRUCTURED MATERIALS

Heterostructures are hybrid nanostructures (HNS) formed by incorporating two or more types of materials to produce a new material that possess characteristics that differ from the starting materials. For example, the formation of metal semiconductor hybrid such as Au-doped CdSe which effectively combines the properties of both the metal (Au) and the semiconductor (CdSe) (Plante *et al.,* 2009). When a metal and a semiconductor combine as one material, the properties of both parent materials could be harnessed in potential applications. For example, the metal can provide the anchor point for electrical connections and self-assembly and the semiconductor enhances the optical and photoluminescence properties (Pullabhotla and Revaprasadu 2009, Chili *et al.,* 2012). According to Mokari *et al*., 2004, the anisotropic growth of Au on the tips of the nanorods resulted in novel functionalities that are independent of the individual components which are achieved through the rational design of such heterostructures and may be tailored to fit a specific application. Through self-organization of single Au/CdTe, Jun Li *et al.,* 2004 obtained photoluminescent nanostructure materials using gold nanoparticles as seeds. In copper (Cu)-doped CdSe, the copper can act as both

the acceptor and donor, which will make it to have large applications in photovoltaics and other fields of electronics (Singh *et al.,* 2008). ZnMnTe nanosheets were synthesised by Bhattacharyya *et* al., 2009 via reaction under autogenic pressure at elevated temperature (RAPET) for ferromagnetism and magneto-electronics applications. The manganese here acted as the catalyst for the formation of nanorods and nanosheet structures. The development of new photocatalytic materials for energy applications is a pressing example of such an application for these hybrid nanostructures (Plante *et al.,* 2009).

1.3 PHOTOCATALYSIS

Semiconductor photocatalysis involves the conversion of solar energy into environmentally friendly fuels, most notably, the production of hydrogen from water (Dukovic *et al.,* 2008). Due to their ability to greatly increase the charge separation and enhance the overall efficiency, semiconductor-metal nanocomposites have been widely employed in photocatalysis (Chen *et al.,* 2009). Semiconductors act as sensitizers for light-induced redox processes due to their electronic structure, which is characterized by a filled valence band and an empty conduction band. "The photocatalytic detoxification of wastewater is a process that combines heterogeneous catalysis with solar technologies" (Beydoun *et al*., 1999). According to Beydoun *et al*., 1999, the illumination of a semiconductor photocatalyst with an ultraviolet (UV) radiation activates the catalyst, establishing a redox environment in the aqueous solution (Beydoun *et al.,* 1999). For metal-semiconductor hybrid materials, depending on the electronic

alignment of the materials, interactions at the metal-semiconductor interface can facilitate charge separation in the semiconductor or energy transfer between the two materials. The combination of catalytically active metals with semiconductor nanowires that absorb strongly in the visible region of the solar spectrum are very promising for renewable energy conversion; especially for photoelectrochemical based cells (Mokari *et al.,* 2004). For photocatalysis with semiconductors, it is necessary to suppress the recombination of the electron-hole pair formed following light absorption (Costi *et al.,* 2008). In the case of a one-dimensional system, the greater surface area along the length creates a larger number of sites for metal nucleation and growth leading to the formation of high-surface-area materials with multiple reactive sites for photocatalysis. In order for photocatalytic applications to be occurring, the one-dimensional morphologies are to render themselves as charge transporters (Plante *et al.,* 2009).

Nanometer-scale materials in particular have attracted considerable attention as the building blocks for light-harvesting applications. Their desirable attributes include tunability of the optical properties with size, amenability to relatively inexpensive low-temperature processing, and a high degree of synthetic sophistication leading to increasingly complex and multi-functional architectures. For photocatalysis in particular, the high surface-to-volume ratios in nanoscale materials should lead to an increased availability of carriers for redox reactions on the nanoparticle surface. Recombination of photoexcited carriers directly competes with photocatalytic activity. Charge separation is often achieved with multi-component heterostructures (Dukovic *et al.,* 2008).

Semiconductor photocatalysis has been applied in solving a variety of problems which are of environmental interest this includes, air and water purification, increase in the efficiency of photocatalytic redox processes and photocatalytic water-splitting reactions. The application of illuminated semiconductors for degradation of undesirable organics dissolved in air or water is well documented and has been successful for a wide variety of compounds (Subramanian *et al.,* 2004).

1.4 SYNTHESIS OF HETEROSTRUCTURED MATERIALS

Hybrid structures can be in the form of alloys or core/shell. Core/shell structure of metal/oxide/silica on metal particles of Ag and Au has been widely reported (Soundeyra and Zhang 2008). Extensive work on the growth of gold tips on anisotropic CdSe particles was done by Mokari *et al*., 2004. In their study, they observed a transition from two sided gold growth to multiple gold growths along the rods or tetrapods when they varied the concentration of gold. The synthesis of these hybrid structures involves two steps. The first step is to synthesize the semiconductor particles followed by growing the metal particles prepared using a separate procedure onto the semiconductor. In 2005, Mokari *et al*., extended this gold deposition method to other CdSe structures. This enables the deposition of single gold tips on quantum dots which manifest a unique semiconductor-metal junction allowing for benchmark studies on the properties of nanoscale interfaces within a single nanoparticle. Wang *et al.*, in 2005 used iron oxide as a seed layer to reduce gold precursor for the assembly of iron oxide and Au core-shell nanostructures. The core shell was produced by coating the pre-

synthesized iron oxide nanoparticles with gold shells. Bao *et al.*, in 2008 reported the deposition of Pt on CdS nanowire using conventional photocatalytic method under visible light. This is an aqueous solution route for larger scale preparation of nanoporous CdS nanostructures at room temperature using air-insensitive inorganic reactants such as $CdCl_2.2.5H_2O$ and $Na_2S.9H_2O$. The photodeposition of Pt on CdSe/CdS semiconductor by Ar-ion laser was reported by Dukovic *et al.,* 2008. The Pt precursor led to the deposition of Pt nanoparticles on the semiconductor surface and stark differences are observed in the Pt nanoparticles located on the colloidal CdS and CdSe/CdS core/shell nanocrystals. Costi *et al.,* (2008) reported on the visible light-induced charge retention and photocatalysis with hybrid CdSe-Au nanodumbbells. The CdSe nanorods were grown by high-temperature pyrolysis of suitable precursors in a coordinating solvent containing a mixture of trioctylphosphineoxide (TOPO) and phosphonic acids. The surface exchange was carried out before the metal can be incorporated in order not to compromise the Au tip quality. Gold growth was performed by dissolving the gold (III) chloride in 4 ml of triple-distilled water and was then added at once to the aqueous nanorods solution under vigorous stirring and ambient light. The result was a black precipitate which shows the formation of Au-CdSe. Plante *et al.*, 2009 synthesized metal-semiconductor hybrid nanowires via metal overgrowth onto solution-liquid-solid grown nanowires. This process involves the use of metals such as Au, Pt, PtNi & PtCo hybrids with CdSe nanowires. Here, the metal salts were reduced using different methods. The Au was reduced by using the Mokari method discussed above

and the Pt was reduced using 1.2-dichlorobenzene at 65 ^{o}C for 10 min to promote the dissolution of the Pt precursor. The fabrication of Pt-CdSe hybrid nanocomposites by using the chemical redox reaction with ethylene glycol as the reducing agent was also reported by Chen *et al.,* (2009). CdSe quantum rods (QRs) were prepared using organometallic reagents via a one-pot approach followed by ligand exchange using 2-mercaptopropanoic acid (MPA). Pt was then prepared by dissolving hexachloroplatinic acid in ethylene glycol. Finally Pt particles were successfully deposited on the CdSe QRs aqueous solution. In 2011 Panda *et al.,* reported high quality ternary CdZnSe quantum dots. These were prepared by alloying CdSe/ZnSe core/shell quantum dots at high temperatures under Argon. The anisotropic selective growth of gold nanoparticles on Fe-Pt to form heterodimers, tad-pole like and necklace like hybrid structures via simple nucleation was reported by Mao *et al.,* 2011. The gold, hexane and oleylamine mixture were prepared and injected into oleylamine solution at room temperature under vigorous stirring. The temperature of the reaction was raised to 80 °C to remove hexane. The mixture became colourless in 5 minutes to form the gold precursor which was then added to Fe-Pt nanoparticle solution under vigorous stirring for 30 minutes to form a heterodimer which consists of one Fe-Pt nanoparticle and one Au nanoparticle. Quantum dot sensitized solar cells were developed from $CdSe_xS_{(s-x)}$ quantum dots via successive ionic layer adsorption and reaction (SILAR) technique (Shu *et al* 2012). The TiO_2 film was dipped in a $Cd(NO_3)_2$ methanol solution for 30 seconds and rinsed with methanol. The $Cd(NO_3)_2$ coated electrodes were then dipped in $Na_2Se_xS_{(x-1)}$ methanol

solution for 30 seconds and rinsed with methanol. This is the SILAR cycle which is repeated *n* times (where n is the number of cycles) and then again at 70 °C for *m* times (where m is the number of times a cycle finishes). The quantum dot sensitized solar cells were sandwiched with the quantum dot sensitized electrode and the Pt-counter electrode by a 25 μm sealing film. Shingchung *et al.*, 2013 reported the hybrid solar cells based on poly (3-hexylthiophene, P3HT) and electrospun TiO_2 nanofibers modified with CdS nanoparticles. The polymer anchors easy fabrication, flexibility, large area production and power conversion efficiencies (PCE). The TiO_2 nanofibres were prepared by electrospinning process to fabricate fibers with high aspect ratio and nanoscale diameter. The size and alignment were controlled by choosing suitable solvents and suitable processing conditions. The CdS layer was then deposited on TiO_2 nanofibres by facile solution process. Liu et al., 2013 reported the fabrication of three-dimensional CdSe films merged with plasmonic Au fabricated by alternating layer-by-layer assembly of Au nanoparticles and CdSe films in a simple electrodeposition process. The gold nanostructures electrodeposited on the conductive ITO-coated glass surfaces were used as conducting scaffolds to anchor CdSe semiconductor for light harvesting. The plasmonic gold nanostructures can be expected as the scattering elements to (i) couple and trap the sunlight into the CdSe absorber film and locally amplify the electromagnetic field when placed on the surface or inside the CdSe (ii) increase the effective absorption cross-section and optical path length inside the absorber. Furthermore, the concentrated resonance energy contained in localized plasmonic

oscillations can be transferred to the semiconductor to induce charge separation in the semiconductor. In a recent development CdS/TiO_2 heterostructures photocatalyst was reported by Wei *et al.,* 2014. The heterostructures were synthesized via a simple and practical electrospinning-assisted technique which gave efficient electron-hole separation ability. The formation of CdS nanoparticles on one dimension TiO_2 nanofibres was carried out by a SILAR method.

1.5 SYNTHESIS OF Au-CdSe NANOSTRUCTURES

Gold (Au) nanoparticles (NPs) have been shown to possess peculiar properties and wider applications. Thus, they are one of the most extensively studied nanostructured materials and are very promising for applications in electronics, catalysis and nanomedicine. This is due to their intriguing high stability, plasmon resonance effect, catalytic activity and biological compatibility (Wang *et al,* 2012). Despite the fact that the bulk metal is inactive in catalysis, Au-nanoparticles have turned out to be highly active in the catalysis reactions (Kaiser *et al,* 2012). Early studies of metal semiconductors dwelled on the core/shell structure of the metal/oxide by depositing oxide shells such as TiO_2, SnO_2 and SiO_2 on metal nanoparticles of Au and Ag (Pullabhotla and Revaprasadu, 2009). Extensive work on the growth of gold on the tips of anisotropic CdSe particles has been reported by Salant *et al*, 2006. The same procedure was used by Mokari group and by varying the concentration of gold they observed a transition from two sided growth to one sided gold growth (Mokari *et al*, 2004; Costi *et al*, 2008). Bulk metallic gold typically exhibits a low chemical and catalytic

activity. Gold is often referred to as the "coinage metal" since it is by far the least reactive in the transition metals, however, due to its unusual catalytic properties when dispersed on some oxide supports, it has become subject of attention (Rodriguez *et al,* 2007).

Water soluble Au-CdSe nanostructures have been synthesized via direct and indirect method. The direct method is when the synthesis is carried out in an aqueous medium while the indirect method is when the synthesis is carried out in an organic medium followed by ligand exchange to produce water soluble material. Mokari *et* al in 2004 reported on the selective growth of Au tips onto CdSe rods and tetrapods. Rods and tetrapods of different dimensions were prepared separately by high-temperature pyrolysis of suitable precursors in a co-ordinating solvent containing a mixture of TOPO and phosphonic acids. In another separate reaction Au solution was prepared by adding $AuCl_3$ in toluene followed by the addition of dodecyldimethylammonium bromide (DDAB) and dodecylamine (DDA). For the growth of the Au tips these two solutions were mixed at room temperature. In this study, the Au tips are natural elements for applications such as scanning tunnelling microscopy studies, transport measurements and the use of DNA-based assembly.

In 2005, Mokari *et al*., further studied the growth process of Au nanoparticles on CdSe nanorods. They observed that at longer reaction times the concentration of $AuCl_3$ in solution dropped to a critical value and the reaction transitioned from a growth state to

a ripening state. This resulted in the disappearance of small Au nanoparticles along the surface of the nanorods and the emergence of large Au nanoparticles on the tips of the nanorods. In 2008, Costi *et al.,* reported the synthesis of Au tips on CdSe rods in an organic medium which later were converted to water soluble using mercaptoundecanoic acid. Pullabotla and Revaprasadu in 2009 reported the direct synthesis of cysteine capped Au-CdSe hybrid nanoparticles. In this method, Au-CdSe was synthesized via a one pot synthetic route by reducing $HAuCl_4$ and Se powder in solution using $NaBH_4$ as the reducing agent, $CdCl_2$ as the cadmium precursor and L-cysteine as the capping agent in an inert atmosphere. In 2010, Shaviv and Banin reported the synergistic effects on second harmonic generation of hybrid CdSe-Au nanoparticles. CdSe quantum dots and nanorods capped with tetradecyphosphonic acid (TDPA), TOPO and HDA were synthesized in co-ordinating solvents using high temperature injection method. $AuCl_3$ was dissolved in toluene, together with DDA and DDAB to produce the Au precursor solution. Au metal tips were deposited onto the CdSe quantum dots and nanorods by adding the Au precursor solution. In 2011, Liu *et al* reported that Au nanoparticles enhanced light emission from CdSe quantum dots. In this work the Au colloids were synthesized by a citrate-seeded method, where a solution of small Au seed colloids was synthesized first followed by larger Au colloids prepared by the citrate-seed method. The Au nanoparticles were then self-assembled on 3-aminopropyltriethoxysilane (APS) modified glass by perpendicularly immersing the slides into the as-prepared Au colloids solution for 12 hours. After drying, the Au colloid films were annealed in oven at

different temperatures for 10 min in N_2 atmosphere and were then coupled with CdSe/PMMA solution. The CdSe\PMMA solution was prepared by dispersing the CdSe in chloroform solution of poly methyl methacrylate, (PMMA). The prepared CdSe/PMMA was subsequently coated on the surface of glass substrates with Au colloid films by dipping the glass substrates into CdSe/PMMA solution.

In 2012, Gao *et al* reported on the charge transfer and retention in directly coupled Au-CdSe nanohybrids. In this work, the Au-CdSe hybrids were synthesized using seeded growth via the heterogeneous nucleation and growth of Au on a CdSe NPs seed. The CdSe NPs were prepared by mixing the cadmium source with hexadecylamine (HDA) and trioctylphosphine oxide (TOPO) and heating to a temperature of 310 ^{o}C in an inert atmosphere. A solution of selenium dissolved in trioctylphosphine (TOP) was injected into the Cd/HDA/TOPO solution to form HDA-capped CdSe QDs. The Au solution was prepared by mixing the Au precursor with water followed by mixing with toluene containing tetra-*n*-octyl ammonium bromide (TOAB) for delamination. Au was extracted to the toluene phase by tetra-*n*-octyl ammonium ions then the Au-toluene solution is decanted and washed with water. Dodecylamine (DDA) was then added to this toluene solution and ultrasonically agitated for 15 min, and kept at room temperature for 3 days to produce the Au precursor capped with DDA. The Au-CdSe hybrids were formed by adding the Au precursor solution drop wise to the CdSe seed solution under vigorous stirring for 20 min. Joo *et al* 2012, reported on the viral-assisted assembly and photoelectric response of individual Au/CdSe core-shell nanowires using M13

bacteriophage as the template for Au nanowire synthesis. The Au nanoparticles which selectively bind to the bacteriophage were used as seed crystals for the deposition. Kawai and Yamamoto 2012 reported the spacer thickness dependence in Au/spacer/CdSe nanoparticle multilayers. In this work, the Au film was fabricated on a glass substrate using the Argon-ion sputtering method. A poly methyl methacrylate (PMMA) film was then spin coated on the Au film as a spacer layer. The distance between the Au film and the CdSe nanoparticles is determined by the thickness of the PMMA films.

Teng and Jia 2012 reported on the synthesis and charge transfer of CdSe-Au hybrid nanowires. In this work, CdSe NPs were synthesized by heating the mixture of cadmium acetate, stearic acid, TOPO and octadecylamine (ODA) in a 3-necked flask at vigorous stirring under argon flow. The results showed that Au^{3+} was reduced to Au atoms while Se^{2-} was oxidized to Se^{4+}. Chili *et al* 2012 reported the synthesis of PVP-capped Au-CdSe hybrids. Au NPs were prepared by reacting chloroauric acid ($HAuCl_4$) with PVP in distilled water. The reaction was carried out under UV irradiation in order to reduce the gold to form gold NPs. The CdSe NPs were prepared by dissolving selenium powder in distilled water in a 3-necked flask in an inert atmosphere under continuous stirring. Aqueous solution of sodium borohydride ($NaBH_4$) was then added to the selenium solution. Cadmium chloride dissolved in water was also added to this solution to produce CdSe NPs. The CdSe solution was then added to the Au metal nanoparticle solution and allowed to completely react for an hour in an inert atmosphere under

continuous stirring. The colour change to a purple-wine-red confirming the formation of Au-CdSe capped with PVP. In 2013, Li and Lappas reported the formation of CdSe-Au nanorods networks welded by gold domains. The synthesis of CdSe nanorods were prepared by colloidal chemistry via a seeded growth approach. Following the Mokari procedure, the gold domains were then selectively grown on to the tips of the CdSe nanorods to form dumbbell structures.

Gadalla *et al.,* 2013 synthesized and characterized Au/CdSe core-shells. In this reaction, a mixture of oleylamine and Au source was heated until the colour changed to red, confirming the formation of the Au nanoparticles. TOPO was then slowly added to this mixture and the temperature was gradually increased from 100 to 150 ^{o}C. To form the shell of CdSe around the Au core the CdSe precursor was added drop wise into the reaction mixture.

1.6 APPLICATIONS OF HETEROSTRUCTURED MATERIALS

The ability to tune the physical properties of semiconductor nanocrystals makes them an important category of materials that have attracted much interest from academia and industry. Since 1998 luminescent semiconductor nanocrystals or QDs have been widely explored as biomedical labeling reagents (Pradhan *et al.,* 2007). Therefore, semiconductor nanocrystals have multiple potential applications such as biosensors, photovoltaic devices, light-emitting devices, memory devices and so on (Schüler *et al.,* 2007). Preparation of non-radioactive biological labels and chemical opto-sensors are

the applications that have risen from the conjugation of semiconductor nanoparticles with biomolecules like starch, nucleic acids and proteins enabling the selective interaction with biochemical species (Oluwafemi and Revaprasadu 2007). Due to quantum confinement of the electronic states and their molecular conjugates, QDs have become increasingly important in biotechnology and medicine. Previously, silica and metal nanoparticles have been used for the detection of proteins and clinical diagnosis but nowadays the use of QDs in imaging and phototherapeutic agents is becoming common (Idowu *et al.,* 2008). Metal-semiconductor hybrid materials have been studied as photocatalysts in photochemical water splitting to produce hydrogen, in photoelectrochemical cells, in photochemical purification of organic contaminants and in bacterial detoxification (Costi *et al.,* 2008). When semiconductor nanorods are close-packed and aligned with their long axes perpendicular to the substrate they can be used for potential applications in field emission, photovoltaic and data storage devices (Zhao *et al.,* 2009).

Application in light-emitting diodes and quantum dot lasers devices make the quantum dots to be promising candidates for many optoelectronic applications (Viswanatha *et al.,* 2008; Oluwafemi *et al.,* 2010; Xei *et al.,* 2011). Ultrafine iron-platinum nanoparticles were prepared using laser solution photolysis (Nkosi *et al.,* 2012). Such materials can be used in a range of applications including ultrahigh density recording media and a number of biological applications. CdSe films emerged with plasmonic gold via layer-to-layer process make novel multilayered photovoltaic material for photovoltaic

applications (Liu *et al.,* 2013). The alternating assembly of the CdS/TiO_2 heterostructures reported by Wei *et al*., 2014 were used for photocatalytic applications. The TiO_2 enhances the surface-to-volume ratio and the composited nanofibers improved the light absorption range and charge separation.

1.7 SYNTHETIC ROUTE PROBLEMS

As a result of the tremendous progress made in nanomaterial synthesis, different methods have been reported to fabricate the semiconductor-metal HNS. This includes substrate assisted metal growth method (Wang *et al.,* 2005), conventional photocatalytic method under visible light (Bao *et al.,* 2008), Ar-ion laser deposition (Dukovic *et al*., 2008), metal overgrowth solution-liquid-solid method (Plante *et al.,* 2009) and chemical redox reaction method (Chen *et al.,* 2009). The preparation of HNS in most of these synthetic approaches involves three stages, (i) preparation of the metal and nanostructures separately in organic solvent (ii) dispersion of these materials in organic solvent to produce HNS (iii) ligand exchange in order to make the as-synthesized HNS water soluble. This is necessary as photocatalysis is most relevant in aqueous solution (Costi *et al.,* 2008 and Chen *et al*., 2009). Though this method is effective, however, rigorous condition, elevated temperature and the use of standard airless techniques are usually involved in the synthesis of the nanostructure materials. This is in addition to the ligand exchange procedure required to make the HNS water soluble, which is time consuming with low-transfer efficiencies, thus, compromising the metal tip quality. The overall process is therefore difficult to realize for large scale

synthesis. In another development, Costi *et al.,* 2008 and Chen *et al.,* 2009 have reported an alternative method for the synthesis of HNS by carrying out ligand exchange on the nanostructure before the addition of the metal precursor in the aqueous medium. In this technique, the ligand exchange procedure is very fast and with high efficiencies, unlike the ligand exchange procedure for the whole HNS. However, the synthesis of the nanostructured material still involves rigorous condition, elevated temperature and the use of standard airless techniques. Therefore, there is need to produce metal-semiconductor HNS via a 'greener' and economical method. In searching for greener method for the synthesis of II-VI semiconductor nanostructures, a facile, economical, bench top and environmentally benign method under a short reaction time was reported for the synthesis of both organically and aqueous soluble selenide nanoparticles by Oluwafemi *et al*. The synthesis involves the use of a selenide source that is stable at room temperature, thus circumventing the major problem associated with the selenide nanostructure synthesis (Oluwafemi and Revaprasadu 2007; Oluwafemi *et al.* 2008; Oluwafemi *et al.* 2008; Oluwafemi and Revaprasadu 2009; Oluwafemi 2009; Oluwafemi *et al.* 64 (2010) 1513; Oluwafemi et al. 79 (2010) 126; Oluwafemi and Songca 2012). This method is 'green' in many aspects, however the selenide source is not stable at room temperature hence there is need for further modification/improvement. In 2010 Shaviv and Banin followed the high-temperature injection method to synthesize the Au-CdSe hybrids but ligand exchange was performed after the metal was incorporated. This ligand exchange technique was highly efficient;

however the synthesis of the nanostructured material still involves high temperature and rigorous conditions. Mokari *et al*., (2011) further modified this procedure to further decorate the CdSe with Pt, PtNi and PtCo but there was still use of elevated temperature and rigorous conditions. Teng and Jia (2012) modified the Mokari *et al*., 2004 procedure to synthesize the Au-CdSe nanoparticles. The new method they implemented was easy to conduct, using moderate reaction temperatures and a more favorable cadmium source. Even though amendments were done to this procedure but other starting materials are still rigorous and not environmentally benign. Reported by Chilli *et al*., (2012) was the UV-irradiation method for the synthesis of hybrid nanoparticles. This method is 'green' in some aspects but the selenide source is not stable at room temperature and therefore cannot be stored for later use. After the needed amount is taken from this source the rest must be discarded, rendering a loss. The organometallic pyrolysis was reported for the synthesis of Ag/CdSe and Au/CdSe (Gadalla *et al.,* 2013). The use of high temperature and rigorous starting materials render this method as not environmentally friendly.

1.8 AIM

The aim of this project is to synthesize Au-CdSe nanostructures via a facile environmentally benign method.

1.9 OBJECTIVES

- To synthesize water soluble and organically soluble CdSe and Au-doped CdSe hybrid nanostructures via a facile environmentally friendly method.
- To investigate the effect of direct aqueous synthesis of the nanostructures as well as the synthesis via ligand exchange on the luminescent properties of the hybrid nanostructures.
- To tune the absorption properties of metal-semiconductor hybrid nanostructures for optimal performance.
- To characterize and study the optical and morphological properties of the hybrid nanostructures.

CHAPTER 2

2. EXPERIMENTAL

2.1 Chemicals

Selenium powder (Se; Aldrich), sodium sulfite (Na_2SO_4), deionized water (HPLC grade), cadmium chloride ($CdCl_2$; Aldrich), cadmium acetate ($Cd(CH_3COO)_2$; ACE), cadmium nitrate ($Cd(NO_3)_2$; ACE), tri-sodium citrate (Unilavar), mercaptopropanoic acid (MPA), potassium sodium tartarate (PST), L-cysteine (Aldrich), propan-2-ol (ACE) hexadecylamine (HDA; Aldrich), trioctylphosphine (TOP; Aldrich) gold (III) chloride ($AuCl_3$; Aldrich), toluene (Aldrich), methanol (Aldrich), ethanol (Aldrich), rhodamine 6G (Aldrich), chloroform (Aldrich), mercaptoundecanoic acid (MUA; Aldrich) and potassium hydroxide (KOH).

2.2 Apparatus

Condenser, heating mantle, stirrer bar, 3-necked flask, beakers, measuring cylinders, 1-necked flasks, syringe with needle, pipette, pipette filler, micropipette, pipette tips, centrifuge tubes.

2.3 Synthesis

2.3.1 Synthesis of water soluble CdSe nanoparticles

The procedure used for the synthesis is a modification of Oluwafemi *et al.*, (2008 a and b) and Ghaedi *et al.*, 2011 for the synthesis of CdSe nanoparticles. In a typical synthesis, a selenium precursor solution was prepared by mixing 2.0 mmol (0.157g) of selenium powder with 50 mL of demonized water followed by the addition of 0.8 g of sodium sulfite. The temperature of the reaction was raised to 70 °C to completely dissolve the selenium. The reaction was allowed to continue for 6 h until the solution become colourless to produce sodium selenosulphate solution as shown in equation (1). In another reaction flask, 3 mL of 0.04 M cadmium chloride solution was added to 20 mL of 0.0034 M sodium citrate solution, followed by the addition of 3 mL 0.04 M selenium precursor prepared above. All the reactions took place at room temperature. The reaction was monitored from 1 hour to 30 days. Aliquots were taken at different time intervals and were dispersed in propanol followed by centrifugation. The precipitate was then redispersed in water for characterization.

$$Na_2SO_3 + Se + H_2O \xrightarrow{\text{Reflux at 70 ° C}} Na_2SeSO_3 + H_2O \quad \ldots\ldots\ldots\ldots\ldots (1)$$

$$CdCl_2 + \text{citrate} \xrightarrow{\text{Room temp}} \text{citrate-Cd complex} \quad \ldots\ldots\ldots\ldots\ldots (2)$$

$$Na_2SeSO_3 + \text{citrate-Cd} \xrightarrow{\text{Room temp}} \text{citrate–CdSe} + Na_2SO_3 \quad \ldots\ldots\ldots\ldots\ldots (3)$$

2.3.1.1 Effect of Cd:Se mole ratio

The reactions were carried out according to the procedure described in section 2.3.1 by varying the Cd:Se ratio from 1:1 to 4:1 while other parameters remain constant. The concentrations of $CdCl_2$ used are 0.04, 0.08, 0.12 and 0.16 M solution.

2.3.1.2 Effect of temperature

The reactions were carried out at room temperature and reflux at 90 ^{o}C in accordance with the procedure described in section 2.3.1 using Cd:Se ratio of 2:1 while other parameters remain constant.

2.3.1.3 Effect of capping agent

The reactions were carried out using Cd:Se ratio (4:1) and different capping agents (citrate, MPS, PST and L-cysteine) following the procedure described in section 2.3.1 while other parameters remain constant. The Cd:Se ratio of 4: 1 was used because it gave the highest luminescence when compared to other Cd:Se ratios. The concentrations of the capping agents used were 0.0034 M citrate, 0.0034 M MPA, 0.0034 M PST and 0.0034 M L-cysteine.

2.3.1.4 Effect of cadmium precursor

The reactions were carried out using Cd:Se ratio of 4:1 and different cadmium precursors (cadmium chloride, cadmium acetate and cadmium nitrate) and according to the procedure described in section 2.3.1 while other parameters remain constant.

2.3.2 Synthesis of water soluble Au-doped CdSe

In a typical synthesis, 3 mL of 1.6 mmol cadmium chloride solution was added to 20 mL of 0.21 mmol L-cysteine solution. This was followed by the addition of 0.024 mmol $AuCl_3$ under continuous stirring. After 15 min, 3 mL of the 0.04 M sodium selenosulphate (Na_2SeSO_3) solution prepared as described in section 2:3:1, was added. The reaction was monitored from 15 minutes to 30 days. Aliquots were taken at different time intervals and were dispersed in propanol followed by centrifugation. The precipitate was then redispersed in water for characterization.

2.3.2.1 Effect of gold ratio

The reactions were carried out in accordance with the procedure described in section 2.3.2 using 2.0 mmol of selenium, 1.6 mmol of $CdCl_2$, and varying $AuCl_3$ between 0.024 mmol, 0.012 mmol and 0.006 mmol at room temperature to give Cd:Au of 1:20, 1:40 and 1:60, respectively.

2.3.3 Synthesis of organic soluble CdSe nanostructures

The synthesis was carried out following Oluwafemi *et al.*, (2008 a and b) method for the synthesis of Mn-doped CdSe NPs with slight modification. In a typical synthesis, 20 mL of 0.04 M selenosulphate solution was prepared according to the procedure in section 2.3.1 and reacted with 20 mL of 0.08 M $CdCl_2$ solution under continuous stirring. After 30 mins excess methanol was added to the reaction mixture followed by centrifugation. The resultant CdSe nanoparticulate was dispersed in 6 mL of

trioctylphosphine (TOP). The CdSe-TOP solution was then injected into hot hexadecylamine (HDA, 6 g) in an inert atmosphere at 160 °C. Aliquots were taken at different reaction times of 0, 5, 10, 20 and 30 minutes to monitor the growth of the nanoparticles and diluted with toluene. Sufficient amount of anhydrous methanol was added to produce flocculate consisting of nanocrystals and to make the supernatant colourless by centrifugation. The flocculate was redispersed in toluene for characterisation

2.3.4 Synthesis of organic soluble Au-doped CdSe nanostructures

In a typical synthesis, the Au-Cd complex solution was prepared by adding (0.0485g) of $AuCl_3$ in 20 mL of 0.4 M $CdCl_2$ solution. 20 mL of 0.04 M selenosulphate solution was added to the complex under continuous stirring. After 30 mins excess methanol was added to the reaction mixture followed by centrifugation. The resultant Au-CdSe nanoparticulate was dispersed in 6 mL of trioctylphosphine (TOP). The Au-CdSe-TOP solution was then injected into hot hexadecylamine (HDA, 6 g) in an inert atmosphere at 160 °C. Aliquots were taken at different reaction times of 0, 5, 10, 20 and 30 minutes to monitor the growth of the nanoparticles and diluted with toluene. Sufficient amount of anhydrous methanol was added to produce flocculate consisting of nanocrystals and to make the supernatant colourless by centrifugation. The flocculate was redispersed in toluene for characterisation

2.3.4.1 Effect of temperature

The reactions were carried out following the procedure described in section 2.3.3 and 2.3.4 for CdSe and doped-CdSe NPs respectively at different growth temperatures of 200 and 240 °C.

2.4 Quantum yield determination

The quantum yield was determined by following the procedure described by Fery-Forgues and Lavabre 1999. Rhodamine 6G was used as the standard. 0.024 g of rhodamine was dissolved in 10 ml ethanol and diluted to give an absorbance of 0.5 at the excitation wavelength of 400 nm. The aliquots of the nanostructures were also diluted until their absorbance reached 0.5 at 400 nm. The photoluminescence measurements were carried out for both the standard and the nanostructures. The data obtained was used in equation 4 to determine the quantum yield of the synthesised NPs.

$$\Phi_x = (A_s / A_x) (F_x / F_s) (n_x / n_s)^2 \Phi_s \quad \text{..... (4)}$$

Φ_x (sample) and Φ_s (standard) are the quantum yields, A_s (standard) and A_x (sample) are the absorbencies at the specific excitation wavelength, F_x (sample) and F_s (standard) are the area under the curve and lastly n_x (sample) and n_s (standard) are the refractive indexes of the solvents.

2.5 Ligand exchange

1 mL of HDA-capped CdSe was dispersed in 10 mL chloroform. 0.02 g of MUA was then added under vigorous shaking to dissolve the nanoparticulate. Then 5 mL of KOH solution prepared by dissolving 0.1 g in 20 mL of H_2O, was added to the mixture and shaken vigorously. The mixture was then centrifuged at 2.05 r.c.f. (relative centrifugal force) for 20 minutes. The aqueous solution was then collected and characterized.

The same procedure was repeated for HDA-capped Au-CdSe NPs.

2.6 Characterization

2.6.1 Ultraviolet/visible (UV/vis) Spectroscopy

The UV/vis spectroscopy uses electromagnetic radiation between 190 nm and 800 nm and is divided into the ultraviolet (190-400 nm) and visible (400-800 nm) regions. This technique is aimed at studying the changes in the energy levels within a molecule during the promotion of electrons from occupied lower energy levels to unoccupied high energy levels. The Perkin Elmer Lambda 20 UV-vis spectrophotometer was used to carry out absorption spectra in the 200-1100 nm wavelength at room temperature. Samples were placed in quartz cuvettes (1cm path length) and placed in a UV-vis compartment for analysis.

2.6.2 Photoluminescence (PL) Spectroscopy

A PL spectroscopy is a contactless, non-destructive method to probe the electronic structure of materials. Various excitation wavelengths can be used to allow varying levels of volume excitation. The intensity and spectral content of the emitted photoluminescence is a direct measure of various important properties. PL spectra were recorded on a Perkin Elmer LS 55 luminescence spectrometer. Samples were placed in quartz cuvettes (1 cm path length).

2.6.3 Fourier Transform Infrared Spectroscopy (FTIR)

FTIR is a technique which gives information about the vibrations and rotations of molecules known as normal modes. These vibrational transitions are a result of quantized energy levels influenced by the bonds that join the molecules (Skoog et al., 2004). The measurements were carried out using Perkin-Elmer FT-IR spectrometer which is equipped with the universal ATR sampling accessory and the measurements were done in the transmission mode within a 4000–400 cm^{-1} range and 4 cm^{-1} resolution maintaining a total of 50 scans for each sample analyzed.

2.6.4 Transmission Electron Microscopy (TEM) and High Resolution TEM (HRTEM)

This technique gives information about the morphology, size and crystallinity of the specimen under study through the use of a series of electromagnetic lenses that help them direct the electron beam produced at a high potential in an electrically heated

filament. As this electron beam penetrates the sample, the diffraction patterns show the structure of the specimen. It is a very powerful tool for the analysis of microstructures at high resolutions. A JEOL 2100 TEM operating at 200 KV was used for transmission electron microscopy (TEM), high resolution transmission electron microscopy (HRTEM) and fast Fourier transform (FFT) measurements. Each sample was prepared by adding a drop of the solution unto the carbon coated copper grid and allow it to dry under ambient condition.

CHAPTER 3

3. RESULTS AND DISCUSSIONS

3.1 Synthesis of water soluble CdSe nanoparticles

3.1.1 Citrate-capped CdSe nanoparticles

3.1.1.1 Optical properties

The addition of selenium precursor to the $CdCl_2$ solution changed the colour of the solution from colourless to a transparent orange (Figure 1) which confirms the formation of the CdSe NPs (Ghaedi *et al*., 2011). The absorption spectra of citrate-capped CdSe NPs at ratio 1:1 (Cd: Se) at different reaction time is shown in Figure 2. All the CdSe NPs are blue shifted in relation to the bulk CdSe 1.73 eV (716 nm) due to quantum confinement effect (Wang *et al*., 2011). The spectra show that as the reaction time increased, the absorption band edges are red shifted indicating increase in particle size (Ingole *et al*., 2010). The sizes of the citrate-capped CdSe particles as calculated from the band edge using effective mass approximation (EMA) method as given in equation 5 (Gupta and Ramrakhiani 2009) are 2.57 nm (1 hour), 2.58 nm (3 hours), 2.83 nm (2 days), 2.85 nm (4 days), 2.88 nm (14 days), 2.92 nm (22 days) and 2.98 nm (30 days). The photoluminescence spectra of the citrate-capped CdSe NPs at ratio 1:1 are shown in Figure 3. The emission spectra show band edge luminescence for excitation at 400 nm (Ingole *et al*., 2010). In correlation with the absorption spectra,

the emission maxima are red-shifted as the reaction time increased. The emission maxima are 536 nm (1 hour), 538 nm (3 hours), 553 nm (2 days), 554 (4 days), 559 (14 days) and 557 nm (30 days). The emission widths are very narrow and increased slightly with time as shown in Table 1. This increase in emission width is attributed to broadening of the size distribution.

$$a^2 = \frac{3.571 \times 10^{-18}}{(\Delta E)\, E_v} \qquad \ldots\ldots\ldots\ldots\ldots (5)$$

Where 'a' is the effective mass, ΔE is the band edge energy difference and E_v is the bulk energy band gap.



Figure 1: A photograph of the colour of the CdSe solution after the addition of selenium precursor.

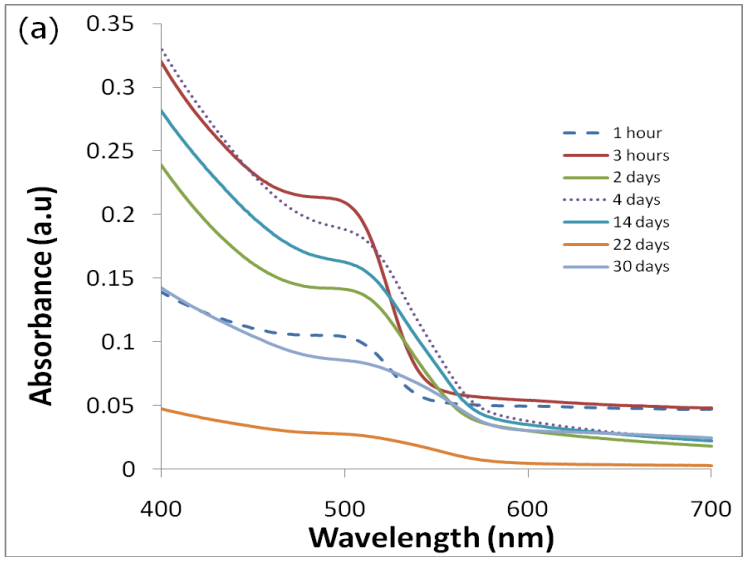


Figure 2: Absorption spectra of citrate-capped CdSe NPs at ratio 1:1 (Cd:Se) at different reaction times.

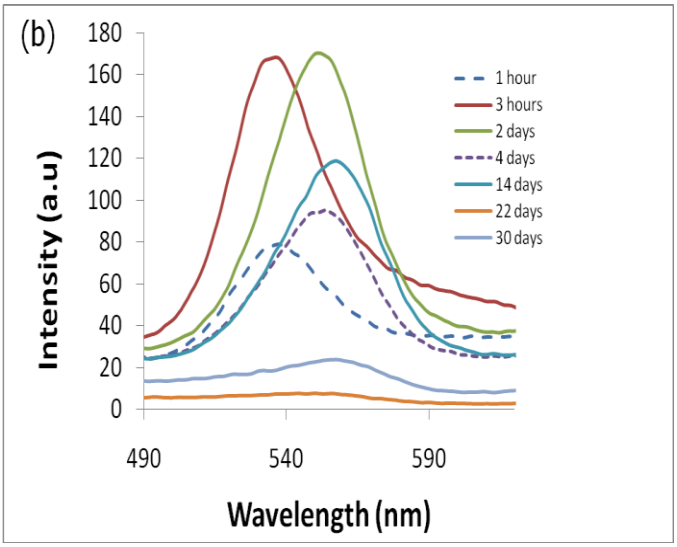


Figure 3: Photoluminescence spectra (λ_{400}) of citrate-capped CdSe NPs at ratio 1:1 (Cd:Se) at different reaction times.

Table 1: Optical properties of citrate-capped CdSe NPs at ratio 1:1 using $CdCl_2$.

Time	Excitonic peak (nm)	Band edge (nm)	PL (nm)	FWHM	Particle size (nm)
1 hour	501	541	536	39	2.57
3 hours	504	545	538	38	2.58
2 days	508	564	553	41	2.83
4 days	513	566	554	45	2.85
14 days	516	567	559	44	2.88
22 days	518	572	-------	-------	2.92
30 days	520	584	557	-------	2.98

*Note: ------- Cannot be determined from the spectrum

3.1.1.2 Structural properties

3.1.1.2.1 Fourier Transform Infrared Spectroscopy (FTIR)

The surface morphology of the as-synthesized citrate-capped CdSe NPs was investigated by IR spectroscopy. Figure 4 shows the FTIR spectra of trisodium citrate and citrate-capped CdSe NPs. The IR spectra of citrate shows characteristic bands at 1622 cm^{-1}, 1352 cm^{1} and 1129 cm^{-1} corresponding to stretching vibration of C=O, C–H and C–O respectively, while the presence of the bands at 1323 and 1542 cm^{-1}

correspond to the symmetric and asymmetric COO^- stretching respectively. The presence of the broad band at 3374 cm^{-1} corresponding to the O-H stretching in the spectrum for the citrate–capped CdSe NPs suggests the successful capping of the nanoparticles by citrate (Hu *et al.*, 2012). The bands at 1688, 1388 and 1132 cm^{-1} corresponding to C=O, C-H and C-O respectively show slight increase in the band position to higher frequency as shown in Table 2. The slight red-shifting of the band position has been attributed to the interaction between the citrate group and the CdSe NPs and thus, confirming the effective passivation of the CdSe NPs surface by the citrate through –C-O- functionalities (Ingole *et al.,* 2010 and Hu *et al.*, 2012).

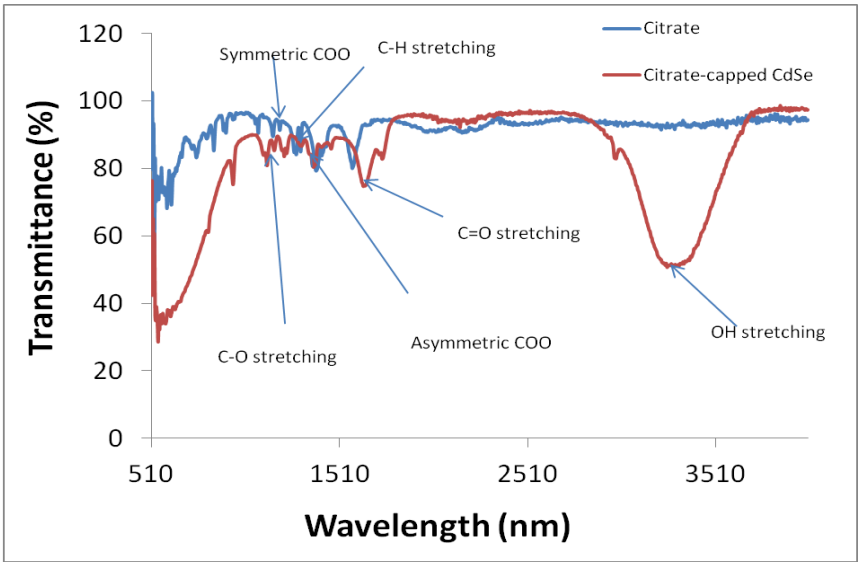


Figure 4: FTIR spectra for citrate and citrate-capped CdSe NPs.

Table 2: IR bands for the citrate and citrate-capped CdSe NPs.

Citrate (cm^{-1})	Citrate-capped CdSe NPs (cm^{-1})	Bands
-------	3374	O-H stretching
1622	1688	C=O stretching
1542	1552	Asymmetric COO
1352	1388	C-H stretching
1323	1351	Symmetric COO
1121	1132	C-O stretching

*Note: ------- Cannot be determined from the spectrum

3.1.1.2.2 TEM, HRTEM and FFT

The representative TEM micrograph of the citrate-capped CdSe NPs at ratio 1:1 is shown in figure 5. The micrograph shows that the materials are nearly spherical in shape with some aggregation due to the smaller nature of the NPs. The presence of the lattice fringes in the high resolution TEM (HRTEM), Figure 5 (c) confirms the highly crystalline nature of the material. The fast Fourier transform (FFT) pattern (Figure 5 b) shows sharp and clear singular reciprocal points supporting the conclusion that the nanoparticles are single crystals.

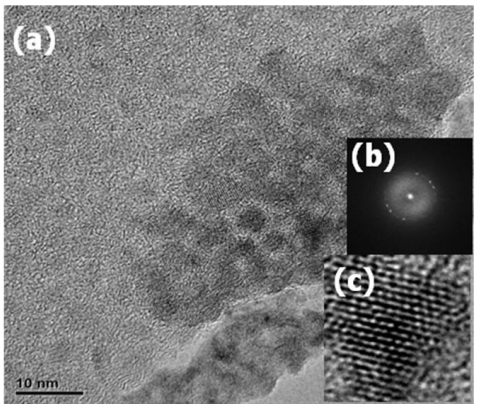


Figure 5: TEM (a) FFT (b) HRTEM (c) images of citrate-capped CdSe at ratio 1:1 at 1 hour.

3.1.2 Effect of cadmium to selenium ratio

The effect of the Cd:Se mole ratio was investigated using trisodium citrate as a capping agent and $CdCl_2$ as a cadmium precursor. The Cd:Se ratio was varied from 1:1 to 4:1 while all other parameters were kept constant.

3.1.2.1 Optical properties

The absorption spectra of citrate-capped CdSe at different mole ratios under 1 hour reaction time are shown in Figure 6 (a). The spectra show that as the mole ratio increases, the absorption band edge is blue shifted indicating decrease in particle size. The 4:1 mole ratio gives the smallest particle size as compared to the other ratios. However, there was neither defined excitonic shoulder nor sharp band edge at this ratio compared to other ratios. This might be attributed to the aggregation of these particles because of their high surface energy due to their smaller nature. The smaller the nanomaterials, the higher the surface energy and the chances of aggregation. The

positions of the excitonic shoulders are 510 nm (1:1), 461 nm (2:1), 455 nm (3:1) and 440 nm (4:1). The sizes of the citrate-capped CdSe particles as calculated according to the EMA as given in equation 5 (Gupta and Ramrakhiani 2009) were 2.57 nm, 2.26 nm, 2.17 nm and 2.08 nm for ratio 1:1, 2:1, 3:1 and 4:1, respectively. The photoluminescence spectra for the citrate-capped CdSe at ratio 1:1, 2:1, 3:1 and 4:1 is shown in figure 6 (b). The emission maximum shows band edge luminescence for excitation at 400 nm. In correlation with the absorption spectra, the emission maxima are blue-shifted as the Cd: Se ratio increases. The emission maxima are 536 nm (1:1), 543.5 nm (2:1), 536 nm (3:1) and 525.5 nm (4:1). The luminescence intensity as well as the emission width increased as the Cd:Se mole ratio increased for the first three hours. The emission widths are; 38 (1:1), 99 (2:1), 106 (3:1) and 102.5 (4:1). The sharp luminescence shows the efficiency of the capping agent in passivating the surface defects which are normally associated with semiconductor NPs.

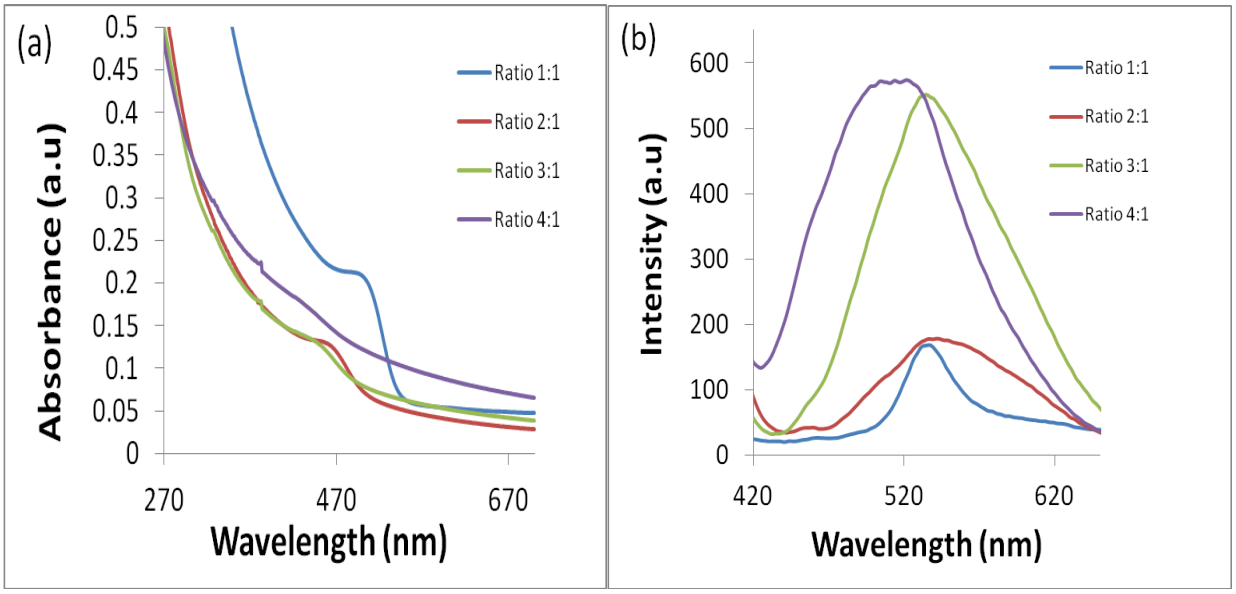


Figure 6: (a) Absorption and (b) photoluminescence ($\lambda_{400\ nm}$) spectra of citrate-capped CdSe NPs at different ratios at 3 h reaction time.

Table 3: Optical properties of citrate-capped CdSe NPs at different ratios at 1 hour reaction time.

Ratio	Excitonic peak (nm)	Band edge (nm)	PL emission (nm)	PL intensity	FWHM	Particle size (nm)
1:1	502	545	536	168	38	2.57
2:1	449	503	544	178	99	2.26
3:1	445	482	536	552	106	2.17
4:1	455	503	525	570	103.5	2.08

3.1.2.2 Structural properties

3.1.2.2.1 Fourier Transform Infrared Spectroscopy

Figure 7 shows the FTIR spectra of trisodium citrate and citrate-capped CdSe samples at different ratios. The IR spectra of citrate show characteristic bands at 1622 cm^{-1}, 1352 cm^{1} and 1129 cm^{-1} corresponding to stretching vibration of C=O, C–H and C–O respectively, while the presence of the bands at 1323 and 1542 cm^{-1} correspond to the symmetric and asymmetric COO^{-} stretching respectively. The spectra for the as-synthesized materials showed all the characteristics peaks present in the capping agent at higher frequency with an increase in the intensities as the mole ratio increases indicating successful passivation of the CdSe surface by the citrate through –C-O- functionalities (Ingole *et al.,* 2010 and Hu *et al*., 2012).

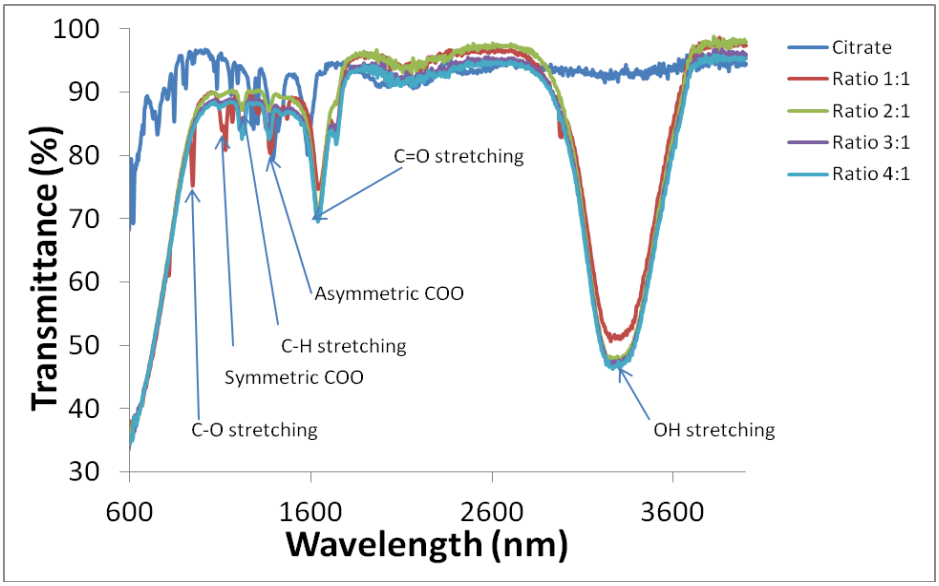
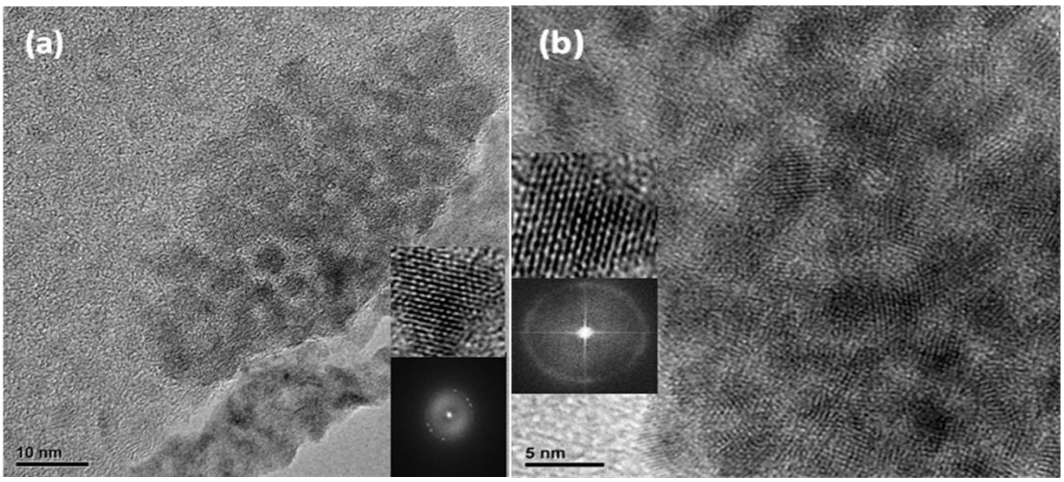


Figure 7: FTIR spectra of citrate and citrate-capped CdSe NPs at different Cd:Se mole ratio.

3.1.2.2.2 TEM, HRTEM and FFT

The representative TEM micrographs of the citrate-capped CdSe at different mole ratio are shown in Figure 8. The micrographs show that all the materials are nearly spherical in shape with some aggregation due to the smaller nature of the Nano particulate. The presence of the lattice fringe in the high resolution TEM (HRTEM) confirms that the as-prepared materials are spherical and consist of well-ordered single crystals with distinct lattice fringes. The clear and uniform lattice fringes confirmed that the spherical particles are highly crystalline (Ayele *et al.*, 2011). The clear singular reciprocal points shown by the fast Fourier transform (FFT) patterns confirmed that the obtained citrate-CdSe NPs are single crystals.



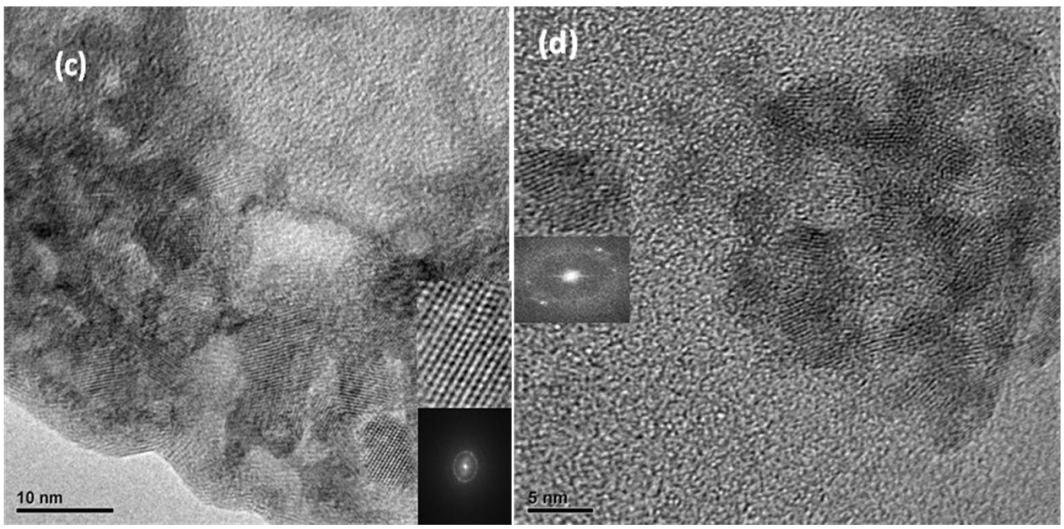


Figure 8: TEM images of citrate-capped CdSe NPs [insets: HRTEM and FFT] at Cd:Se ratio of (a) 1:1 (b) 2:1 (c) 3:1 (d) 4:1.

3.1.3 Effect of temperature

The synthesis of citrate capped CdSe at ratio 2:1 was carried out under reflux to investigate the effect of temperature on the particles size, emission width and intensity. During the reaction, the colour of the solution changed from light orange (at room temperature) to mud brown as the reaction time increased as shown in Figure 9 indicating increase in particle size.

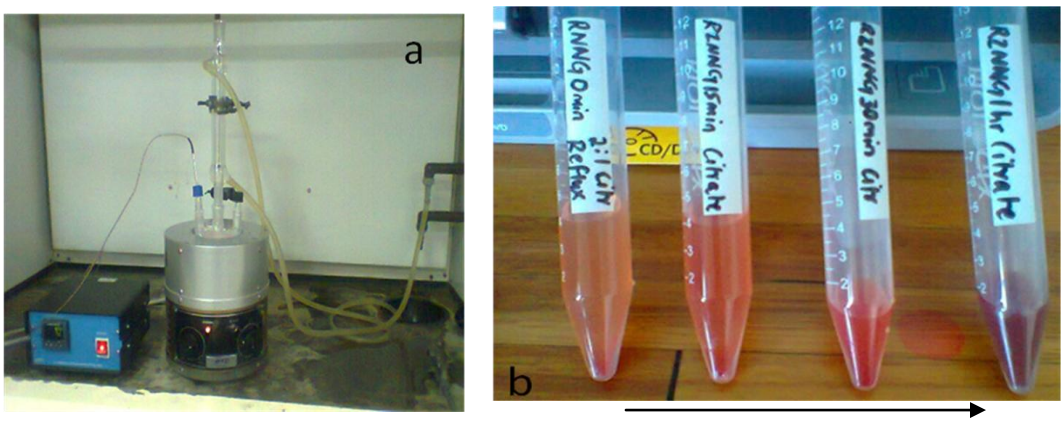


Figure 9: Photographs showing the (a) reflux setup (b) colour change during the reaction of citrate-capped CdSe at ratio 2:1 in the order 0 mins, 15 mins, 30 mins and 1h.

3.1.3.1 Optical properties

The typical absorption spectra of citrate-capped CdSe NPs synthesised at room temperature (R.T) and under reflux at 30 minutes reaction times are shown in figure 10 (a). The absorption band edges are 505 nm (RT) and 582 nm (reflux). The red-shift of the absorption band edge under the reflux indicates increase in the particle size. This shows that bigger particles are produced at higher temperatures (Deng *et al* 2005). The increase in the particle size for the material synthesized under reflux can be attributed to the association and dissociation processes at higher temperature. Under the reflux, the materials break down into smaller particles (digestive ripening) which then combined together due to their high surface energy to form larger particles. The particle sizes as calculated from the band edge using the EMA method as given in equation 5 (Gupta and Ramrakhiani 2009) are 2.27 nm (R.T) and 3.54 nm (reflux). The photoluminescence spectra of the citrate-capped CdSe NPs at room temperature and

under reflux are shown in figure 10 (b). Unlike the one synthesized at room temperature, the luminescence for the CdSe NPs synthesized under the reflux (Fig. 10 b inset) was very low, hence it appeared as if there was no luminescence at all when plotted together with the one obtained at room temperature. The lower intensity of the luminescence obtained under reflux is attributed to the presence of surface defects which serves as trap for the exciton recombination. This arose from both the smaller nature of the material and aggregation after digestive ripening, thus leading to ineffective passivation by the capping agent (Wang *et al.*, 2011).

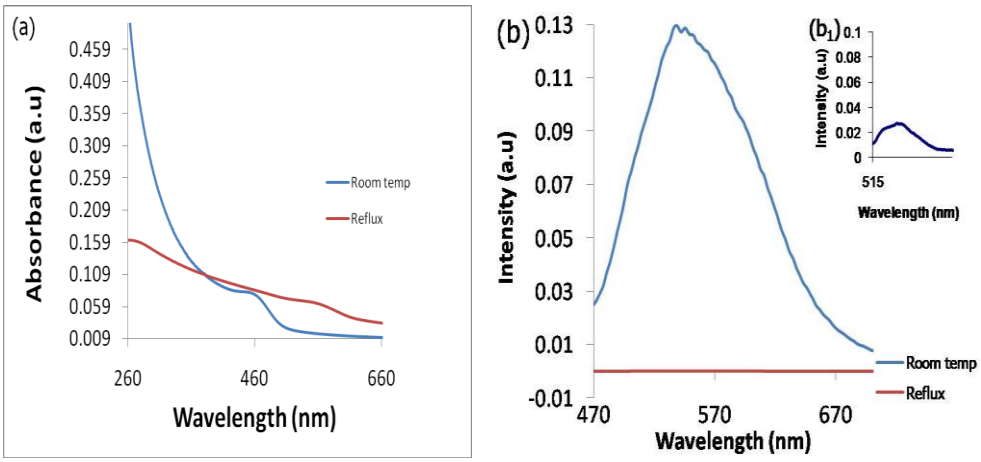


Figure 10: Typical (a) Absorption and (b) photoluminescence (PL $\lambda_{400\ nm}$) spectra of citrate-capped CdSe NPs at room temperature and under reflux [Inset: PL under reflux].

3.1.3.2 Structural properties

3.1.3.2.1 TEM, HRTEM and FFT

The representative TEM micrographs of the citrate-capped CdSe NPs at room temperature and under reflux is shown in Figure 11. The micrograph shows that at both temperatures the materials are nearly spherical in shape with some aggregation due to the smaller nature of the nanomaterial. The HRTEM confirms that the as-prepared materials are spherical and consist of well ordered single crystals with distinct lattice fringes, confirming that the particles are highly crystalline. The FFT patterns on Figure 11 show sharp and clear singular reciprocal points supporting the conclusion that the nanoparticles are single crystals.

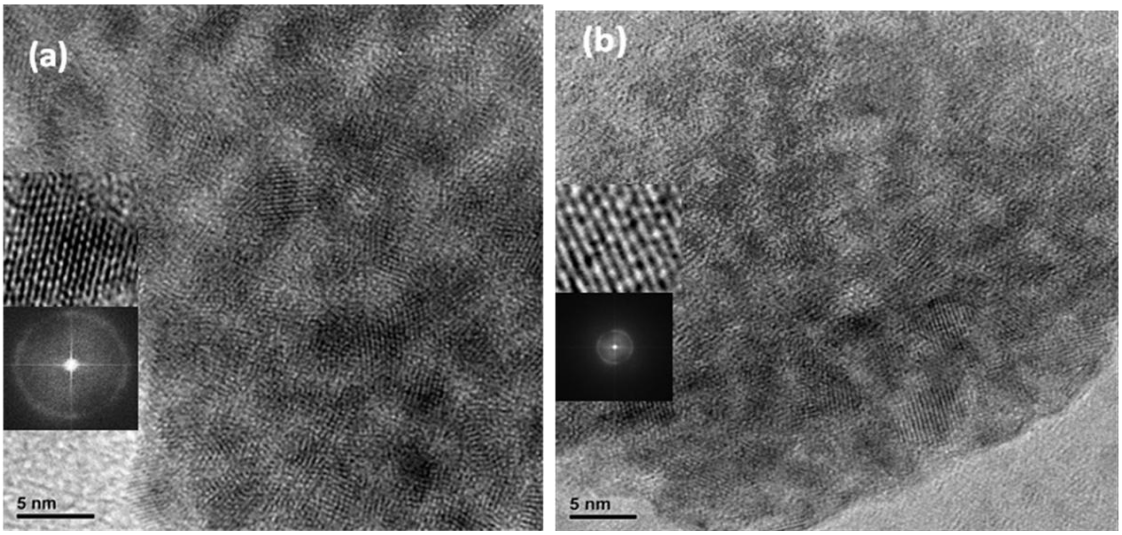


Figure 11: TEM images of citrate-capped CdSe NPs [insets: HRTEM and FFT] for Cd:Se ratio 2:1 at (a) room temperature (b) reflux.

3.1.4 Effect of capping agent

The effect of capping agent was investigated using different passivating molecules which are potassium sodium tartarate (PST), mercaptopropanoic acid (MPA), sodium citrate and L-cysteine. The Cd:Se ratio of 4:1 was used for the investigation because it gave the highest luminescence intensity among the other Cd:Se ratio studied (Fig. 5b) while other parameters remained constant. After the addition of selenium precursor to the Cd-capping agent complex solution, the colour of the solution changed from colourless to transparent orange (citrate), transparent yellow (MPA), bright yellow (cysteine) and milky white colour which later turned into a grayish colour (PST). The change in colour is indicative of particle with different diameter.

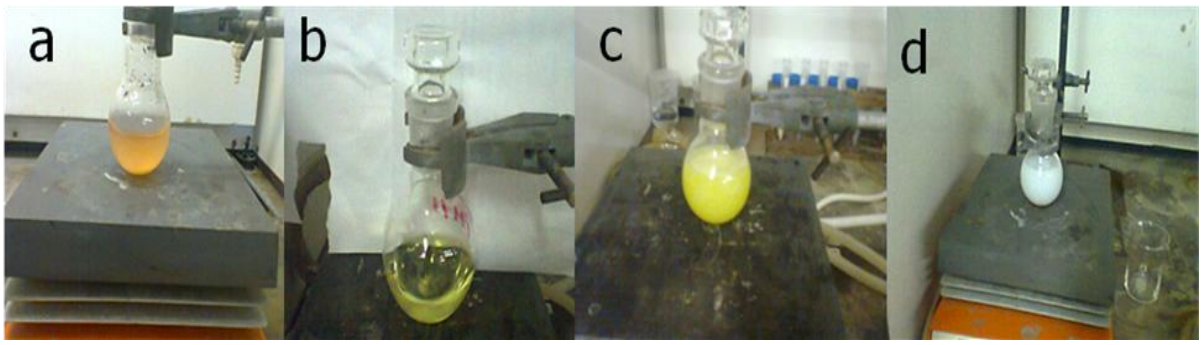


Figure 12: The colour of the CdSe NPs after the addition of selenium precursor to the (a) Cd-citrate complex (b) Cd-MPA complex (c) Cd-cysteine complex and (d) Cd-PST complex solution.

3.1.4.1 Optical properties

Typical absorption spectra of CdSe NPs synthesised using different capping agents is shown in Figure 13 (a). All the particles are blue shifted in relation to the bulk CdSe band gap (716 nm). The band edge of the nanoparticles are red-shifted in the order MPA < cysteine <PST < citrate. The sizes of the CdSe particles as calculated using the EMA method as given in equation 5 (Gupta and Ramrakhiani 2009) are 2.08 nm, 2.25 nm 2.26 nm and 2.30 nm for MPA, cysteine, PST and citrate respectively. Due to smaller particle size, the MPA-capped CdSe NPs absorption was blue shifted with stronger quantum confinement effect than the other NPs (Li *et al.,* 2007). The photoluminescence spectra in Figure 13 (b) show that PST capped CdSe NPs has emission maximum at 566 nm while the CdSe NPs capped with cysteine and citrate have emission maximum at nearly the same position of about 529 nm and 531 nm respectively. The MPA capped-CdSe NPs show very poor luminescence properties. The luminescence intensity decreased in the order citrate > cysteine > PST > MPA. This indicates that citrate gave better passivation than the other capping agent under this reaction condition.

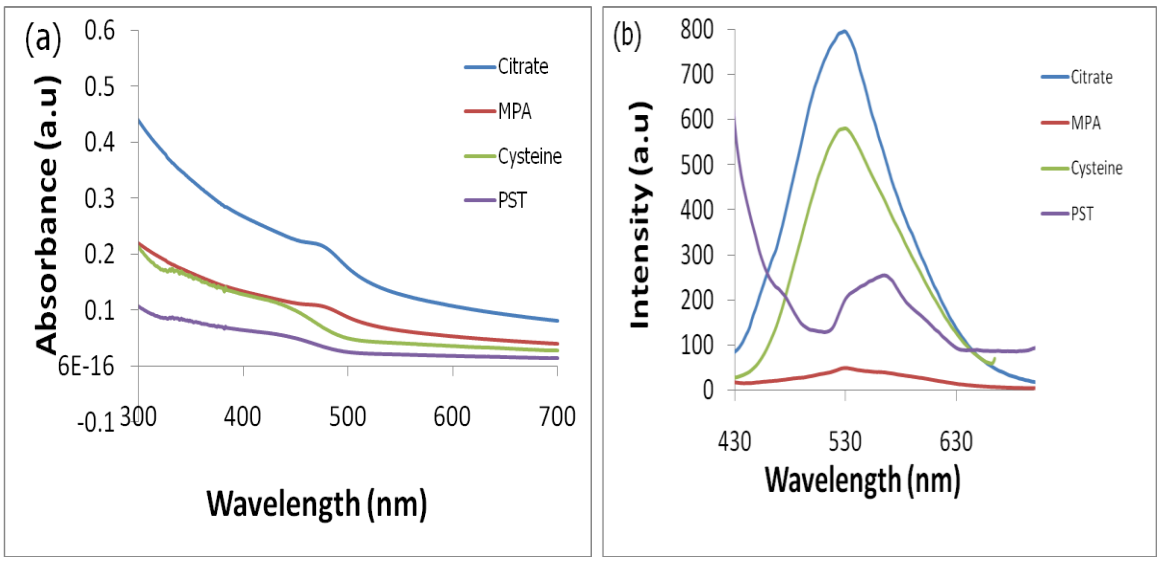


Figure 13: (a) Absorption and (b) photoluminescence ($\lambda_{400\ nm}$) spectra of CdSe NPs using different capping agents

Table 4: Optical properties of CdSe NPs using different capping agents.

Capping agent	Excitonic peak (nm)	Band edge (nm)	PL emission (nm)	PL intensity (nm)	FWHM	Particle size (nm)
Citrate	469	521	531	795	96	2.30
MPA	433	478	529	48	-------	2.08
Cysteine	454	502	529	581	100	2.25
PST	459	503	566	254	-------	2.26

*Note: ------- Cannot be determined from the spectrum

3.1.5 Effect of growth time

The stability of the nanoparticles synthesized using the $CdCl_2$ precursor and different capping agents were investigated by ageing the materials for several days.

3.1.5.1 Optical properties

The absorption spectra for the citrate-capped CdSe NPs using $CdCl_2$ precursor in Figure 14 (a) show that at lower ageing time there are no distinct absorption features until 7 days when a sharp excitonic peak appeared. The excitonic shoulder disappeared after 34 days. The spectra show that the absorption band edges are red-shifted as the ageing time increases. The optical properties of the citrate-capped CdSe NPs are shown in Table 5. The spectra for the MPA-capped CdSe NPs shows that the band edges are red shifted at the beginning of the reaction and became blue shifted after 3 hours (Figure 14 b). The NPs have distinct sharp excitonic peaks with no significant shift in the position except at 3 hours. After 7 days there is a drastic red shift in the band edge position meaning bigger particles are formed at higher reaction times (Xia *et al.*, 2008). The optical properties of the MPA-capped CdSe NPs are shown in Table 6. Figure 14 (c) shows the absorption spectra for cysteine-capped CdSe NPs at different reaction times. A red shift in the band edge was observed as the reaction time increased due to the increase in particle size (Park *et al.*, 2010). The intensity of the peaks also increased as the reaction times increased, however, no peak was observed at 1 hour. In the absorption spectra for the PST-capped CdSe shown in Figure 14 (d) neither excitonic

peaks nor band edge was observed throughout the ageing time. The optical properties for cysteine-capped CdSe NPs using $CdCl_2$ precursor are shown in Table 7.

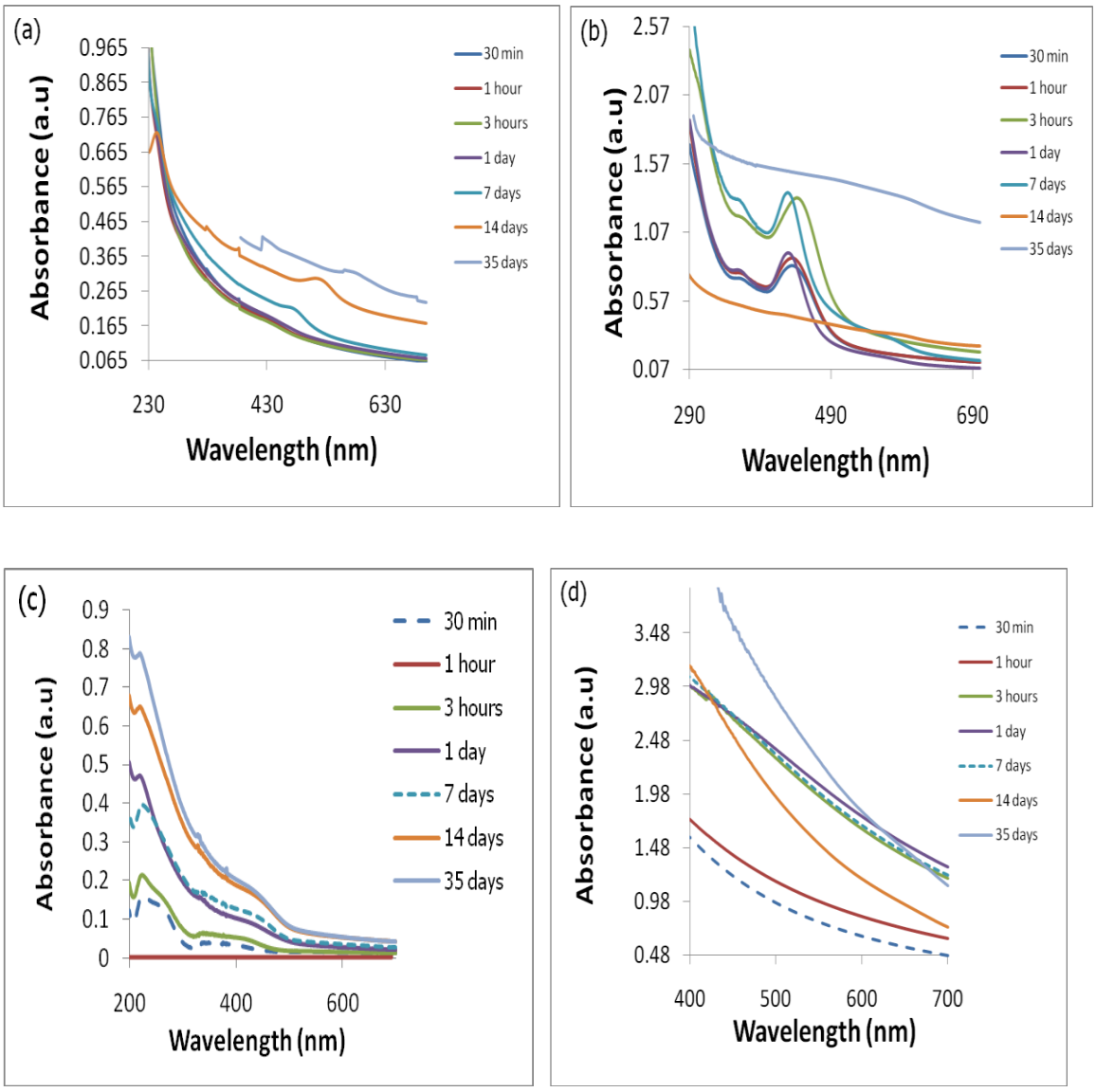


Figure 14: Absorption spectra of CdSe NPs using different capping agents: (a) citrate (b) MPA (c) cysteine and (d) PST at different reaction times.

The photoluminescence spectra in Figure 15 (a) for citrate-capped CdSe NPs shows that as the reaction time increased, the intensity increased with slight shifting of the emission maxima position. The emission maximum varied from 529 nm (30 min) to 568 nm (35 days). The particles are transparent orange in colour but do not fluoresce under UV light. It is observed that the luminescence was lost at 14 and 35 days respectively. MPA-capped CdSe NPs shows very poor luminescence at the beginning of the reaction (Figure 15 b). This improves with time but was not symmetrical and contains a lot of defects. The as-synthesised NPS did not show any fluorescence under the UV light. The PL spectra for the L-cysteine capped CdSe NPs (Figure 15 c), shows an increase in the emission intensity with slight increase in the emission wavelength at the beginning of the reaction. As the reaction time increased further, a severe decrease in the intensity was observed after 1 day. The broad emission width could be attributed to recombination from the surface defects (Oluwafemi *et al.*, 2008). Further aging of the nanoparticles improves the luminescence intensity with narrower emission width compared to the result obtained at the beginning of the reaction. The NPs emit a bright yellow colour under the UV light with highest quantum yield (32 %) at 7 days. Figure 15 d shows that there was no significant shift in the emission peak position for the PST capped CdSe NPs. However, the intensity increased as the reaction time increased up to 3 hrs followed by decrease in emission intensity. This study shows cysteine as a better capping agent under these synthetic conditions. In addition, it is observed from the optical properties (Table 5-7), that all the samples with emission maxima at 532 nm and

beyond show featureless absorption band edges. Therefore, it can be concluded that the featureless band edge for some of the capping agents, especially PST is due to the formation of large particle sized CdSe NPs.

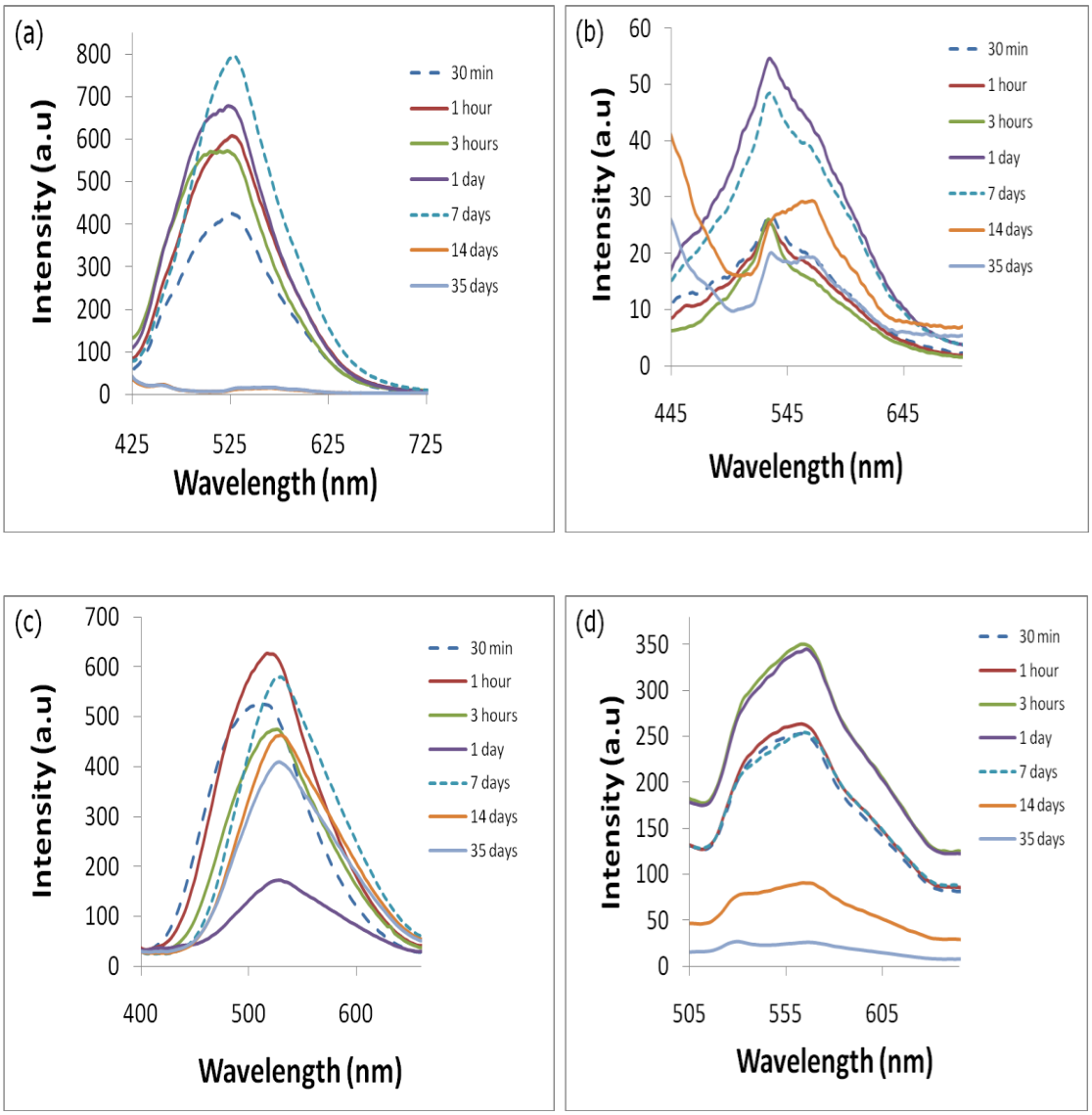


Figure 15: Photoluminescence ($\lambda_{400\ nm}$) spectra of CdSe NPs using different capping agents: (a) citrate (b) MPA (c) cysteine and (d) PST at different reaction times.

Table 5: Optical properties of citrate-capped CdSe NPs using $CdCl_2$ precursor.

Reaction time	Excitonic peak (nm)	Band edge (nm)	PL emission (nm)	PL intensity (nm)	FWHM	Particle size (nm)
30 min	451	501	530	422	105	2.06
1 hour	455	501	531	605	103	2.06
3 hours	455	503	526	570	104	2.08
1 day	454	511	528	676	104	2.16
7 days	469	521	531	795	96	2.30
14 days	511	549	564	18	-------	2.70
35 days	586	645	568	16	-------	3.75

*Note: ------- Cannot be determined from the spectrum

Table 6: Optical properties for MPA-capped CdSe NPs.

Reaction time	Excitonic peak (nm)	Band edge (nm)	PL emission (nm)	PL intensity (nm)	FWHM	Particle size (nm)
30 min	437	501	529	27	-------	2.24
1 hour	437	501	529	25	-------	2.24
3 hours	433	500	529	26	-------	2.23
1 day	430	478	530	55	-------	2.08
7 days	433	478	529	48	-------	2.08
14 days	574	630	534	27	-------	3.60
35 days	584	657	533	20	-------	3.87

*Note: ------- Cannot be determined from the spectrum

Table 7: Optical properties of cysteine-capped CdSe NPs.

Time	Excitonic peak (nm)	Band edge (nm)	PL emission (nm)	PL intensity (nm)	FWHM	Particle size (nm)	PL QE (%)
30 min	410	491	511	526	107	2.03	25
1 hour	-------	-------	517	628	102	-------	28
3 hours	426	493	527	475	100	2.19	28
1 day	435	501	527	173	90	2.24	25
7 days	448	502	529	581	100	2.25	32
14 days	455	503	529	463	100	2.26	27
35 days	456	506	529	410	101	2.28	30

*Note: ------- Cannot be determined from the spectrum

3.1.6 Effect of cadmium precursor

The effect of different cadmium precursors on the size and optical properties was investigated using Cd $(CH_3COO)_2$ and Cd $(NO_3)_2$ in addition to the $CdCl_2$ precursor used above with different capping agents.

3.1.6.1 Optical properties

The absorption spectra of citrate-capped CdSe NPs using $Cd(CH_3COO)_2$ is shown in Figure 16 (a). The spectra were featureless at the beginning of the reaction after which

the spectra show distinct absorption feature. After 1 day, the absorption band edge become red-shifted as the aging time increased. The band edges varied between 601 nm (1 day) and 610 nm (35 days) with particle diameter between 3.37 nm (1 day) and 3.53 nm (35 days). The particles were bigger and the absorption features were observed for longer period when compared to those synthesized using $CdCl_2$ precursor. In the absorption spectra of the citrate-capped CdSe NPs using $Cd(NO_3)_2$ shown in Figure 16 (b) it was observed that at the beginning of the reaction, there were no distinct absorption features. After day 1, absorption features were observed and the band edges became red-shifted as the reaction time was increased. The particle sizes ranged from 3.40 nm (1 day) to 3.75 nm (35 days) (Table 9). The particle sizes of these materials were bigger than those produced using $CdCl_2$ and $Cd(CH_3COO)_2$ as precursors.

Figure 16 (c) shows the photoluminescence spectra of citrate-capped CdSe NPs using $Cd(CH_3COO)_2$. It was observed that at the beginning of the reaction the peaks were very broad which was in agreement with the observation from the absorption spectra, however, the intensity was highest at this instance. At day 1, the intensity decreased dramatically with red-shifting of the emission position. The intensity of these particles was quenched when compared to those produced using $CdCl_2$ as precursor. The particles do not fluoresce under UV light. The photoluminescence spectra in Figure 16 (d) for citrate-capped CdSe NPs show well defined and broad peaks at the beginning of the reaction with high intensity compared to those obtained at the later stage. A slight

red shift was observed at day 1 with narrow emission width. The intensity of these particles is slightly more than those obtained with $Cd(CH_3COO)_2$ precursors but less than those of $CdCl_2$ precursor. The particles did not fluoresce under UV light.

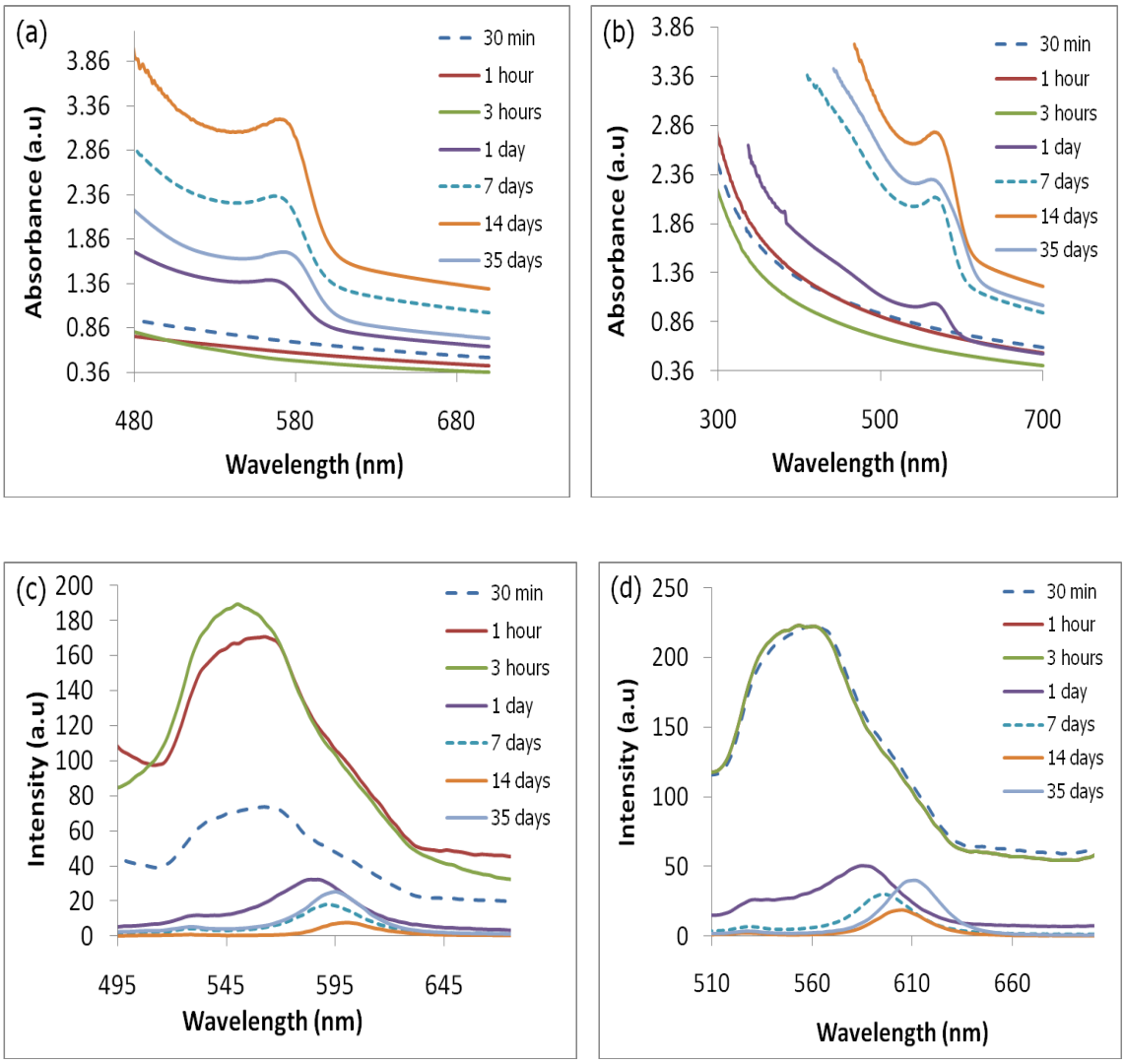


Figure 16: Absorption spectra of citrate-capped CdSe NPs using (a) $Cd(CH_3COO)_2$ and (b) $Cd(NO_3)_2$ precursors and Photoluminescence ($\lambda_{400\ nm}$) spectra of citrate-capped CdSe NPs using (c) $Cd(CH_3COO)_2$ and (d) $Cd(NO_3)_2$ precursors at different reaction times.

Table 8: Optical properties of citrate-capped CdSe NPs using $Cd(CH_3COO)_2$ precursor.

Reaction time	Excitonic peak (nm)	Band edge (nm)	PL emission (nm)	PL intensity (nm)	FWHM	Particle size (nm)
30 min	-------	-------	567	73	-------	-------
1 hour	-------	-------	562	171	-------	-------
3 hours	-------	-------	556	186	-------	-------
1 day	565	601	585	32	-------	3.37
7 days	571	603	592	18	-------	3.39
14 days	573	605	600	8	-------	3.43
35 days	573	610	595	25	-------	3.53

*Note: ------- Cannot be determined from the spectrum

Table 9: Optical properties of citrate-capped CdSe NPs using $Cd(NO_3)_2$ precursor.

Reaction time	Excitonic peak (nm)	Band edge (nm)	PL emission (nm)	PL intensity (nm)	FWHM	Particle size (nm)
30 min	-------	-------	563	223	-------	-------
1 hour	-------	-------	563	234	-------	-------
3 hours	-------	-------	563	222	-------	-------
1 day	567	603	586	51	-------	3.40
7 days	573	598	595	30	-------	3.31
14 days	579	607	604	19	-------	3.46
35 days	570	621	609	40	-------	3.75

*Note: ------- Cannot be determined from the spectrum

The absorption spectra for the MPA-capped CdSe NPs using $Cd(CH_3COO)_2$ as cadmium precursor is shown in Figure 17 (a). The band edges varied between 508 nm (30 min) and 644 nm (35 days). The particle size ranged from 2.02 to 3.65 nm when compared to the one obtained when $CdCl_2$ was used as the precursor (2.08 to 3.87 nm). The absorption spectra of MPA-capped CdSe NPs synthesized using $Cd(NO_3)_2$ as precursor (Figure 17 b) did not show significant shift in the excitonic peak at the beginning of the reaction until after 14 days. The band edges of the materials as calculated using direct

band gap method are 507 nm (30 min), 494 nm (1 hour), 502 nm (3 hours), 482 nm (1 day), 474 nm (7 days), 630 nm (14 days) and 650 nm (35 days). The particle size as shown in Table 3.12 ranged between 2.30 nm (30 min) and 3.73 nm (35 days). When assessing all the absorption spectra, $CdCl_2$ gives distinct features as compared to the other two cadmium precursors. The photoluminescence spectra of MPA-capped CdSe NPs using $Cd(CH_3COO)_2$ as cadmium precursor is shown in Fig. 17 (c). The spectra show the presence of defect emission and the intensity is very low. The particles did not fluoresce under the UV light. Figure 17 (d) shows the photoluminescence spectra of the MPA-capped CdSe NPs using $Cd(NO_3)_2$ as precursor. Poor luminescence properties were observed during the course of the reaction which might be due to the pH of the nanoparticles (Ruedas-Rama *et al.*, 2011). The particles did not fluoresce under the UV light.

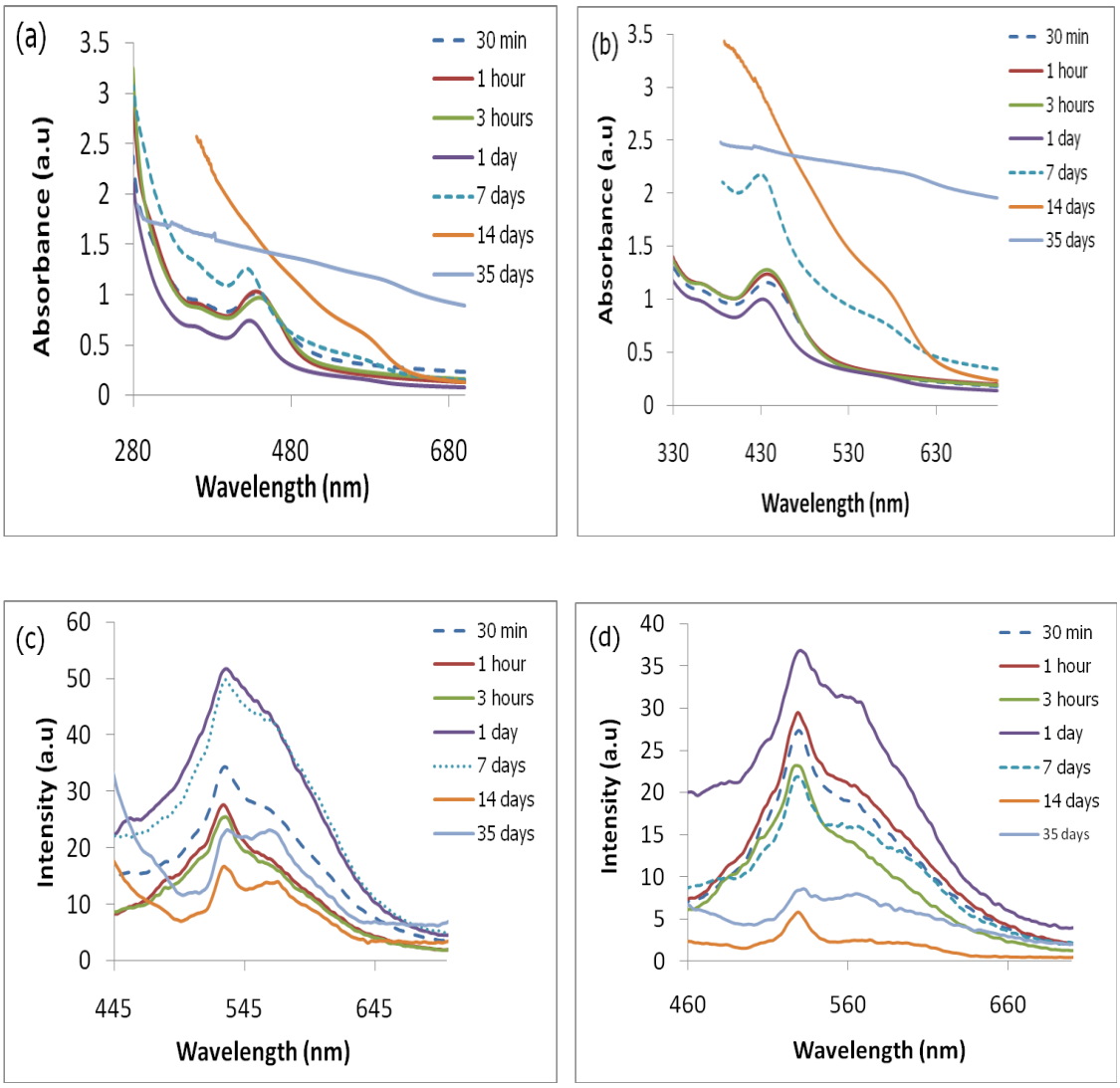


Figure 17: Absorption spectra of MPA-capped CdSe NPs using (a) $Cd(CH_3COO)_2$ and (b) $Cd(NO_3)_2$ and Photoluminescence ($\lambda_{400\ nm}$) spectra of MPA-capped CdSe NPs (c) $Cd(CH_3COO)_2$ and (d) $Cd(NO_3)_2$ at different reaction times.

Table 10: Optical properties of MPA-capped CdSe NPs using $Cd(CH_3COO)_2$ precursor.

Reaction time	Excitonic peak (nm)	Band edge (nm)	PL emission (nm)	PL intensity (nm)	FWHM	Particle size (nm)
30 min	444	509	529	34	-------	2.30
1 hour	446	506	529	28	-------	2.27
3 hours	454	511	529	26	-------	2.32
1 day	438	582	530	52	-------	3.03
7 days	434	481	529	50	-------	2.02
14 days	582	625	528	17	-------	3.46
35 days	604	644	534	23	-------	3.65

*Note: ------- Cannot be determined from the spectrum

Table 11: Optical properties of MPA-capped CdSe NPs using $Cd(NO_3)_2$ precursor.

Reaction time	Excitonic peak (nm)	Band edge (nm)	PL emission (nm)	PL intensity (nm)	FWHM	Particle size (nm)
30 min	437	507	531	27	-------	2.29
1 hour	440	494	530	29	-------	2.20
3 hours	437	502	531	23	-------	2.25
1 day	435	482	530	37	-------	2.11
7 days	435	474	530	22	-------	2.06
14 days	576	630	531	6	-------	3.53
35 days	603	650	533	9	-------	3.73

*Note: ------- Cannot be determined from the spectrum

The absorption spectra of the cysteine-capped CdSe NPs using $Cd(CH_3COO)_2$ as the precursor is shown in Figure 18 (a). The spectra show a red-shift in the band gap as the reaction time was increased indicating an increase in particle size (Table 12). The band edges of the materials vary from 480 nm (30 min) to 510 nm (35 days). The size of these NPs ranges between 2.10 and 2.31 nm. This is higher than the result obtained when $CdCl_2$ was used as the precursor (2.03 – 2.28 nm). A red-shift as the reaction time increased was also observed in the absorption spectra of the cysteine-capped

CdSe NPs using $Cd(NO_3)_2$ as the precursor (Figure 18 b). The band edges of the materials vary from 470 nm (30 min) to 517 nm (35 days). The particle size ranges between 2.03 nm (30 min) and 2.37 nm (35 days) as shown in Table 13. The particle size range for these cadmium precursors increased in the order $CdCl_2$ < $Cd(CH_3COO)_2$ < $Cd(NO_3)_2$. The PL spectra of the cysteine-capped CdSe NPs using $Cd(CH_3COO)_2$ show that the positions of the peaks were red-shifting as the time increased (Figure 18 c). The emission intensity is still high but lower compared to the particles synthesised with $CdCl_2$. In addition, the quantum yield at 7 days is lower than that obtained for $CdCl_2$. The highest quantum yield was observed at 14 days (31 %). The particles emit a yellow colour under the UV light which is the same as in the nanoparticles synthesized using $CdCl_2$. The PL spectra of the cysteine-capped CdSe NPs using $Cd(NO_3)_2$ as the precursor show a slight red shift in the emission maximum position as the reaction time increased but no significant shift is observed after 7 days (Figure 18 d). The emission intensity is slightly higher compared to those synthesized using $Cd(CH_3COO)_2$ but lower than those obtained with $CdCl_2$ precursor. The quantum yield (Q.Y) at day 7 is the same with that of $Cd(CH_3COO)_2$ but less than those obtained with $CdCl_2$ precursor (32 %). The Q.Y at day 14 (33 %) is higher than those obtained at the same day when $CdCl_2$ and $Cd(CH_3COO)_2$ were used as the precursor. The Q.Y obtained at 3 h (34 %) was the highest. The particles emit at yellow region under the UV light like those of $CdCl_2$ and $Cd(CH_3COOH)_2$.

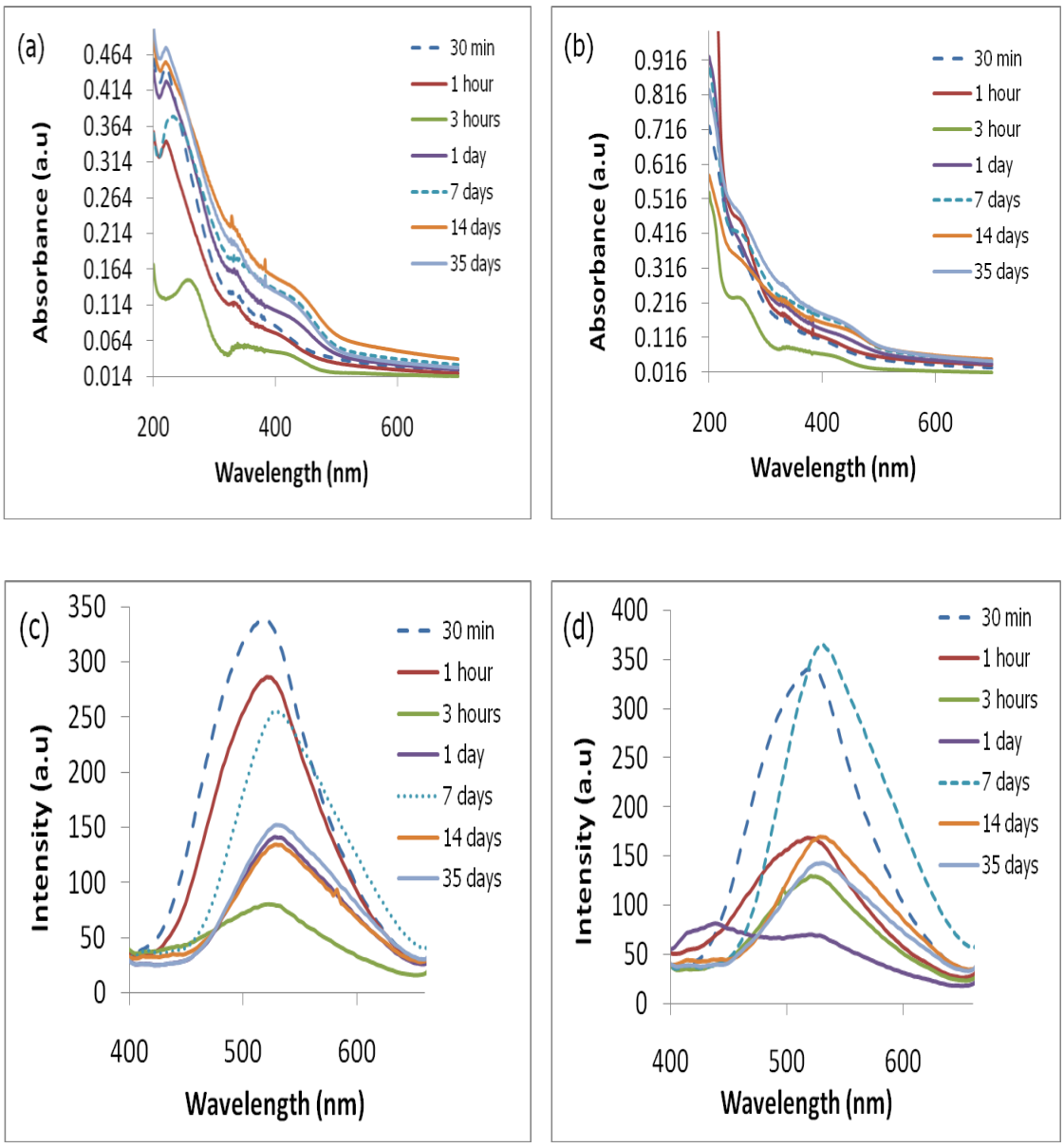


Figure 18: Absorption spectra of cysteine-capped CdSe NPs using (a) $Cd(CH_3COO)_2$ and (b) $Cd(NO_3)_2$ and Photoluminescence ($\lambda_{350\ nm}$) spectra of cysteine-capped CdSe NPs (c) $Cd(CH_3COO)_2$ and (d) $Cd(NO_3)_2$ at different reaction times.

Table 12: Optical properties of cysteine-capped CdSe NPs using $Cd(CH_3COO)_2$ precursor.

Time	Excitonic peak (nm)	Band edge (nm)	PL emission (nm)	PL intensity (nm)	FWHM	Particle size (nm)	PL QE (%)
30 min	421	480	523	337	101	2.10	28
1 hour	423	483	526	285	100	2.12	25
3 hours	430	488	526	80	81	2.15	30
1 day	444	494	531	141	95	2.19	26
7 days	449	505	531	255	96	2.27	27
14 days	454	509	531	135	94	2.30	31
35 days	456	510	531	152	100	2.31	29

Table 13: Optical properties of cysteine-capped CdSe NPs using $Cd(NO_3)_2$ precursor.

Time	Excitonic peak (nm)	Band edge (nm)	PL emission(nm)	PL intensity (nm)	FWHM	Particle size (nm)	PL QE (%)
30 min	429	470	519	340	100	2.03	29
1 hour	431	481	519	169	93	2.10	26
3 hours	444	482	524	129	90	2.11	34
1 day	452	500	524	66	-------	2.24	24
7 days	461	510	532	169	101	2.31	27
14 days	465	512	532	363	93	2.33	33
35 days	469	517	532	143	96	2.37	25

*Note: ------- Cannot be determined from the spectrum

Figure 19 (a) show the absorption spectra of the PST-capped CdSe NPs using $Cd(CH_3COO)_2$ as the precursor. The spectra shows slight red shift in the band edge as the reaction time increased. The optical properties are shown in Table 14. The as-synthesised material show distinct absorption features unlike when $CdCl_2$ was used as the precursor. In the absorption spectra of PST-capped CdSe NPs using $Cd(NO_3)_2$ the absorption features were not observed at the beginning of the reaction until after 3 h (figure 19 b). A red shift in the band gap was observed as the reaction time increased.

These particles are bigger when compared to the CdSe NPs produced using $CdCl_2$ and $Cd(CH_3COO)_2$. Figure 19 c show that there is no significant shift in the emission maxima at the beginning of the reaction for the PST-capped CdSe NPs using $Cd(CH_3COO)_2$. A red shift in the emission maxima was then observed after 1 day until the end of the reaction. In addition, the intensity increased for the first 3 hours and decreased significantly after 1 day. There was no significant change in the intensity between these particles and those that were produced using $CdCl_2$. The particles did not fluoresce under UV light. Figure 19 d shows the photoluminescence spectra of PST-capped CdSe NPS using $Cd(NO_3)_2$. No significant shift in the emission maximum peak position was observed earlier in the reaction and the intensity was highest at this instance. A red shift was later observed after day 1 until the end of the reaction whereas the intensity decreased with time. There was no significant change in the intensity between these particles and those produced using $Cd(CH_3COO)_2$ and $CdCl_2$. The particles did not fluoresce under UV light.

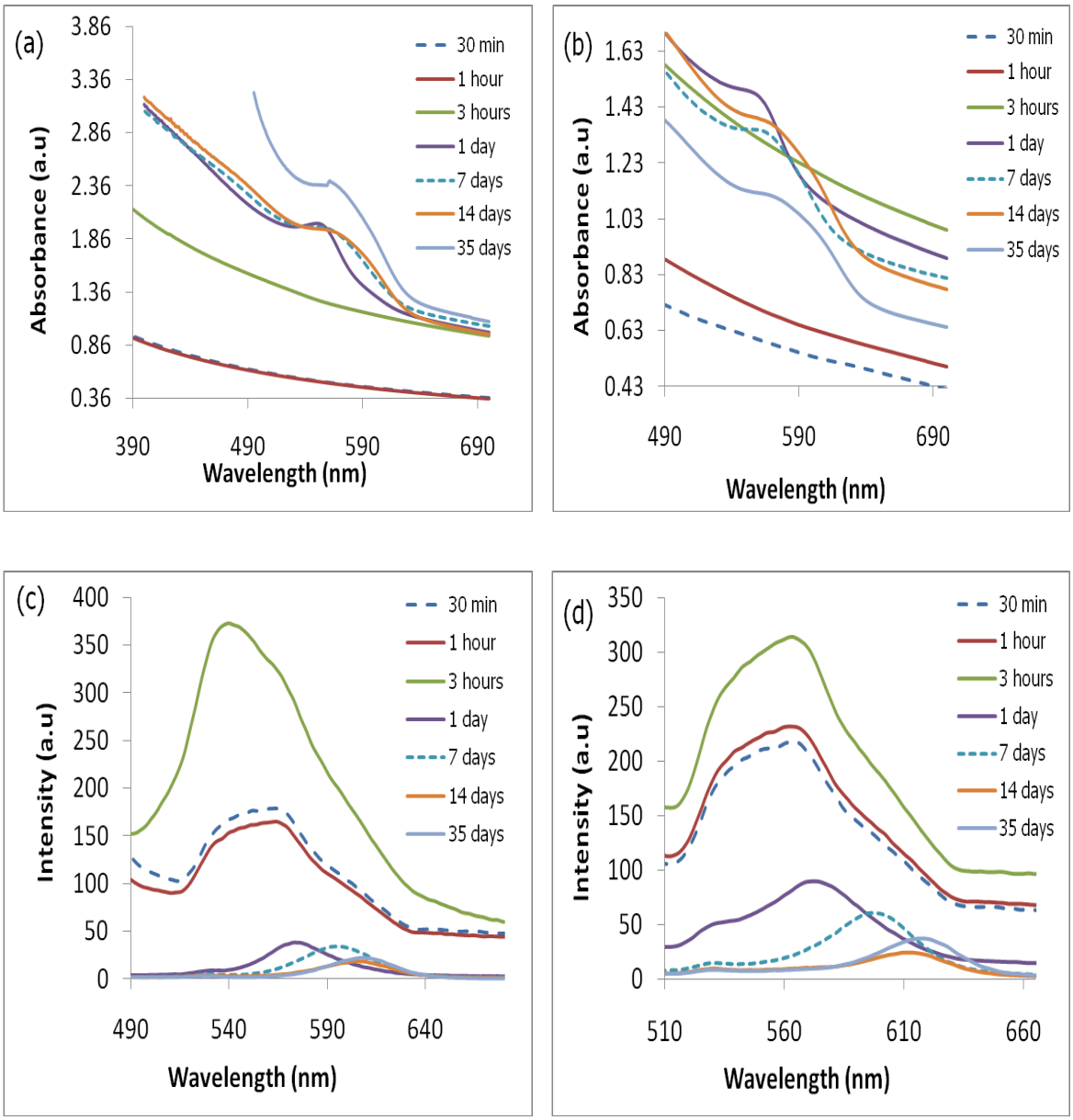


Figure 19: Absorption spectra of PST-capped CdSe NPs using (a) $Cd(CH_3COO)_2$ and (b) $Cd(NO_3)_2$ and Photoluminescence ($\lambda_{400\ nm}$) spectra of PST-capped CdSe NPs (c) $Cd(CH_3COO)_2$ and (d) $Cd(NO_3)_2$ at different reaction times.

Table 14: Optical properties for PST-capped CdSe NPs using $Cd(CH_3COO)_2$ precursor.

Reaction time	Excitonic peak (nm)	Band edge (nm)	PL emission (nm)	PL intensity (nm)	FWHM	Particle size (nm)
30 min	-------	-------	564	179	-------	-------
1 hour	-------	-------	564	165	-------	-------
3 hours	-------	-------	540	374	-------	-------
1 day	551	587	574	37	-------	3.13
7 days	558	623	593	34	-------	3.80
14 days	564	627	605	18	-------	3.90
35 days	565	630	608	23	-------	3.97

*Note: ------- Cannot be determined from the spectrum

Table 15: Optical properties of PST-capped CdSe NPs using $Cd(NO_3)_2$ precursor.

Reaction time	Excitonic peak (nm)	Band edge (nm)	PL emission (nm)	PL intensity (nm)	FWHM	Particle size (nm)
30 min	-------	-------	564	218	-------	-------
1 hour	-------	-------	564	232	-------	-------
3 hours	-------	-------	564	314	-------	-------
1 day	551	592	572	89	-------	3.21
7 days	566	620	594	60	-------	3.73
14 days	567	633	612	24	-------	4.06
35 days	574	632	616	38	-------	4.03

*Note: ------- Cannot be determined from the spectrum

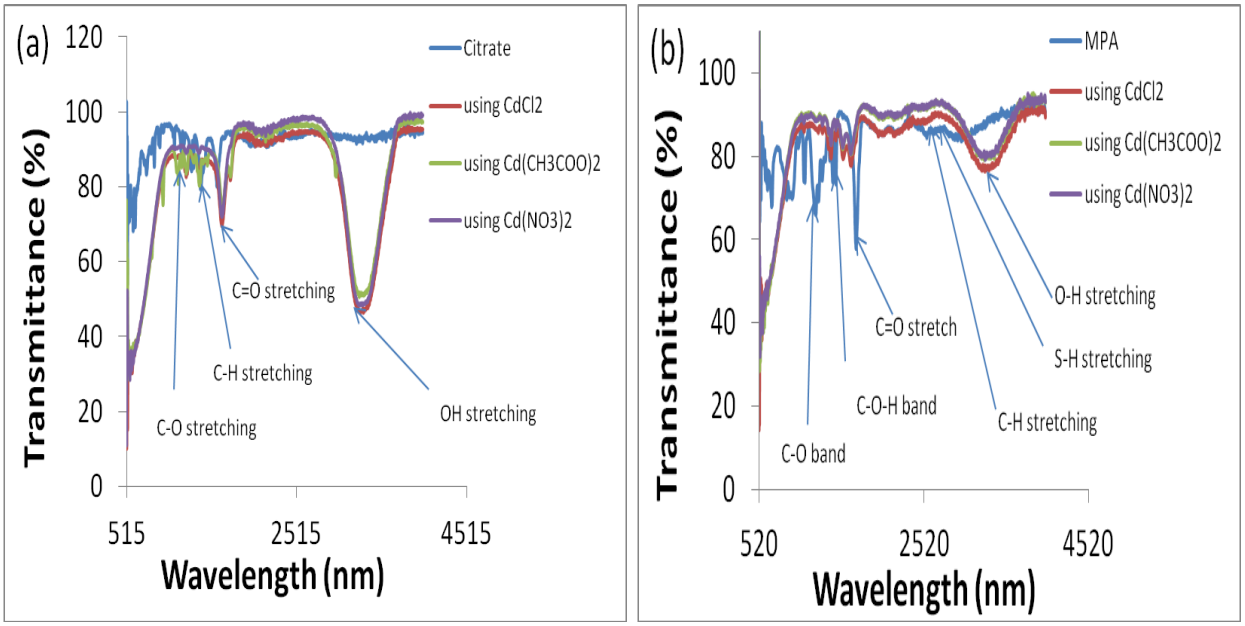
3.1.6.2 Structural properties

3.1.6.2.1 Fourier Transform Infrared Microscopy (FTIR)

The FTIR of the citrate-capped CdSe using different cadmium sources is shown in Figure 20 (a). For comparison, the spectrum recorded for pure tri-sodium citrate is also superimposed in the same figure. The IR spectra of citrate show characteristic bands at 1638 cm^{-1}, 1392 cm^{1} and 1129 cm^{-1} corresponding to stretching vibration of C=O, C–H and C–O, respectively. In the CdSe NPs the bands were slightly shifted towards the

higher frequency. The broad band observed around 3374 corresponds to the O-H stretching. The low intensity of C-O band is attributed to the interaction of the CdSe NPs with citrate. Figure 20 (b) is the FTIR of the MPA and MPA-capped CdSe NPs using different cadmium precursors. The spectra of MPA show characteristic bands at 3300 cm^{-1} corresponding to O-H stretching. The S-H band is observed between 2668 and 2575 cm^{-1} on account of hydrogen bonding between the acid and thiol group. A C-H stretch at 2947 cm^{-1} and a shoulder at 2927 cm^{-1} are superimposed on the OH stretch. The peaks observed at 1707 cm^{-1}, 1423 cm^{-1} and 1248 cm^{-1} are assigned to the C=O stretch, C-O-H band and C-O band respectively. The bands for the MPA-capped CdSe NPs were shifted to lower frequencies. The O-H band is wide and the intensity on the 1505 cm^{-1} corresponding to C=O is lower indicating successful capping with the MPA. The cysteine spectrum shows prominent bands at 3372 cm^{-1} and 1654 cm^{-1} corresponding to stretching vibration of NH_3 and COO^- asymmetric respectively (Figure 20 c). Bands at around 2511 cm^{-1}, 1180 cm^{-1} and 1552 cm^{-1} corresponding to S-H, C-N and N-H asymmetric bands were also observed. The spectra of the as-synthesised cysteine-capped CdSe NPs show a shift to the higher frequency. The spectra using different cadmium sources are almost identical and show a decrease in the intensities when compared to the pure cysteine, with the $Cd(CH_3COO)_2$ having highest intensity compared to other cadmium sources. In addition, the S-H bond at around 2500 cm^{-1} for the thiols is not visible in the thio-capped CdSe NPs. This has been attributed to the cleavage of the S-H bond and the formation of a new S-Cd bond on the surface of the

CdSe NPs (Oluwafemi *et al.*, 2008).This indicates the passivation of the CdSe NPs surface by the thiols. Figure 20 (d) shows the FTIR spectra for PST and PST-capped CdSe NPs. The pure PST has two hydroxyl groups hence two bands can be expected for the stretching vibration of the hydroxyl groups. The spectra of the PST shows a band between 3000 and 3642 cm^{-1} attributed to the stretching vibration of hydroxyl and C-H groups which overlap. The presence of the O-H bands at 3355 and 1057 cm^{-1}, C-H bands at 2961 and 1120 cm^{-1}, carbonyl C=O bands at 1628 and 1406 cm^{-1}, C-O band at 1406 cm^{-1} and C-C band at 1291 cm^{-1} were also observed. The PST-capped CdSe show a wide band around 3350 cm^{-1} due to the overlapping of O-H and C-H groups. The C=O band was shifted to the higher frequency while the intensity of other band disappeared.



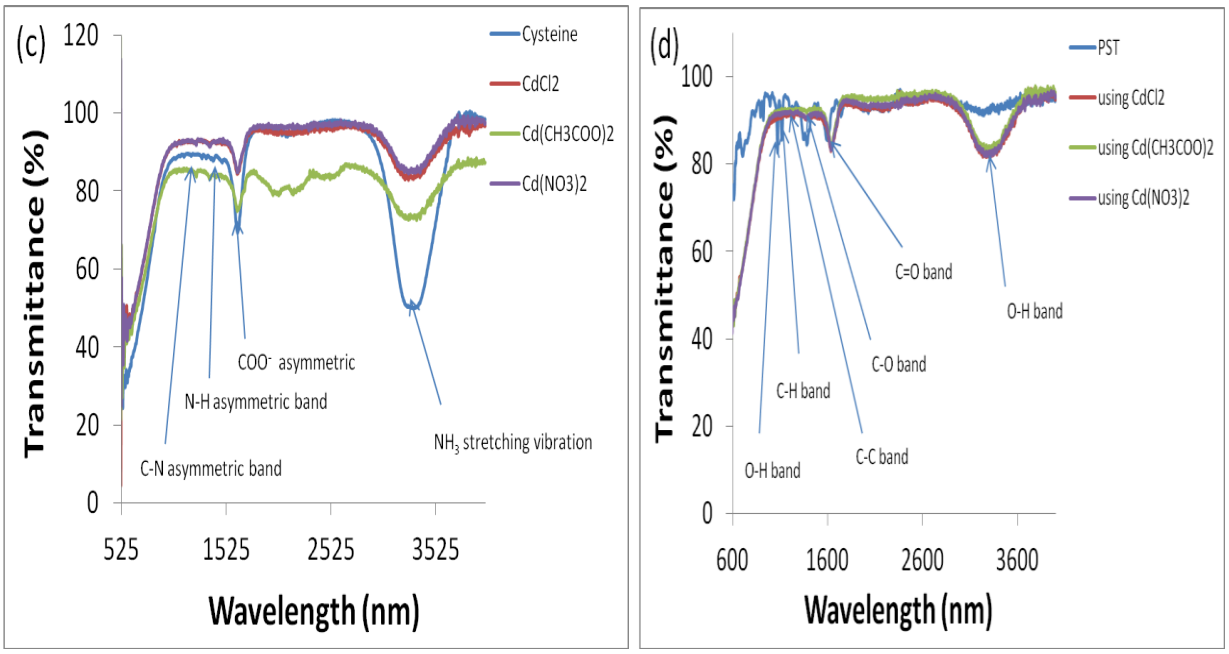


Figure 20: FTIR spectra of CdSe NPs synthesised using different cadmium precursors capped with (a) citrate (b) MPA (c) cysteine and (d) PST.

3.1.6.2.2 TEM, HRTEM and FFT

The representative TEM micrograph and size distribution of the MPA-capped CdSe NPs synthesized using $Cd(CH_3COO)_2$ is shown in Figure 21. The micrograph shows most of the particles are small, spherical in shape and highly monodispersed with the presence of very scantly short nanorods. The nanorods formed when using cadmium acetate as the cadmium precursor agree with Maseko *et al.*, (2010) report where rods, bipods and tripods were produced when cadmium acetate was used as the cadmium precursor. The diameters of the spherical particles are within 1.00 nm to 4.365 nm, with average particle diameter of 3.005 nm ± 0.342 nm. The averaged diameter of the rods is 5.31 nm and length of 5.53 nm with aspect ratio of 1.104 nm. The presence of the lattice

fringes in the high resolution TEM (HRTEM) confirms that the as-prepared materials are highly crystalline. The FFT patterns in Figure 21 (c) show sharp and clear singular reciprocal points supporting the conclusion that the nanoparticles are single crystals.

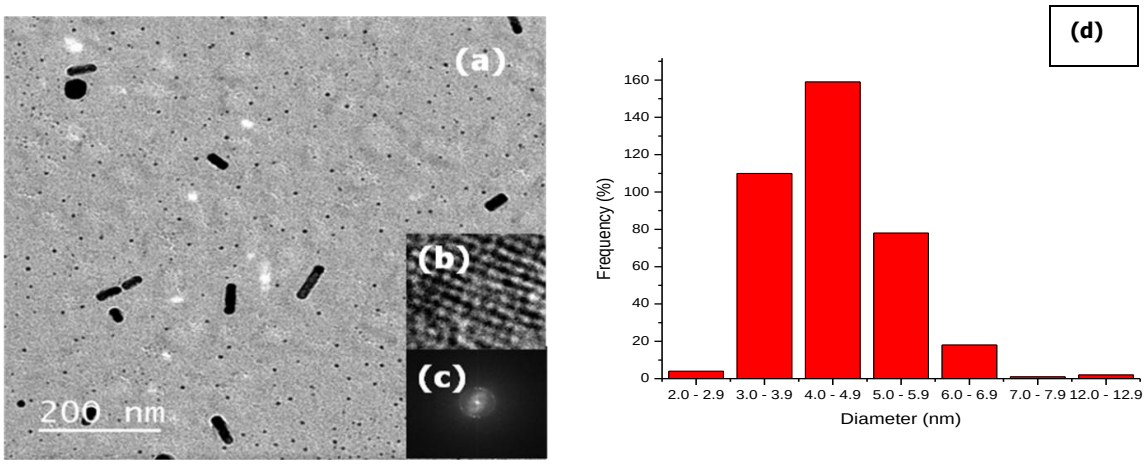


Figure 21: (a) TEM (b) HRTEM (c) FFT images and (d) size distribution of MPA-capped CdSe NPs synthesised using $Cd(CH_3COO)_2$.

3.2 Synthesis of water soluble Au-CdSe nanostructures

After carefully investigating the effect of cadmium source, mole ratio, temperature, growth time and capping agent on the optical and structural properties of CdSe NPs under this synthetic route, water soluble, Au-doped CdSe NPs were synthesized using the optimum reaction conditions; Cd:Se ratio of 4:1, $CdCl_2$ as the cadmium precursor and cysteine as the capping agent. The reaction was carried out at room temperature with varied amount of Au.

3.2.1 Cysteine-capped Au-CdSe nanostructures

3.2.1.1 Optical properties

The absorption spectra of cysteine-capped Au-doped CdSe NPs using Cd: Au ratio of 1:20 is shown in Figure 22 (a). A red shift in the absorption band edge as the reaction time was increased. All the absorption band edges of the doped CdSe NPs were blue-shifted from the 716 nm bulk value of CdSe as a result of quantum confinement (Oluwafemi *et al*., 2008). The absorption band edge was red–shifted as the reaction time was increased indicating an increase in particle size. The excitonic peaks were not observed at the early stages of the reaction but as the time was increased, the peaks started to emerge (from day 2) and showed more distinct features as the reaction progressed. The particle size ranged from 2.19 nm to 3.25 nm as the reaction and aging time was increased. These sizes are higher compared to the results obtained for the undoped CdSe NPs which ranged from 2.03 nm to 2.28 nm. The photoluminescence spectra in Figure 22 (b) indicate that there was no significant shift in the emission maxima position at the beginning of the reaction. The spectra showed irregular shapes which might be attributed to the presence of surface defects due to the presence of Au in the material and insufficient passivation. However, the intensity of the doped material increased as reaction time was increased at the beginning of the reaction. After 45 min, the intensity showed reduction and an increase again at 1 hour followed by another drastic reduction after 2 days of aging. The doped-CdSe NPs synthesized at the earlier period of the reaction (15 min - 3 hours) fluoresce in the yellow region but the

fluorescence stopped after 2 days. The materials fluoresced for a shorter period due to the presence of the dopant as compared to the undoped CdSe NPs where all the samples fluoresced for a longer period. However, due to the presence of the dopant the 3 hour sample gave the highest photoluminescence quantum yield (PLQY) as compared to the undoped material at the same reaction time.

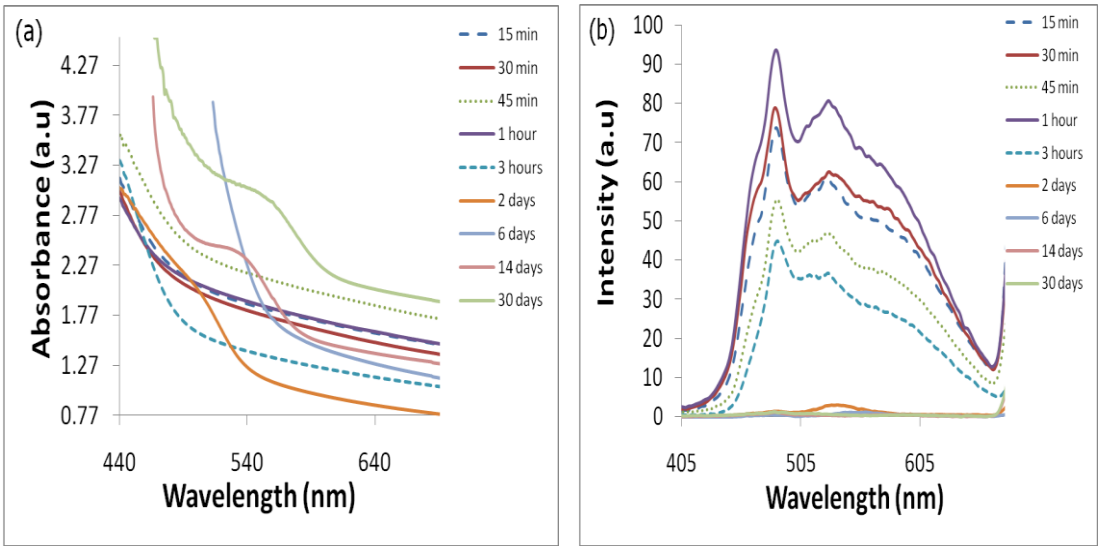


Figure 22: (a) Absorption and (b) photoluminescence ($\lambda_{400\ nm}$) spectra of cysteine-capped Au-doped CdSe NPs using 1:20 Cd:Au ratio at different reaction times.

3.2.2 Effect of Au ratio

3.2.2.1 Optical properties

Figure 23 (a) shows the absorption spectra of the cysteine capped Au-doped CdSe NPs at Cd:Au ratio of 1:40. As observed for the ratio 1:20 all the particles were blue shifted as compared to the bulk CdSe (716 nm). However, unlike the particles synthesized at

ratio 1:20 the absorption spectra did not show any distinctive features. The particle size ranged from 1.97 nm to 2.48 nm as compared to both the 2.19 nm to 3.25 nm for 1:20 ratio and 2.03 nm to 2.28 nm for the undoped materials. The photoluminescence spectra in Figure 23 (b) showed improved emission curves as the reaction time was increased with slight red-shift in the emission position. Unlike the doped material at ratio 1:20, all the as-synthesized doped-CdSe NPs fluoresced in the yellow to the orange region as the reaction was increased. On the other hand, the NPs fluoresced in the yellow region for the entire duration of the reaction for the undoped CdSe NPs.

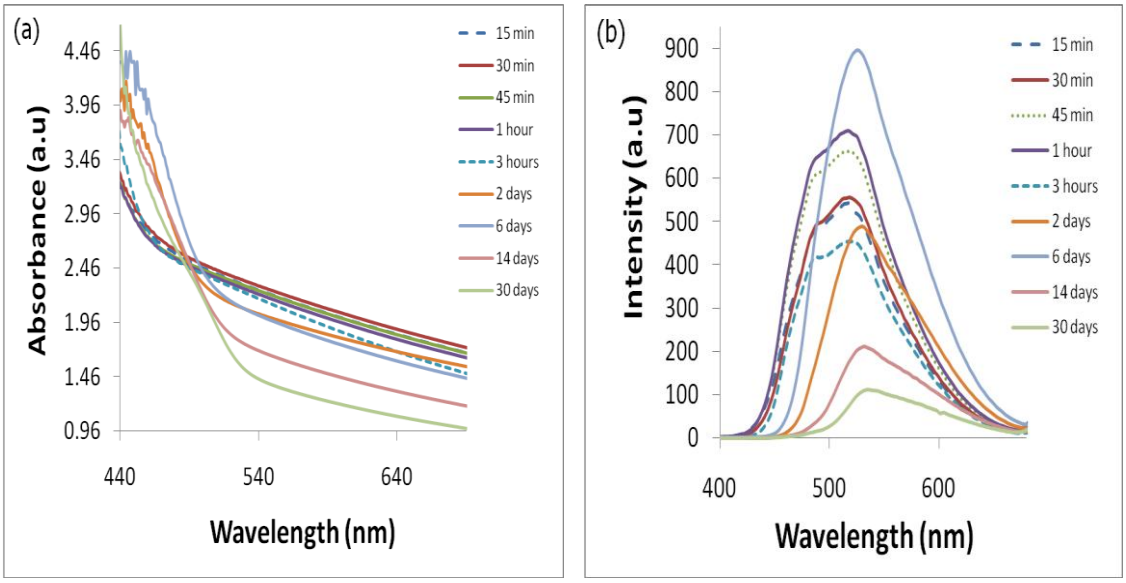


Figure 23: (a) Absorption and (b) photoluminescence ($\lambda_{400\ nm}$) spectra of cysteine-capped Au-doped CdSe NPs using 1:40 Cd: Au ratio at different reaction times.

Table 16: Optical properties of cysteine-capped Au-doped CdSe NPs at ratio 1:40.

Time	Band edge (nm)	PL emission (nm)	PL intensity (nm)	FWHM	Particle size (nm)	PL QE (%)
15 min	460	516	541	106	1.97	28
30 min	460	516	555	106	1.97	32
45 min	461	516	662	107	1.98	37
1 hour	468	516	709	108	2.02	27
3 hours	477	516	454	108	2.08	32
2 days	505	531	487	97	2.27	38
6 days	511	529	889	99	2.32	29
14 days	520	531	211	93	2.39	-------
30 days	530	536	111	96	2.48	27

*Note: ------- Cannot be determined from the spectrum

The absorbance spectra of cysteine-capped Au-doped CdSe NPs at ratio 1:60 in Figure 24 (a) also showed featureless spectra similar to those obtained at ratio 1:40. The particle size ranged from 1.98 nm to 2.26 nm which was smaller when compared to the 2.19 nm to 3.25 nm (1:20), 1.97 nm to 2.48 nm (1:40) and 2.03 nm to 2.28 nm (undoped) materials, respectively. The photoluminescence spectra in Figure 24 (b)

showed a red shift in the emission maxima at 3 h and beyond with an increase in intensity up to 6 days. After 6 days, the intensity started to decrease with increasing particle size. The materials showed fluorescence in the yellow to orange region as the reaction time was increased. The PLQY increased with the aging time with 38 % being the highest which is the same for ratio 1:40 but is higher when compared to the 35 % for ratio 1:20 and 32 % for the undoped CdSe.

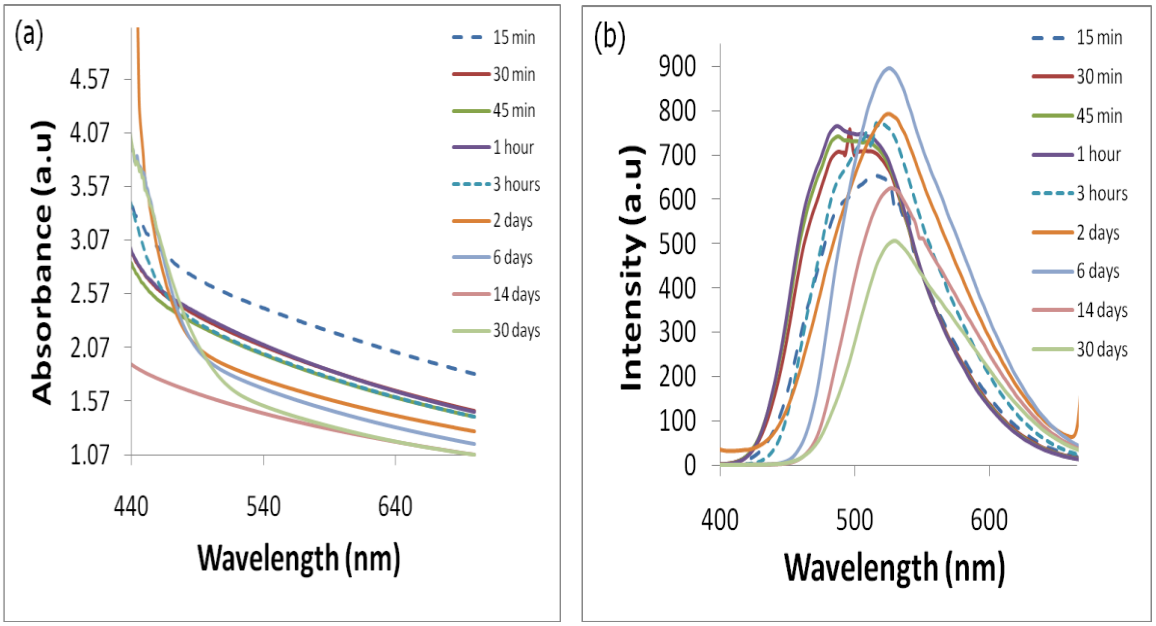


Figure 24: (a) Absorption and (b) photoluminescence ($\lambda_{400\ nm}$) spectra of cysteine-capped Au-doped CdSe NPs using 1:40 ratio at different reaction times.

Table 17: Optical properties of cysteine-capped Au doped CdSe NPs at ratio 1:60.

Time	Band edge (nm)	PL emission (nm)	PL intensity (nm)	FWHM	Particle size (nm)	PL QE (%)
15 min	463	515	653	103	1.99	34
30 min	461	494	712	105	1.98	35
45 min	461	491	737	105	1.98	38
1 hour	461	490	759	104	1.98	34
3 hours	480	520	777	104	2.10	38
2 days	495	526	792	106	2.20	29
6 days	503	525	896	100	2.26	34
14 days	515	527	627	98	2.35	26
30 days	517	529	507	95	2.37	38

3.2.2.2 Structural properties

3.2.2.2.1 Fourier Transform Infrared Microscopy (FTIR)

Figure 25 shows the FTIR spectra of cysteine and cysteine-capped Au doped CdSe NPs at different Cd:Au ratios. The IR spectra of cysteine, shows a very broad band of NH_3 stretch at 3345 cm^{-1}, S-H band at around 2507 cm^{-1}, COO^- asymmetric stretch at 1640

cm^{-1}, C-N stretch at 1160 cm^{-1} and an N-H bending vibration at 1565 cm^{-1}. The spectra of the as-synthesized materials show a shift to the higher frequency and an increase in the intensities as the mole ratio increased, however the intensity of the broad NH_2 stretch decreases. These observations confirm the successful capping of the doped-CdSe NPs surface.

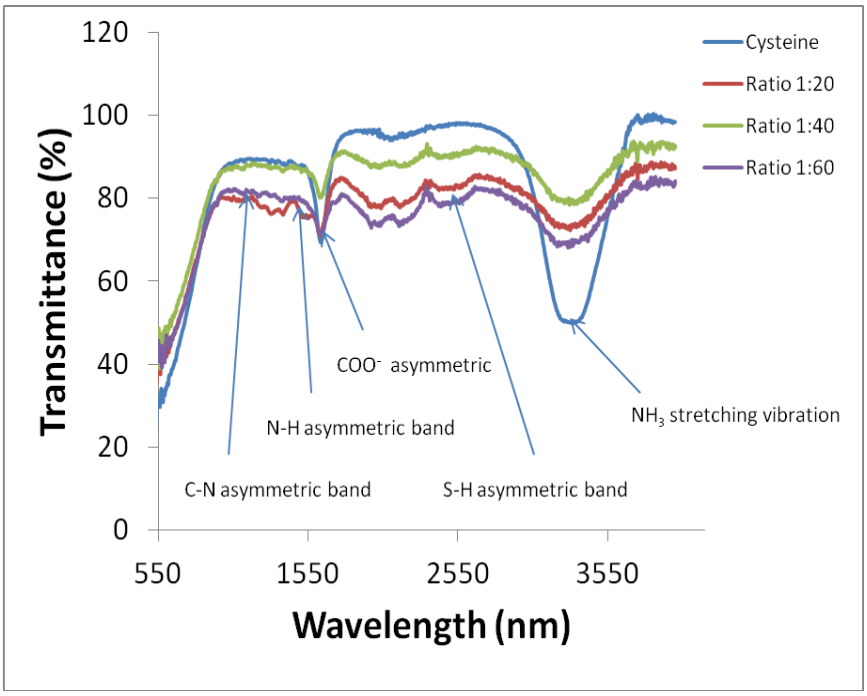


Figure 25: FTIR spectra of cysteine and cysteine-capped Au doped CdSe NPs using different Cd:Au ratio.

3.3 Synthesis of organic soluble CdSe nanostructures

3.3.1 HDA-capped CdSe nanostructures

The addition of selenium precursor to the $CdCl_2$ resulted in an instant change in the colour of the solution from colourless to milky yellow. The intensity of the colour increased as the reaction continued as shown in Figure 26. The dispersion of the CdSe in TOP after centrifugation produced TOP-CdSe which was then injected into the HDA solution at 160 ^{o}C to produce HDA-capped CdSe NPs.

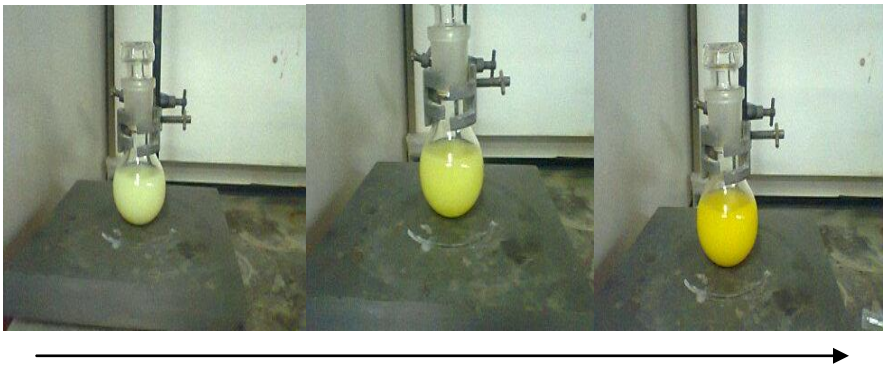


Figure 26: A photograph showing the change in the colour of the CdSe NPs as at reaction time of 0, 8 and 15 mins.

3.3.1.1 Optical properties

The absorption spectra of HDA-capped CdSe NPs at different reaction times are shown in Figure 27 (a). All the as-synthesized CdSe NPs at different reaction time are blue-shifted in relation to the CdSe bulk band gap due to quantum confinement (Oluwafemi *et al.*, 2008). All the particles show sharp excitonic shoulder indicative of monodispersed materials. The absorption shoulder becomes slightly red-shifted as the reaction time

increased. The excitonic shoulder and sharp absorption edge is indicative of particles with narrow size distribution. The photoluminescence spectra show that at 5 mins the emission maximum position was blue-shifted as compared to the 0 min. No further significant shift from this point was observed till the end of the reaction (figure 27 b). The intensity increased at 5 minutes then dropped drastically at 10 minutes and increased again as the reaction progressed, with 5 minutes having the highest emission maxima. The narrow emission width is attributed to the efficiency of the HDA in electronically passivating the surface defects which are normally associated with the semiconductor nanoparticles (Oluwafemi *et al.*, 2009). The PLQY of the materials ranged between 51 and 64 % throughout the reaction. The particles emit in the yellow region under the UV light as shown in Figure 28.

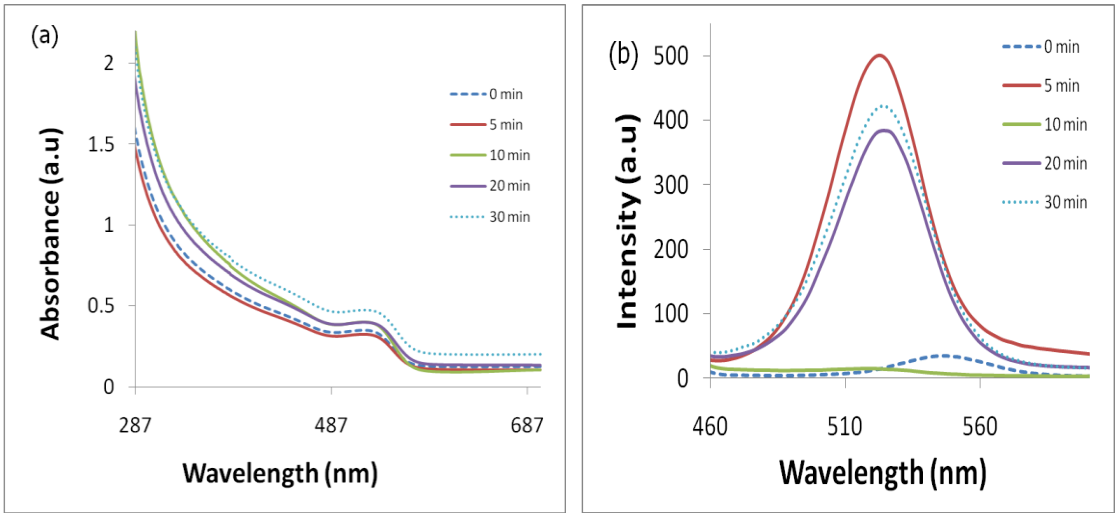


Figure 27: (a) Absorption and (b) photoluminescence ($\lambda_{400\ nm}$) spectra of HDA-capped CdSe NPs at 160 °C at different reaction times.

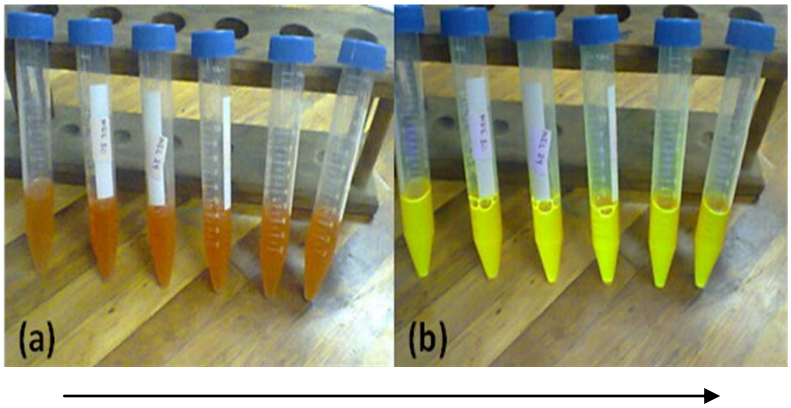


Figure 28: Photographs showing the colour of HDA-capped CdSe NPs at 160 °C under (a) visible light and under (b) UV light at 0, 5, 10, 20, 30 and 60 min.

Table 18: Optical properties of HDA-capped CdSe NPs at 160 °C.

Time	Excitonic peak (nm)	Band edge (nm)	PL emission (nm)	PL intensity (nm)	FWHM	Particle size (nm)	PL QE (%)
0 min	525	572	543	33	39	2.63	64
5 min	525	572	519	489	44	2.63	51
10 min	529	572	519	14	48	2.68	64
20 min	525	572	520	370	42	2.63	59
30 min	530	571	520	413	44	2.70	-------

*Note: ------- Cannot be determined from the spectrum

Figure 29 (a) showed the absorption spectra of the HDA-capped CdSe NPs at 200 °C. The absorption spectra showed no significant shift in the absorption band edge as the reaction time proceeded. This might indicate that the particles were of the same average diameter. In the PL spectra shown in Figure 29 (b) narrow emission curves were observed with emission maxima ranging between 586 and 589 nm. There was no significant shift in the position of the peaks. The PLQY of the materials ranged between 52 and 68 % throughout the reaction. The materials were red under normal light and emit an orange colour under UV light (Figure 30), which confirmed what was observed in both the UV and PL.

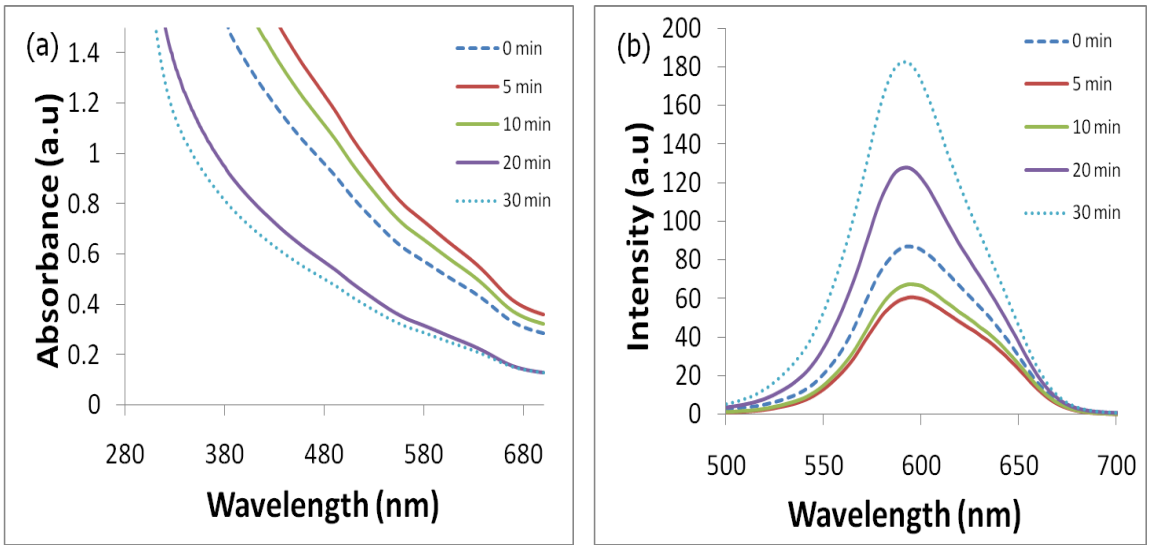


Figure 29: (a) Absorption and (b) photoluminescence ($\lambda_{400\ nm}$) spectra of HDA-capped CdSe NPs at 200 °C at different reaction times.

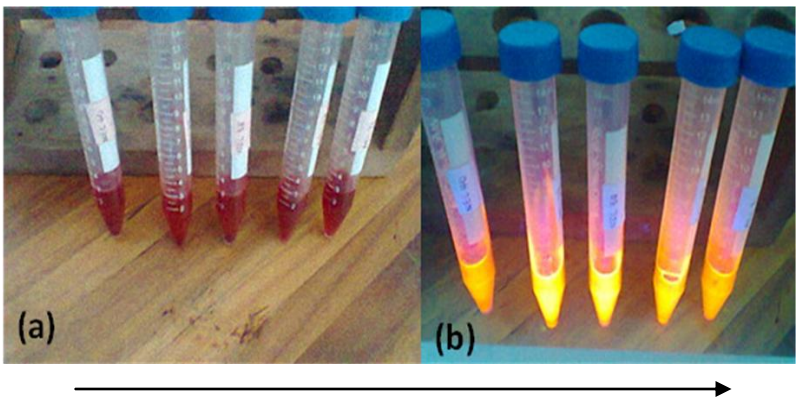


Figure 30: Photographs showing the colour of HDA-capped CdSe NPs at 200 °C under (a) visible light and under (b) UV light at 0, 5, 10, 20, 30 and 60 min.

Table 19: Optical properties of HDA-capped CdSe NPs at 200 °C.

Time	Excitonic peak (nm)	Band edge (nm)	PL emission (nm)	PL intensity (nm)	FWHM	Particle size (nm)	PL QE (%)
0 min	667	664	589	84	68	5.35	55
5 min	666	664	589	54	68	5.35	55
10 min	666	664	589	66	69	5.35	68
20 min	667	662	586	124	65	5.39	54
30 min	667	662	587	180	66	5.39	52

3.3.2 Structural properties

3.3.2.1 Fourier Transform Infrared Microscopy (FTIR)

The surface chemistry of the HDA-capped CdSe NPs at different temperature was investigated using FTIR spectroscopy. The spectra in Figure 31 show that the bands are shifted to higher frequencies when compared to the free ligand. The IR spectra of HDA show characteristic bands at 3331 cm^{-1}, 2929 cm^{-1}, 2919 cm^{1}, 1463 cm^{-1} and 1061 cm^{-1} corresponding to stretching vibration of N–H, C–H (CH_3), C–H (CH_2), CH_2/CH_3 and C–N respectively. The spectra of the as-synthesised materials show a shift to the higher frequency and a decrease in the intensities as the temperature increases. This shift has been reported for amine bound CdSe and may be due to the coordination to the nanocrystallites (Oluwafemi and Revaprasadu, 2008).

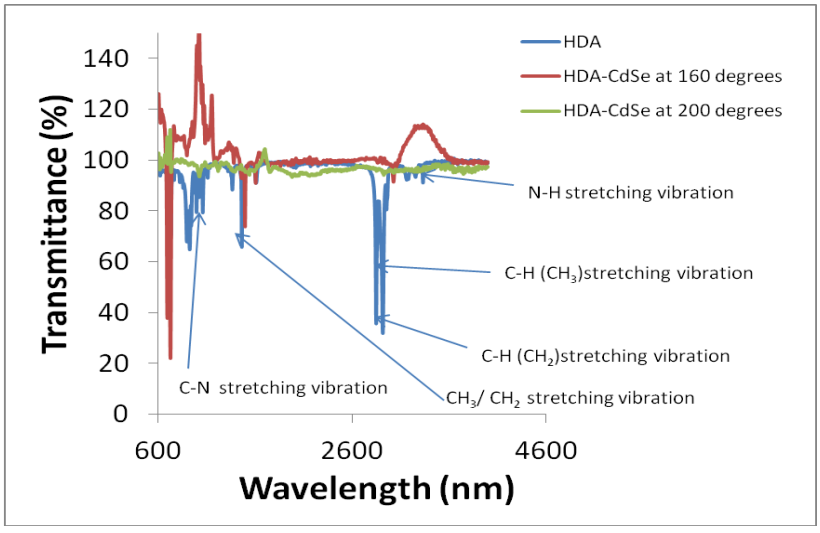


Figure 31: FTIR spectra for HDA and HDA-capped CdSe NPs at 160 and 200 °C.

3.3.2.2 TEM, HRTEM and FFT

The representative TEM micrograph of the HDA-capped CdSe NPs is shown in Figure 32 (a). The TEM results indicate that the materials are small, well dispersed and spherical in shape. The diameters of the spherical particles are within 2.941 nm to 4.388 nm range, with average particle diameter of 3.175 nm ± 0.458 nm. The presence of the lattice fringe in the high resolution TEM (HRTEM) confirms that the as-prepared materials are highly crystalline. The FFT patterns on figure 32 (c) show sharp and clear singular reciprocal points supporting the conclusion that the nanoparticles are single crystals.

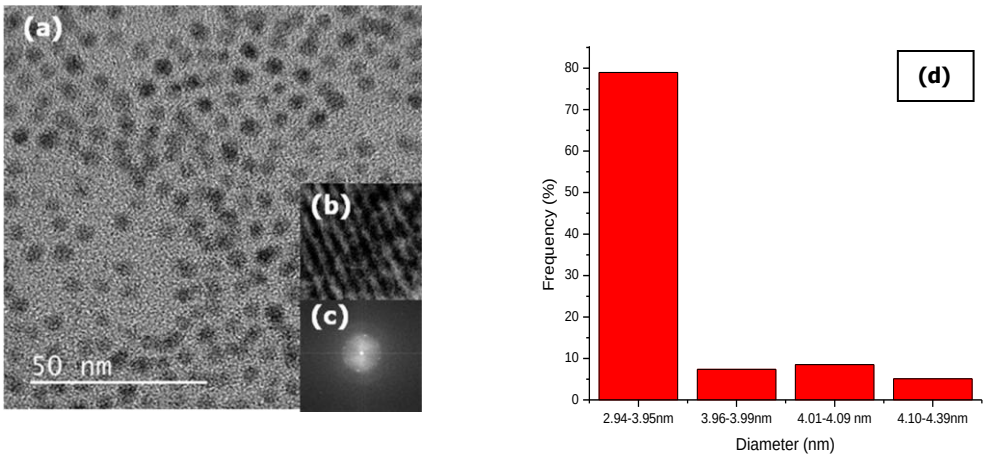


Figure 32: TEM (a) HRTEM (b) FFT (c) images and size distribution (d) of HDA-capped CdSe NPs at 200 °C.

3.4 Synthesis of Au doped CdSe nanostructures

3.4.1 HDA-capped Au-CdSe nanostructures

The colour of the CdSe solution changed from milky white to an intense yellow within the first 15 minutes after the addition of selenium precursor and black colour after the addition of gold salt.



Figure 33: A photograph showing the colour of the CdSe NPs after the addition of selenium precursor to the Au-Cd complex.

3.4.1.1 Optical properties

Figure 34 (a) shows the absorption spectra of HDA-capped Au doped CdSe NPs at 160 °C and different reaction times. At the beginning of the reaction neither excitonic shoulder nor sharp absorption edge was observed but later appeared at 5 minutes. The 30 mins peak overlay the 20 minutes peak, indicating no further increase in the absorption spectra (Oluwafemi *et al.*, 2014). It was also observed that the band edge red shifted as the reaction time was increased due to the increase in particle size and

blue shifted when compared to the bulk CdSe due to quantum confinement effects. The photoluminescence spectra of HDA-capped Au doped CdSe NPs at 160 °C and at different reaction times are shown in Figure 34 (b). The emission intensity also increased with time and dropped at 30 minutes with 20 minutes having maximum intensity. The highest PLQY throughout the reaction was 87 %. Figure 35 show that the particles were black under normal light (a) and emit at green region under UV light (b).

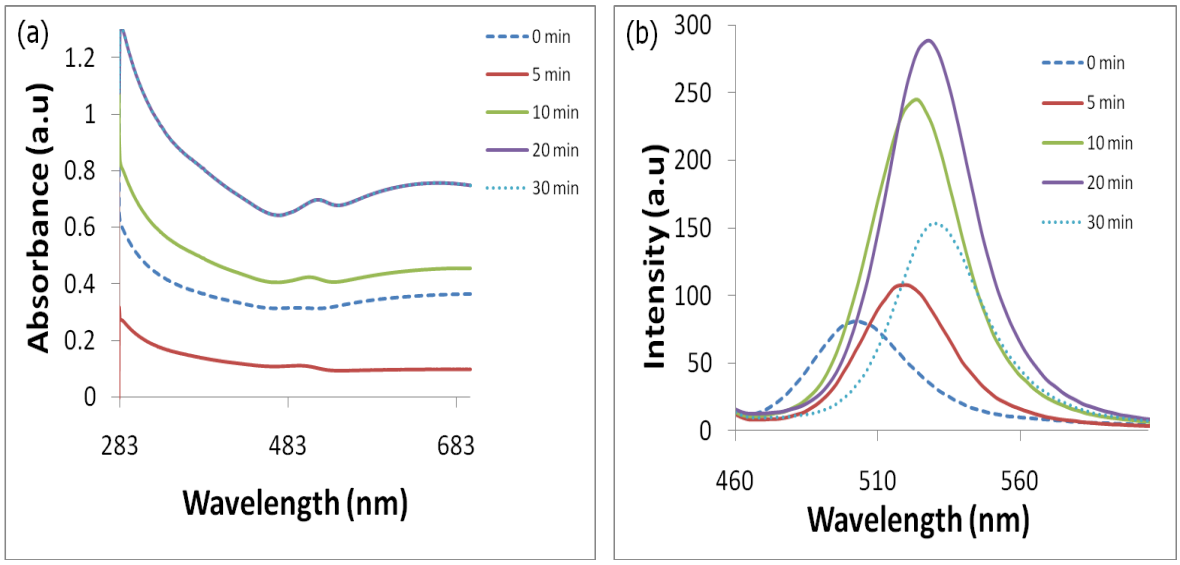


Figure 34 (a) Absorption and (b) photoluminescence ($\lambda_{400\ nm}$) spectra of Au doped HDA-capped CdSe at 160 °C at different reaction times.

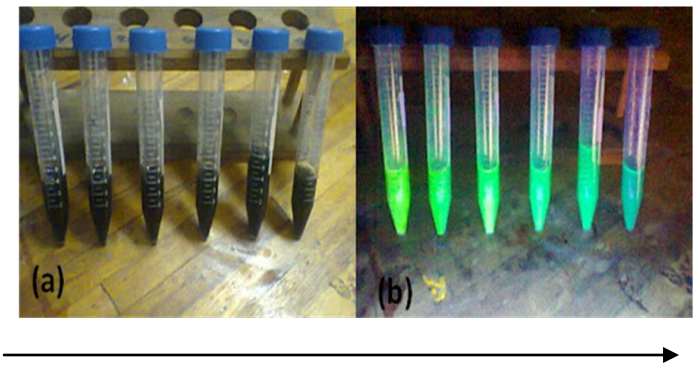


Figure 35: Photographs showing the colour of Au-doped HDA-capped CdSe NPs at 160 °C under (a) visible light and under (b) UV light at 0, 5, 10, 20, 30 and 60 min.

Table 20: Optical properties of HDA-capped Au doped CdSe NPs at 160 °C.

Time	Excitonic peak (nm)	Band edge (nm)	PL emission (nm)	PL intensity (nm)	FWHM	Particle size (nm)	PL QE (%)
0 min	-------	-------	501	73	42	-------	48
5 min	497	536	517	98	38	2.53	43
10 min	508	536	519	242	40	2.53	87
20 min	511	540	524	280	39	2.57	-------
30 min	511	540	525	146	42	2.57	83

*Note: ------- Cannot be determined from the spectrum

Figure 36 (a) shows the absorption spectra for HDA-capped Au doped CdSe NPs at 200 °C and at different reaction times. The spectra showed that there was a clear red shift in the excitonic peak as the reaction time was increased while the band edge slightly red shifted as shown on Table 21. Due to quantum confinement effects all the materials

were blue-shifted when compared to the bulk CdSe. Figure 36 (b) is the photoluminescence spectra of HDA-capped Au doped CdSe at 200 °C and at different reaction times. In these spectra a slight shift towards the red region as the reaction time increased was observed. The intensity slightly increased with time, with maximum intensity observed at 20 minutes. The FWHM ranged from (55 – 58) nm during the course of the reaction in the order shown in Table 21. The materials were brownish in colour under normal light and emit a dark orange colour under the UV light, which confirmed the emitting position observed in both the UV and PL shown in Figure 37.

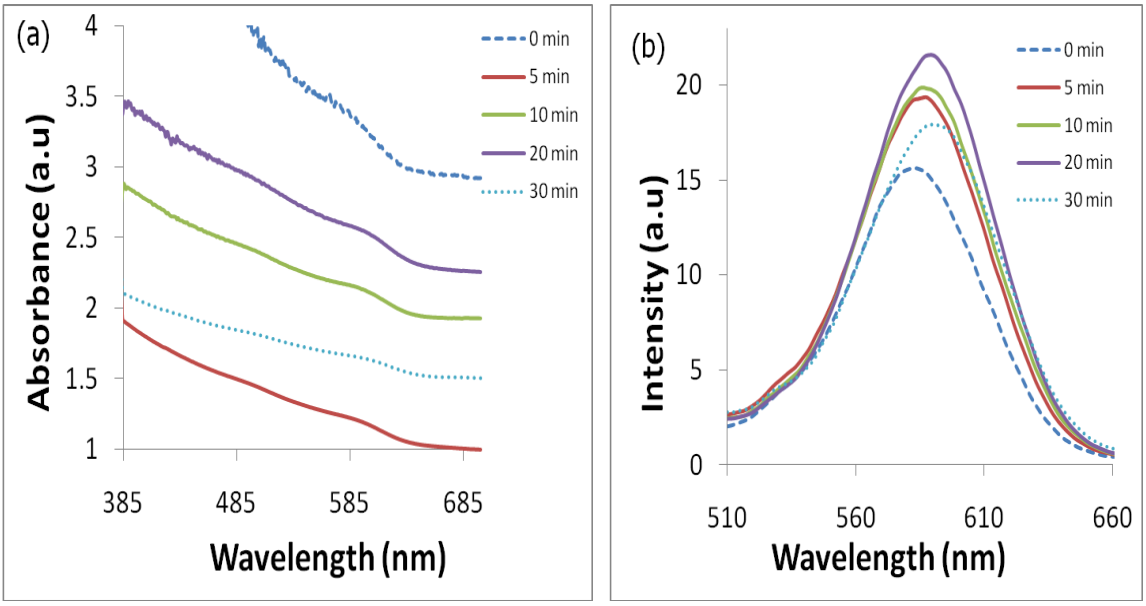


Figure 36: (a) Absorption and (b) photoluminescence ($\lambda_{400\ nm}$) spectra of Au doped HDA-capped CdSe NPs at 200 °C at different reaction times.

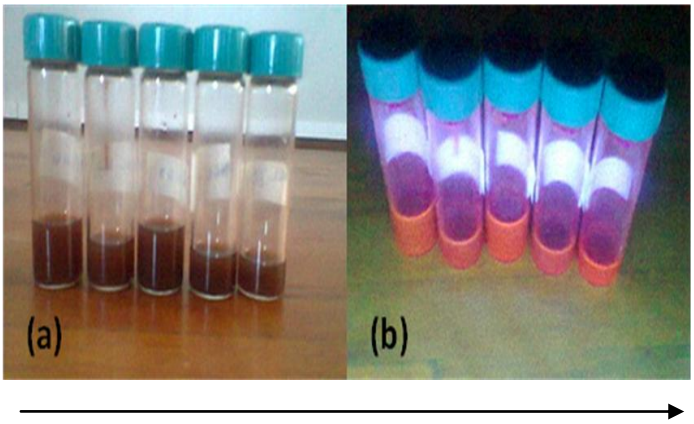


Figure 37: Photographs showing the colour of Au-doped HDA-capped CdSe NPs at 200 °C under (a) visible light and under (b) UV light at 0, 5, 10, 20 and 30 min.

Table 21: Optical properties of HDA-capped Au doped CdSe NPs at 200 °C.

Time	Excitonic peak (nm)	Band edge (nm)	PL emission (nm)	PL intensity (nm)	FWHM	Particle size (nm)	PL QE (%)
0 min	597	629	578	16	57	4.45	93
5 min	600	630	583	19	55	4.58	99
10 min	605	630	584	20	56	4.81	-------
20 min	610	631	585	21	56	5.06	99
30 min	613	633	587	19	58	5.21	99

*Note: ------- Cannot be determined from the spectrum

The absorption spectra of HDA-capped Au doped CdSe at 240 ^{o}C are shown in Figure 38 (a). There was a little shift in the position of the band edge as the reaction time increased. This indicated that increasing the reaction time did not have any pronounced

effect on the band gap thus; the reaction can be terminated within a short period of time. Due to quantum confinement all the materials were blue-shifted when compared to the bulk CdSe. Figure 38 (b) shows the photoluminescence spectra for HDA-capped Au doped CdSe at 240 °C. Similar to the UV spectra there was no significant shift in the position of the peaks which confirmed the earlier proposition that the reaction time does not have significant effect at this temperature. However, the intensity of the materials drastically decreases after 2 minutes. This indicated that continuation of the reaction resulted in disordering the surface of the materials. This resulted in surface defect which prevented radiative recombination of the exciton. Thus, reduction in the emission intensity as the reaction time increased. Similar observations have been reported by Hu *et al.*, 2012. The FWHM range was (46 – 52) nm and the PLQY range was (25 – 37) % in the order shown in Table 22. The materials are black under normal light and emit are red colour under UV light (Figure 39).

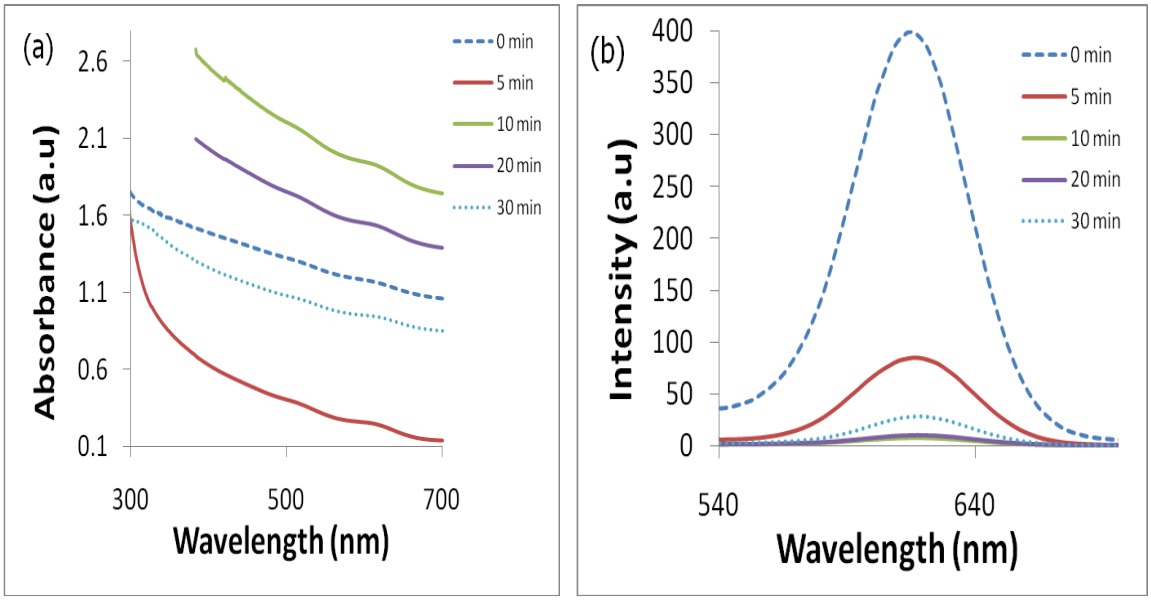


Figure 38: (a) Absorption and (b) photoluminescence ($\lambda_{400\ nm}$) spectra for Au doped HDA-capped CdSe NPs at 240 °C at different reaction times.

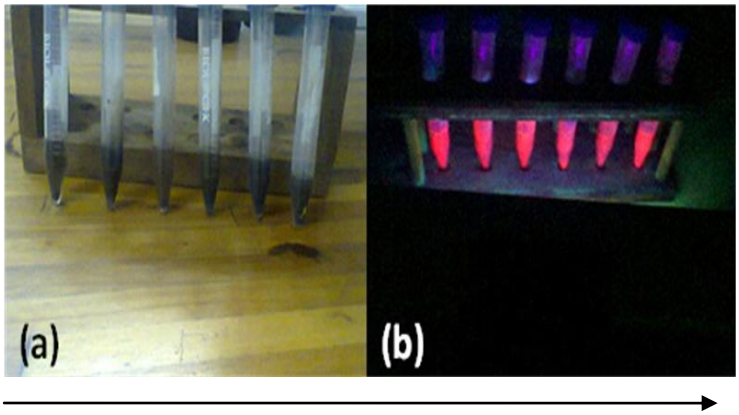


Figure 39: Photographs showing the colour of Au-doped HDA-capped CdSe NPs at 240 °C under (a) visible light and under (b) UV light at 0, 5, 10, 20, 30 and 60 min.

Table 22: Optical properties of HDA-capped Au doped CdSe NPs at 240 °C.

Time	Band edge (nm)	PL emission (nm)	PL intensity (nm)	FWHM	Particle size (nm)	PL QE (%)
0 min	638	610	391	51	4.20	33
5 min	641	613	84	52	4.29	25
10 min	646	612	7	50	4.45	34
20 min	649	612	9	48	4.56	37
30 min	641	613	28	46	4.29	34

3.4.2 Structural properties

3.4.2.1 Fourier Transform Infrared Microscopy (FTIR)

The surface morphology of the CdSe NPs was investigated by IR to confirm the capping of the particles by HDA. The IR spectra of HDA (Figure 40) show characteristic bands at 3331 cm^{-1}, 2929 cm^{-1}, 2919 cm^{1}, 1463 cm^{-1} and 1061 cm^{-1} corresponding to the stretching vibration of N–H, C–H (CH_3), C–H (CH_2), CH_2/CH_3 and C–N respectively. The spectra of the as-synthesized materials show a shift to higher frequency and a decrease in the intensities as the temperature increases. The shift has been reported for amine bound CdSe and may be due to the coordination to the nanocrystallites (Oluwafemi and Revaprasadu, 2008).

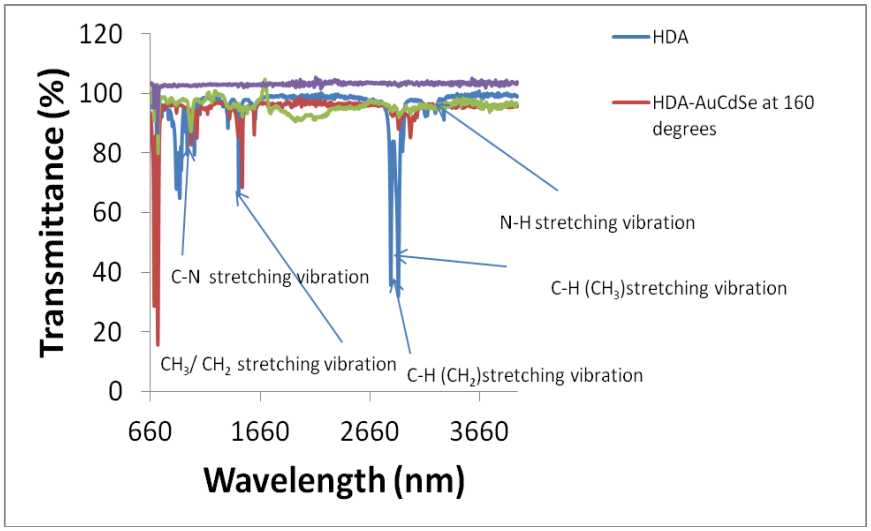


Figure 40: FTIR spectra for HDA and HDA-capped Au doped CdSe NPs at 160, 200 and 240 ° C.

3.4.2.2 TEM, HRTEM and FFT

The TEM image of the Au doped HDA-capped CdSe materials at 160 ^{o}C shows that the materials are small, well dispersed and spherical in shape (Figure 41 a). The diameters of the spherical particles are within 2.97 nm to 10.89 nm, with an average particle diameter of 3.53 nm with standard deviation of 1.315 nm as shown in the size distribution graph in Figure 41 (d). The presence of the lattice fringe in the high resolution TEM (HRTEM) in Figure 3.41 (b) confirms the highly crystalline nature of the as-prepared materials. The FFT patterns in Figure 3.41 (c) show sharp and clear singular reciprocal points supporting the conclusion that the nanoparticles are single crystals.

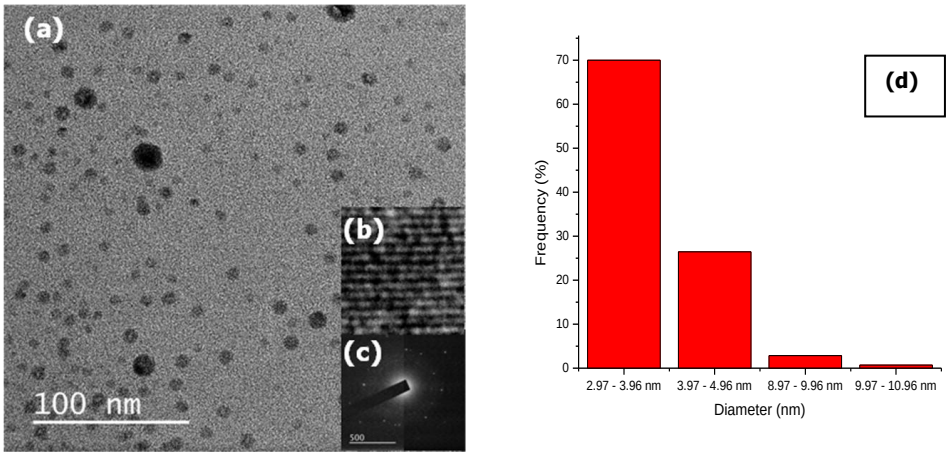


Figure 41: TEM (a) HRTEM (b) FFT (c) images and size distribution (d) of HDA-capped Au-CdSe NPs at 160 °C

3.5 Ligand Exchange

3.5.1 Optical Properties

The absorption spectra of doped and undoped water soluble nanoparticles CdSe NPs after ligand exchange are shown in Figure 42. The spectra shows that the particles synthesized at 160 °C (doped and undoped) are blue shifted compared to the organically capped CdSe NPs. Excitonic peaks are observed for those particles at 200 °C with a band edge that is slightly red-shifted for the undoped and doped compared to the organic soluble particles. A blue shift is also observed for the particles at 240 °C when compared to the organic particles. These shifts may be attributed to the increase and decrease in the size of the particles. The photoluminescence showed no fluorescence and there was no luminescence under the UV light.

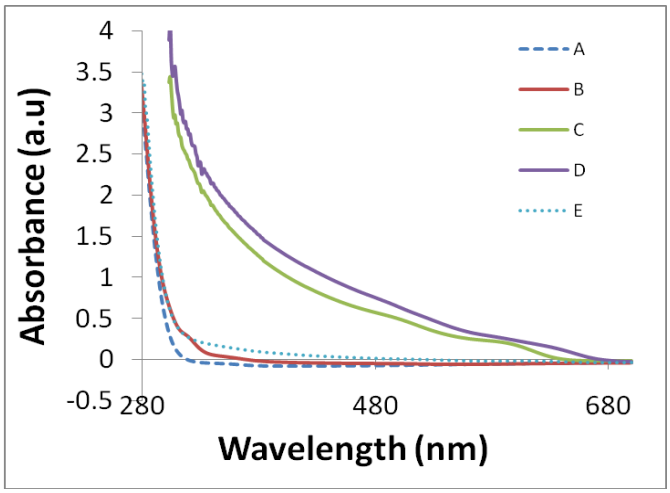


Figure 42: Absorption spectra after ligand exchange for (A) Au doped CdSe NPs at 160 °C, (B) HDA-capped CdSe NPs at 160 °C, (C) Au doped CdSe NPs at 200 °C, (D) HDA-capped CdSe NPs at 200 °C and (E) Au -doped CdSe NPs at 240 °C.

Table 23: Optical properties after ligand exchange for both doped and undoped CdSe NPs at 160, 200 and 240 °C.

Sample	Excitonic peak (nm)	Band edge (nm)	PL emission (nm)	Intensity (1st day)	Intensity (7 days)	Intensity (28 days)	Particle size (nm)
Au (160)	-------	316	598.19	10.46	13.98	14.85	1.31
HDA(160)	-------	330	610.66	16.03	22.64	23.20	1.36
Au (200)	593	633	610.66	3.57	2.59	2.12	4.05
HDA(200)	633	670	610.66	5.66	3.65	2.57	5.60
Au (240)	-------	321	610.66	7.53	8.19	7.66	1.33

*Note: ------- Cannot be determined from the spectrum

CHAPTER 4

4.1 Conclusion

A facile synthetic method for the synthesis of aqueous soluble and organic soluble CdSe NPs doped with gold was reported. Selenium powder was successfully reduced using sodium sulphite to produce a stable selenium precursor that can be stored for a long period. A systematic study of the effects of parameters like mole ratio, temperature, capping agent, growth time and cadmium precursor on the size, optical properties and morphology of the nanoparticles were investigated. The as-synthesized materials were characterized using UV-Visible spectroscopy, PL spectroscopy, FTIR, TEM and HRTEM.

The effect of the mole ratio showed that there was a blue shift in the band edge position as the ratio increased indicating decrease in particle size. Due to their smaller nature, the particles synthesized under the 4:1 ratio gave the highest luminescence intensity. The TEM micrographs show that the as-synthesized materials at ratios 1:1, 2:1, 3:1 and 4:1 are spherical in shape. The effect of temperature showed a red shift in the position of the band edge as the temperature increased, indicating an increase in the particle size. High temperatures resulted in the presence of surface defects which serve as traps for the exciton recombination. Hence, the intensity became extremely low as compared to the materials synthesized at room temperature. The shape of the materials was not affected by the change in temperature, they were all spherical. Looking at the different capping agents the band edge of the nanoparticles are red-

shifted in the order MPA < cysteine <PST < citrate, indicating that the particle size increases in the order of 2.08 nm < 2.25 nm < 2.26 nm < 2.30 nm for MPA, cysteine, PST and citrate respectively. The intensities however increase in a different order of MPA < PST < cysteine < citrate but only cysteine capped CdSe NPs fluoresced under the UV light in the yellow region. The effect of growth time indicated that MPA-capped CdSe NPs showed very distinct excitonic peaks and band edges which shift to the red region after ageing for seven days. The peaks became less distinct as compared to the early stages of the reaction. The PST- capped CdSe NPs on the other hand showed complete opposite trend to the MPA- capped CdSe NPs. It showed no absorption features throughout the growth time while for the cysteine- capped CdSe NPs and citrate-capped CdSe NPs, the peaks were not as visible as the ones obtained for MPA-capped CdSe NPS. However, a slight red shift was observed as growth time increased. The PL spectrum of the MPA- capped CdSe NPs showed very poor luminescence at the beginning of the reaction. Growth time did improve the luminescence intensity but it was not symmetrical and contained a lot of defects. The luminescence intensity of the citrate-capped CdSe NPs increased with time with a slight shift in the position of the emission maxima. However, the intensity became reduced drastically after 7 days and no fluorescence was observed under the UV light. Ageing improved the fluorescence intensity and width of the cysteine-capped CdSe NPs throughout the growth time. Better and higher luminescence intensity was observed for the PST- capped CdSe NPs as compared to the MPA-capped CdSe NPs. However, growth time did not have any

impact on the materials inability to fluoresce under the UV light. The effect of cadmium precursor on the citrate- capped CdSe NPs showed that absorption features are observable from the beginning of the reaction when cadmium chloride was used but were only observed after 3 hours when cadmium acetate and cadmium nitrate were used. The particle size range from 1 day to 35 days are (2.16 – 3.75) nm, (3.37 – 3.53) nm and (3.40 – 3.75) nm for $CdCl_2$, $Cd(CH_3COO)_2$ and $Cd(NO_3)_2$ respectively. The fluorescence intensity of the materials when cadmium acetate and cadmium nitrate were used was quenched with broad peaks as compared to when cadmium chloride is used. Changing the cadmium source did not hinder any fluorescence under the UV light. For the cysteine-capped CdSe NPs, red shifts in the band edge position was observed when $Cd(CH_3COO)_2$ and $Cd(NO_3)_2$ were used. The particle size for these cadmium precursors increased in the order $CdCl_2$ < $Cd(CH_3COO)_2$ < $Cd(NO_3)_2$. The luminescence intensity also increased in this order however, the quantum yield at 7 days is the same when $Cd(CH_3COO)_2$ and $Cd(NO_3)_2$ were used but higher when $CdCl_2$ was used. Varying the cadmium precursor did not produce any change in the region the materials emit under UV light. For the PST- capped CdSe NPs no absorption features were observed when $CdCl_2$ was used, however a positive turnaround was observed as absorption features appeared after 3 hours of reaction time when $Cd(CH_3COO)_2$ and $Cd(NO_3)_2$ were used. The particle size was (3.13 – 3.97) nm and (3.21 -4.03) nm for $Cd(CH_3COO)_2$ and $Cd(NO_3)_2$ respectively. There was no significant change in the intensity nor the width of the peaks for nanoparticles produced using the three

precursors. Although, varying the cadmium precursor had a positive effect on the absorption features, it did not have any effect on the fluorescence of the materials. The MPA-CdSe NPs showed that the band edge was more or less in the same area and the particle size range from (2.08 – 3.87) nm, (2.02 – 3.65) nm and (2.06 – 3.73) nm for $CdCl_2$, $Cd(CH_3COO)_2$ and $Cd(NO_3)_2$ respectively. Varying the cadmium precursor neither improved the poor luminescence intensity, symmetry nor the fluorescence of the materials. However, it did have an effect on the shape of the materials as both spherical and short rods were observed from the TEM micrographs when $Cd(CH_3COO)_2$ was used as the precursor.

After carefully studying these parameters, the reaction carried out using the mole ratio of 4:1 with cysteine and $CdCl_2$ as the capping agent and cadmium precursor respectively gave the best optical properties. These conditions were used to investigate the effect of the dopant on the optical properties of the as-synthesized CdSe NPs. The results showed that the doped CdSe NPs have high luminescence intensity as compared to the undoped ones indicating that, the impurity which is the dopant increased the intensity of the materials. The doped nanoparticles emitted in the yellow region, however, the fluorescence only lasted for a few days compared to the undoped materials. The emission intensity increased with decrease in the Cd:Au ratio in the order 1:20 < 1:40 <1:60. The particle size were in the range 2.19 -3.25 nm, 1.97-2.48 nm and 1.99 -2.37 nm for the Cd:Au ratio of 1:20, 1:40 and 1:60 respectively. This indicates the Cd:Au ratio is directly proportional to the particle size and inversely

proportional to the intensity. The presence of the dopant improved the quantum yield of the as-synthesized CdSe NPs

The organically synthesized CdSe NPs followed the same trend as water soluble CdSe NPs. The doping increased the fluorescence intensity of the CdSe NPs synthesized at 160 °C but decreased at 200 °C and 240 ^{o}C. However for the undoped CdSe NPs, the emission intensity increased as the temperature increased. The particle size increased as the temperature and reaction time increased for both the CdSe and Au-CdSe nanostructures. The Au-CdSe synthesized at 200 °C had the highest quantum yield of 99%. The TEM images show that the CdSe nanoparticles are monodispersed, spherical in shape and have a narrow size distribution. The HRTEM images confirmed the nanocrystalline nature of the as-synthesized CdSe NPs while the FTIR confirmed the passivation of the nanoparticles by the capping agents.

Comparing the direct aqueous synthesis and the synthesis via ligand exchange it was observed that the intensity was very low for the ligand exchange particles. The particle size of the materials synthesized at 160 °C and 240 °C are smaller after the ligand exchange as compared to original sample except for those at 200 °C.

4.2 Recommendations

In this work, the effect of Cd:Se ratio, temperature, capping agent, growth time and cadmium precursor on the particle size, shape, optical properties and structural properties were investigated on the as-synthesized CdSe NPs before incorporating the metal. From the results of the analyses it is recommended that, the effect of pH should be investigated as this might have a significant effect on the capping agents. In addition, the energy dispersive spectroscopy (EDS) as well as x-ray photoelectron spectroscopy (XPS) analyses should be carried out to ascertain the presence of the corresponding elements as well as to know whether the dopant is on the surface or inside the nanoparticles. Furthermore, application of these materials in photocatalytic devices will be a good area to venture into due to the high luminescence efficiency of the as-synthesized materials.

PRESENTATIONS AT ACADEMIC CONFERENCES

(1) Nelisa N. Gaxela, Oluwatobi S. Oluwafemi, Sandile P. Songca and Olisoji O. Olujimi (2012): Effect of II-VI ratio on the luminescence of water soluble CdSe nanoparticles. 5th Walter Sisulu University International Research Conference, East London, 22-24 August.

(2) Nelisa N. Gaxela, Oluwatobi S. Oluwafemi and Sandile P. Songca (2013): Effect of temperature on the size and optical properties of HDA-capped Au doped CdSe nanoparticles. Inorg2013 Conference, Kwazulu Natal, 30 June – 4 July.

(3) Nelisa N. Gaxela, Oluwatobi S. Oluwafemi and Sandile P. Songca (2013): A facile synthesis of water soluble cysteine-capped CdSe nanoparticles using different cadmium sources. SACI National 2013 Convention, East London, 1-6 December 2013.

REFERENCES

Ayele, D. W., Chen, H.-M., Su, W.-N., Pan, C.-J., Chen, L.-Y., Chou, H.-L., Cheng, J.-H., Hwang, B.-J. and Lee, J.-F. 2011. Controlled synthesis of CdSe quantum dots by a microwave-enhanced process: A green approach for mass production. *Chem. Eur. J.*, 17, pp.5737-5744.

Bao, N., Shen, L., Takata, T. and Domen, K. 2008. Self-templated synthesis of nanoporous CdS nanostructures for highly efficient photocatalytic hydrogen production under visible light. *Chem. Mater.*, 20, pp. 110-117.

Beydoun, D., Amal, R., Low, G. and McEvoy, S. 1999. Role of nanoparticles on photocatalysis. *Journal of Nanoparticle Research*, 1, pp.439-458.

Bhattacharyya, S., Zitoun, D., Estrin, Y., Moshe, O., Rich, D. H. and Gedanken, A. 2007. A one-step, template-free synthesis, characterization, optical and magnetic properties of ZnMnTe nanosheets. *Chemistry of Materials*, 21, pp.326-335.

Chen, X., Lou, Y. and Burda, C. 2004. Spectroscopic investigation of II-VI core-shell nanoparticles: CdSe/CdS. *International Journal of Nanotechnology*, 1, pp. 105-118.

Chen, J., Zhao, D. W., Lei, W., Sun, X. W., Song, J. and Deng, W. 2009. A highly effective method for synthesizing hybrid Pt-CdSe nanocomposites. *Applied Surface Science*, 256, pp. 1526-1529.

Chili, M.M., Rajasekhar Pullabhotla, V. S. R. and Revaprasadu, N. 2012. Synthesis of PVP-capped Au-CdSe hybrid nanoparticles. *ISRN Metallurgy,* 2012, pp. 1-4.

Costi, R., Saunders, A. E., Elmalem, E., Salant, A. and Banin, U. 2008. Visible light–induced charge retention and photocatalysis with hybrid CdSe-Au nanodumbbells. *Nano Letters*, 8, pp. 637-641.

Deng, Z., Cao, L., Tang, F. and Zou, B. 2005. A new route to zinc-blende CdSe nanocrystals: Mechanism and Synthesis. *J. Phys. Chem. B*, 109, pp. 16671-16675.

Dukovic, G., Merkle, G. M., Nelson, J. H., Hughes, S. M. and Alivisatos, A. P. 2008. Photodeposition of Pt on colloidal CdS and CdSe @ CdS semiconductor nanostructures. *Advanced Materials*, 20, pp. 4306-4311.

Gadalla, A., Mohamed, M. and Hamad, D. 2013. Synthesis and characterization of Au/CdSe and Ag/CdSe core/shell nanoparticles. *International Journal of Metallurgical & Materials science and Engineering (IJMMSE),* 3, pp. 59-68.

Ghaedi, M., Amirad, S. Z., Marahel, F., Kokhdan, N. S., Sahraei, M. and Daneshfar, A., 2011. Synthesis and characterization of cadmium selenide nanoparticles loaded on activated carbon and its efficient application for removal of muroxide from aqueous solution. *Spectrochimica Acta Part A: Molecular and Biomolecular Spectroscopy,* 83, pp. 47-51.

Gao, B., Lin, Y., Wei, S., Zeng, J., Liao, Y., Chen, L., Goldfeld, D., Wang, X., Luo, Y., Dong, Z. and Hou, J. 2012. Charge transfer and retention in directly coupled Au-CdSe nanohybrids. *Nano Research*, 5, pp. 88-98.

Green, M. A. and O'Brien, P. 1999. Recent advances in the preparation of semiconductors as isolated nanometric particles: new routes to quantum dots.

Chemical Communications, pp. 2235-2241.

Gupta, P. and Ramrakhaini, M. 2009. Influence of the particle size on the optical properties of CdSe nanoparticles. *The Open Nanoscience Journal*, 3, pp. 15-19.

Hines, M. A. and Guyot-Sionnest, P. J. 1996. Synthesis and characterization of strongly luminescing ZnS-capped CdSe Nanocrystals. *Journal of Physical Chemistry*, 100, pp. 468-471.

Hu, M., Yu, H., Wei, F., Xu, G., Yang, J., Cia, Z. and Hu, Q. 2012. Citrate-capped Mn-modified CdSe/Cds quantum dots as luminescent probes for levodopa detection in aqueous solution. *Spectrochimica Acta part A: Molecular and Biomolecular Spectroscopy*, 91, pp. 130-135.

Idowu, M., Lamprecht, E. and Nyokong, T. 2008. Interaction of water-soluble thiol capped CdTe quantum dots and bovine serum albumin. *Journal of Photochemistry and Photobiology A: Chemistry*, 198, pp. 7-12.

Ingole, P. P., Abhyankar, R. M., Prasad, B. L. V. and Haram, S. K. 2010. Citrate-capped quantum dots of CdSe for the selective photometric detection of solver ions in aqueous solutions. *MaterialScience and Engineering B*, 168, pp. 60-65.

Joo, J. H., Hodelin, J. F., Hu, E. L. and Haberer, E. D. 2012. Viral-assisted assembly and photoelectric response of individual Au/CdSe core-shell nanowires. *Materials Letters,* 89, pp. 347-350.

Kaiser, J., Leppert, L., Welz, H., Polzer, F., Wunder, S., Wanderka, N., Albrecht,

M., Lunkenbein, T., Breu, J., Ku¨mmel, S., Lu, Y., and Ballauff, M., 2012. Catalytic activity of nanoalloys from gold and palladium. *Phys. Chem. Chem.Phys.,* 14, pp. 6487-6495.

Kawai, M. and Yamamoto, A. 2012. Spacer thickness dependence of photoluminescence and raman scattering spectra in Au/spacer/CdSe-nanoparticle monolayers. *Physics Procedia,* 29, pp. 25-29.

Li, J., Li, D., Hong, X., Wang, L., Zhao, K., Li, J., Bai, Y. and Li, T. 2004. Unique structure and photoluminescence of Au/CdTe nanostructure materials. *Chem. Commun.,* pp. 982-983.

Li, J. H., Ren, C. L., Liu, X. Y., Hu, Z. D. and Xue, D. S. 2007. "Green" synthesis of starch capped CdSe nanoparticles at room temperature. *Materials Science and Engineering*, 458, pp. 319-322.

Li, P. and Lappas, A. 2013. CdSe-Au nanorods networks welded by gold domains – a promising structure for nano-optoelectronic components. *Journal of Nanoparticle Research,* 14, pp. 1-12.

Liu, L., Xu, X., Lei, J., Liu, Y. and Yang, Z. 2011. Annealing structured Au nanoparticles enhanced light emission from CdSe quantum dots. *Thin Solid Films,* 519, pp. 5582-5587.

Liu, A., Rena, Q., Yuan, M., Xu, T., Tan, M., Zhao, T., Dong, W. and Tang, W. 2013. Layer-by-layer assembled porous CdSe films incorporated with plasmonic gold and improved photoelectrochemical behaviors. *Electrochimica Acta*, 108, pp. 680-689.

Lo, S., Liu, Z., Li, J., Chan, L. H. and Yang, F. 2013. Hybrid solar cells based on poly(3-hexylthiophene) and electrospun TiO2 nanofibers modified with CdS nanoparticles. *Progress in Natural Science: Materials International*, 23, pp. 514-518.

Mahmoud, W. E., Al-Amri, A. M., Yaghmour, S. J. 2012. Low temperature synthesis of CdSe capped 2-mercaptoethanol quantum dots. *Optical Materials*, 34, pp. 1082-1086.

Malik, M. A., O'Brien, P. and Revaprasadu, N. 2000. Semiconductor nanoparticles: their properties, synthesis and potential for application. *South African Journal of Science,* 96, p.55.

Malik, M. A., O'Brien P. and Revaprasadu, N. 2005. Precursor routes to semiconductor quantum dots. *Phosphorus, sulphur and silicon and the Related Elements*, 180, pp. 689-712.

Mao, J., Cao, X., Zhen, J., Shao, H., Gu, H., Lu, J. and Ying, J. Y. 2011. Facile synthesis of hybrid nanostructures from nanoparticles, nanorods and nanowires. *Journal of Material Chemistry,* 21, pp. 11478-11481.

Maseko, N. N., Revaprasadu, N., Rajasekhar Pullabotla, V. S. R., Karthik, R. and O'Brien, P. 2010. The influence of the cadmium source on the shape of CdSe nanoparticles. *Materials Letters*, 64, pp. 1037-1040.

Mokari, T., Ronthenberg, E., Popov, I., Costi, R. and Banin, U. 2004. Selective Growth of Metal Tips onto Semiconductor Quantum Rods and Tetrapods. *Science*, 304, pp. 1787-1790.

Mokari, T., Sztrum, C. G., Salant, A., Rabani, E. and Banin, U. 2005. Formation of asymmetric one-sided metal-tipped semiconductor nanocrystal dots and rods. *Nature Materials,* 4, pp. 855-863.

Mokari, T. 2011. Synthesis and characterization of hybrid nanostructures. *Nano Reviews*, 2, pp. 5983-5991.

Nkosi, S. S., Mwakikunga, B. W., Sideras-Haddad, E. and Forbes, A. 2012. Synthesis and characterization of potential iron-platinum drugs and supplements by laser liquid photolysis. *Nanotechnology, Science and Applications,* 5, pp. 27-36.

Oluwafemi, O. S. and Revaprasadu, N. 2007. A novel method to prepare cysteine capped cadmium selenide nanoparticles. *Materials Research Society Proceedings*, 0951, pp. E03-12.

Oluwafemi, S. O., Revaprasadu, N. and Ramirez, A. J., 2008. A novel one-pot route for the synthesis of water-soluble cadmium selenide nanoparticles. *Journal of Crystal Growth*, 310, pp. 3230-3234.

Oluwafemi, O. S. and Revaprasadu, N., 2008. A new synthetic route to organically capped cadmium selenide nanoparticles. *New Journal of Chemistry*, 10, pp. 1432-1437.

Oluwafemi, S. O. and Revaprasadu, N. 2009. Study on growth kinetics of hexadecylamine capped CdSe nanoparticles using electronic properties. *Physica B*, 404, pp. 1204-1208.

Oluwafemi, O. S. 2009. A novel "green" synthesis of starch-capped CdSe nanostructures. *Colloids and Surfaces B: Biointerfaces*, 73, pp. 382-386.

Oluwafemi, O. S., Revaprasadu, N. and Adeyemi, O. O. 2010. A facile "green" synthesis of ascorbic acid-capped ZnSe nanoparticles. *Colloids and Surfaces B: Biointerfaces*, 79, pp. 126-130.

Oluwafemi, O. S., Revaprasadu, N. and Ayedemi, O. O. 2010. A new synthesis of hexadecylamine-capped Mn-doped wurtzite CdSe nanoparticles. *Materials Letters*, 64, pp. 1513-1516.

Oluwafemi, O. S. and Songca, S. P. 2012. A simple one-pot environmentally benign synthesis of ascorbic acid-capped CdSe nanoparticles at room temperature. *Materials Letters*, 75, pp. 84-86.

Oluwafemi, O. S., Ncapayi, V., Adeyemi, O. O. and Songca, S. P. 2014. Size tunable synthesis of monodispersed hexadecylamine-capped CdSe nanostructures. *Materials Letters*, 123, pp. 165-168.

Panda, S. K., Hickey, S. G., Waurisch, C. and Eychmuller, A. 2011. Gradated alloyed CdZnSe nanocrystals with high luminescence quantum yield and stability for optoelectronic and biological applications. *Journal of Material Chemistry,* 21, pp. 11550-11555.

Park, Y. S., Dmytruk, A., Dmitruk, A., Kasuya, A., Takeda, M., Ohuchi, N., Okamoto, Y., Kaji, N., Tokeshi, M. and Baba, Y. 2010. Size-selective growth and stabilization of small CdSe nanoparticles in aqueous solution. *ACS Nano*, 4, pp. 121-128.

Peng, Z. A. and Peng, X. 2001. Mechanism of the shape evolution of CdSe nanocrystals. *Journal of The American Chemical Society*, 123, pp. 1398-1395.

Plante, I. J., Habas, S. E., Yuhas, B. D., Gargas, D. J. and Mokari, T. 2009. Interfacing metal nanoparticles with semiconductor nanowires. *Chemistry of Materials,* 21, pp. 3662-3667.

Pradhan, N., Battaglia, D. M., Liu, Y. and Peng, X. 2007. Efficient, stable, small and wWater-stable doped ZnSe nanocrystal emitters as non-cadmium biomedical labels. *Nano Letters*, 7, pp. 312-317.

Rajasekhar Pullabhotla, V. S. R. and Revaprasadu, N. 2009. A novel route to cysteine capped Au – CdSe hybrid nanoparticles. *Materials Letters*, 63, pp. 2097-2099.

Rodriguez, J. A., Liu, P., Wen, W., Hanson, J. C., Hrbek, J., Perez, M. and Evans, J. 2007. Gold nanoparticles on ceria: importance of O vacancies in the activation of gold. *Topics in Catalysis,* 44, pp. 73-81.

Ruedas-Rama, M. J., Orte, A., Hall, E. A. H., Alvarez-Pez, J. M. and Talavera, E. M. 2011. Quantum dot photoluminescence lifetime-based pH nanosensors. *Chem. Commun.*, 47, pp. 2898-2900.

Salant, A., Amitay-Sadovsky, E. and Banin, U., 2006. Directed self-assembly of gold-tipped CdSe Nanorods. *Journal of American Chemical Society*, 128, pp. 10006-10007.

Schüler, A., Python, M., Valle del Olmo, M. and De Chambrier, E. 2007, Quantum dot containing nanocomposites thin films for photoluminescent solar concentrators. *Solar Energy*, 81, pp. 1159-1165.

Shaviv, E. and Banin, U. 2010. Synergetic effects on second harmonic generation of hybrid CdSe-Au nanoparticles. *American Chemical Society Nano,* 4, pp. 1529-1538.

Singh, S. B., Limaye, M. V., Lalla, N. P. and Kulkarni, S. K. 2008. Copper-ion-induced photoluminescence tuning in CdSe nanoparticles. *Journal of Luminescence*, 128, pp. 1909-1912.

Sounderya, N. and Zhang, Y. 2008. Use of core/shell structured nanoparticles for biomedical applications. *Recent Patents on Biomedical Engineering*, 1, pp. 34-42.

Subramanian, V., Wolf, E. E. and Kamat, P. V. 2004. Catalysis with TiO_2/gold nanocomposites. effect of metal particle size on the fermi level equilibration. *Journal of The American Chemical Society*, 126, pp. 4943-.4950

Shu, T., Zhou, Z., Wang, H., Liu, G., Xiang, P., Rong, Y., Han, H. and Zhao, Y. 2012. Efficient quantum dot-sensitized solar cell with tunable energy band $CdSe_xS_{(1-x)}$ quantum dots. *Journal of Material Chemistry,* 22, pp.10525-10529.

Teng, X. and Jia, X. 2012. Cadmium selenide-gold (CdSe-Au) hybrid nanowires: synthesis and study of charge transfer. *Nanowires-Recent Advances*. [INTECH]: available through http://dx.doi.org/10.5772/52828.

Viswanatha, R., Battaglia, D. M., Curtis, M. E., Mishima, T. D., Johnson, M. B. and Peng, X. 2008. Shape control of doped semiconductor nanocrystals (d-Dots). *Nano Research*, 1, pp. 138-144.

Wang, L. Y., Lou, J., Maye, M. M., Fan, Q., Rendeng, Q., Engelhard, M. H., Wang, C., Lin, Y. and Zhong, C. J. 2005. Iron oxide-gold core-shell nanoparticles and thin film assembly. *Journal of Material Chemistry,* 15, pp. 1821-1832.

Wang, Y., Yang, H., Xia, Z., Tong, Z. and Zhou, L. 2011. One-pot synthesis of CdSe quantum dots using selenium dioxide as a selenium source in aqueous solution. *Bull. Korean Chem. Soc.*, 32, pp. 2316-2318.

Wang, F., He, C., Han, M., Wu, H. and Xu, G. Q. 2012. Chemical controlled reversible gold nanoparticles dissolution and reconstruction at room temperature. *Chemical communications*, 48, pp. 6136-6138.

Wei, Z., Li, Y., Luo, S., Liu, C., Meng, D., Ding, M. and Zeng, G. 2014. Hierarchical heterostructure of CdS nanoparticles sensitized electrospun TiO_2 nanofibers with enhanced photocatalytic activity. *Separation and Purification Technology*, 122, pp. 60-66.

Xia, Y. S. and Zhu, C. Q. 2008. Aqueous synthesis of luminescent magic sized CdSe nanoclusters. *Materials Letters*, 62, pp. 2103-2105.

Xei, R., Li, L., Li, Y., Liu, L., Xiao, D. and Zhu, J. 2011. Fe:ZnSe semiconductor Nanocrystals: synthesis, surface capping, and optical properties. *Journal of Alloys and Compounds*, 509, pp. 3314-3318.

Zhao, N., Liu, K., Greener, J., Nei, Z. and Kumacheva, E. 2009. Close-packed superlattices of side-by-side assembled Au-CdSe nanorods. *Nano Letters*, 9, pp. 3077-3081.

Appendix A

WSU
Walter Sisulu University

DIRECTORATE OF RESEARCH DEVELOPMENT

Research Ethics Clearance Certificate

DVC(AA&R)/DRD/SREC.....30/05/2012 (No. 03)

After due consideration and recommendation by the Senate Research Ethics Committee meeting held on 30 May 2012 this is to certify that Ethical Clearance is given for the following project:

Project title: **A facile effective method for the synthesis of Au and Pt-CdSe nanostructures and their characterizations.**

Name of Student: **Nelisa Ncumisa Gaxela**

Qualification: **MASTERS**

Student No: **202607763**

Date of commencement of Research: **2012**

Expected date of completion of Research: **31 December 2015**.

Comments:

This clearance is given with the understanding that the research activities to be carried out will be in conformity to those detailed in the research proposal.

Faculty of Natural Sciences
Chair of Faculty Higher Degrees Committee
Dr A. Niba

WALTER SISULU UNIVERSITY
FACULTY OF NATURAL SCIENCES
15 FEB 2016
NELSON MANDELA DRIVE
PRIVATE BAG X1
MTHATHA CAMPUS, 5117

APPENDIX K

WALTER SISULU UNIVERSITY
DIRECTORATE OF POSTGRADUATE STUDIES
MANDATORY CONSENT FORM: ELECTRONIC THESES & DISSERTATIONS (ETD) AND PLAGIARISM REQUIREMENT (For postgraduate research outputs from 2009 September)

TEMPLATE FOR THE STUDENT AND SUPERVISOR CONSENT FOR PUBLICATION OF ELECTRONIC RESEARCH OUTPUT ON INTERNET AND WSU INTRANET

FACULTY: _____

QUALIFICATION NAME: _____ ABBREVIATION: _____ YEAR: _____

STUDENT'S FULL NAME: _____ STUDENT NUMBER _____

TYPE OF RESEARCH OUTPUT: RESEARCH PAPER/MINI-DISSERTATION/DISSERTATION/THESIS (TICK ONE)

TITLE OF THE RESEARCH OUTPUT: _____
_____

CONSENT: I HEREBY GIVE MY CONSENT TO WALTER SUSULU UNIVERSITY TO PUBLISH MY RESEARCH OUTPUT FOR THE QUALIFICATION ABOVE ON THE WSU INTRANET AND INTERNET. I CERTIFY THAT TO THE BEST OF MY KNOWLEDGE, THERE IS NO PLAIGARISM IN THE RESEARCH OUTPUT AS SUBMITTED. I HAVE TAKEN REASONABLE CARE TO ENSURE THAT THE RESEARCH OUTPUT MEETS THE QUALITY LEVEL EXPECTED FOR THE PRESENT QUALIFICATION LEVEL BOTH IN TERMS OF CONTENT AND TECHNICAL REQUIREMENTS. I FULLY UNDERSTAND THE CONTENTS OF THIS DECLARATION.

_____ _____
SIGNATURE OF STUDENT DATE

ENDORSEMENTS BY:

SUPERVISOR:

FULL NAME: _____ SIGNATURE: _____ DATE: _____

CO-SUPERVISOR(S):

1 FULL NAME: _____ SIGNATURE: _____ DATE: _____

2. FULL NAME: _____ SIGNATURE: _____ DATE: _____